MICROMECHANICAL CHARACTERIZATION OF SURFACE TREATED REINFORCING FIBERS IN DUCTILE POLYMER MATRICES

Author: W. A. Fraser

Supervisor: F. H. Ancker

Project No.: 597M02

File No.: 4280

Research and Development Department
Chemicals and Plastics
Union Carbide Corporation
Bound Brook, New Jersey

RECEIVED
FEB 5 1975

PLAINTIFF'S EXHIBIT
tabbies
UC-1507

Published by AsbestosClaims.Law
asbestosclaims.law/library/16612/1

TABLE OF CONTENTS

		Page
Summary		1
Introduction		2
1.	Fiber Reinforcement Theory	4
	1.1 Composite Properties: "Thermoelastic" and "Strength"	4
	1.2 Continuous Fiber Reinforcement: Tensile Failure Modes	6
	1.3 Discontinuous Fiber Reinforcement	7
2.	Experimental Method	10
	2.1 Constituents	11
	2.2 Procedure	12
3.	Experimental Data	13
	3.1 Effect of Total Specimen Strain on ℓ/d Distributions	13
	3.2 Fiber/Matrix Interactions	13
	3.3 Thermal Stability of Fiber/Matrix Interactions	14
	3.4 Pitch Based Graphite and Thornel 300	15
	3.5 Data Interpretation Guidelines	16
4.	Theoretical Analysis	16
	4.1 Statistics of Brittle Fracture	17
	4.1.1 Weakest Link Strength Models	17
	4.1.2 The Weibull Distribution Function	19
	4.2 The Assumed Fiber Strength Model	22
	4.3 Stochastic Fiber Fragmentation Model	25
	4.3.1 Proof Testing and Truncated Breaking Strength Distributions	25
	4.3.2 Computer Simulated Fiber Fragmentation	26
	4.4 Parameter Estimation Procedure	28
	4.4.1 Objective Function & Search Method	29
	4.4.2 Parameter Constraints	29
	4.5 Data Analysis	32
5.	Conclusions	33
	Acknowledgements	34
	References	35

TABLES AND FIGURES

		Page
TABLE I:	Components of a Typical Glass Treatment	38
TABLE II:	Fiberglass Descriptions	38
TABLE III:	Properties of Thornel 300	39
TABLE IV:	Properties of Pitch Based Graphite	39
TABLE V:	Matrix Resin Properties	40
FIGURE 1:	Stress Transfer to an Embedded Fiber	41
FIGURE 2:	Critical Fiber Length Concept	41
FIGURE 3:	Fiber Length Efficiency Factor	42
FIGURE 4:	Multiple Fiber Fracture	43
FIGURE 5:	Compression Mold and Fiber Fork	44
FIGURE 6a:	Fragment ℓ/d Cum. Dist'n. (OCF 885-PP)	45
6b:	ℓ/d Histogram	46
6c:	ℓ/d Frequency Curve	47
FIGURE 7:	Effect of Specimen Strain on ℓ/d Dist'n.	48
FIGURE 8:	ℓ/d Dist'ns.; OCF 885, OCF 415 in Nylon 6	49
FIGURE 9:	OCF 885, OCF 415 in Polypropylene	50
FIGURE 10:	OCF 885, OCF 415 in HDPE	51
FIGURE 11:	Summary Plot, OCF 885 in Nylon 6,PP.,HDPE	52
FIGURE 12:	Summary Plot, OCF 415 in Nylon 6,PP.,HDPE	53
FIGURE 13:	Effect of Temperature, OCF 885 in Nylon 6	54
FIGURE 14:	Effect of Temperature, OCF 415 in HDPE	55
FIGURE 15:	Pitch Based Graphite in Nylon 6, PP.	56
FIGURE 16:	Thornel 300 in Nylon 6, PP.	57
FIGURE 17:	Pitch Based Graphite in Epoxy (ERLA 4617)	58
FIGURE 18:	OCF 885, OCF 415, Pitch Fiber, Thornel 300 in PP.	59
FIGURE 19:	OCF 885, OCF 415, Pitch Fiber, Thornel 300 in Nylon 6	60
FIGURE 20:	General Strength-Length Relationship for Glass	61
FIGURE 21:	Assumed Link Strength Dist'n. Function	62
FIGURE 22:	Hypothetical Fiber Strength Length Curves	63
FIGURE 23:	Proof Testing Effects	64
FIGURE 24:	Stochastic Fiber Fragmentation	65
FIGURE 25:	Strength-Length Behavior - Flaw Free Fiber	66
FIGURE 26:	Theoretical ℓ/d Dist'n.'s -Flaw Free Fiber	67
FIGURE 27:	Strength-Length Behavior-Flawed Fiber	68
FIGURE 28a:	Theoretical ℓ/d Cum. Dist'n.-Flawed Fiber	69
28b:	Theoretical ℓ/d Frequency Curve	70
FIGURE 29:	Experimental and Optimized Theoretical ℓ/d Cum. Dist'ns.-OCF 885 in PP.	71
FIGURE 30:	Computed Strength-Length Curve-OCF 885 in PP.	72

Union Carbide trial exhibit UC-1507: W. A. Fraser, Micromechanical Characterization of Surface Treated Reinforcin... Published by AsbestosClaims.Law
ACL Doc 16612 · Page 3 of 88 asbestosclaims.law/library/16612/3

Page

FIGURE 31: Experimental and Optimized Theoretical ℓ/d Cum. Dist'ns.-OCF 985 in Nylon 6 73
FIGURE 32: Computed Strength-Length Curve-OCF 885 in Nylon 6 74

APPENDICES

A. Data Smoothing and Differentiation 75
B. Probabilistic Derivation for the Effect of Specimen Size on Strength 77
C. The Mixed Element, Weakest Link, Fiber Strength Model 79
D. The Sequential Fragment Proof Testing Equations 81
E. Data Reduction Program Listing 84
F. Data Analysis Program Listing 98

Union Carbide trial exhibit UC-1507: W. A. Fraser, Micromechanical Characterization of Surface Treated Reinforcin... Published by AsbestosClaims.Law
ACL Doc 16612 · Page 4 of 88 asbestosclaims.law/library/16612/4

BUSINESS CONFIDENTIAL PROJECT REPORT

MICROMECHANICAL CHARACTERIZATION OF SURFACE TREATED REINFORCING FIBERS IN DUCTILE POLYMER MATRICES

AUTHORS: W. A. Fraser

SUPERVISOR: F. H. Ancker

DATE: January 30, 1975

PROJECT NO.: 597M02

FILE NO.: 4280

SUMMARY

The present report discusses reinforcing fibers and fiber surface treatments in terms of the micromechanics theories of bulk composite strength. A new single filament technique is discussed which enables direct experimental determination of the fundamental micromechanics parameters which control the strength properties of a composite. A brief outline of this technique has been reported earlier in the form of a paper submitted to the 1975 SPI conference on Reinforced Plastics/Composites[1].

The present report expands on this subject in several distinct areas.

(1) A review of pertinent fiber reinforcement theory is presented to illustrate the importance of coupling and sizing agents in enhancing bulk composite properties.

(2) Additional data are presented including fragment ℓ/d distributions for an experimental sample of Carbon Products' new continuous filament pitch based graphite and "Thornel" 300 in both nylon 6 and polypropylene. Also discussed is a preliminary effort in extending the procedure to include thermoset resins. ℓ/d distributions are presented for the pitch fiber in an epoxy matrix (ERLA 4617) tested at room temperature and 150° C.

(3) A more detailed and comprehensive discussion of the statistics of brittle fracture describes the development and evolution of the assumed probabilistic fiber strength model.

(4) Detailed listings of the computer programs used for both data reduction and data analysis are included in an appendix.

This report is intended to serve as a reference manual for future utilization of the fiber fragmentation, coupling/sizing agent evaluation procedure.

Research and Development Department
Chemicals and Plastics
Union Carbide Corporation
Bound Brook, New Jersey

Union Carbide trial exhibit UC-1507: W. A. Fraser, Micromechanical Characterization of Surface Treated Reinforcin... Published by AsbestosClaims.Law
ACL Doc 16612 · Page 5 of 88 asbestosclaims.law/library/16612/5

INTRODUCTION

The U. S. market for fiber reinforced plastics is approaching two billion pounds per year with an above average projected rate of growth. Union Carbide Corporation supplies many components for the composites market, e.g. polymers and chemicals (C & P), silane coupling agents (C & P), asbestos fibers (Mining & Metals), and graphite fibers (Carbon Products).

Within the last decade, significant advances have been made in the theoretical analysis of composite properties. The initial incentive was the need for super performance materials for space and aircraft applications but, now, the mechanics theories are increasingly being applied to the design of lower cost, mass produced composite parts. At the same time, however, these theories have received only limited use by raw material producers in optimizing the constituents of composite materials. The present report discusses current composite theories and applies them to the problem of optimizing fiber surface treatments.

High strength, high modulus, reinforcing fibers such as glass or graphite are brittle materials which are suceptible to severe property deterioration due to surface damage in handling. Furthermore, when incorporated in a composite, efficient utilization of the fiber reinforcement requires high fiber/matrix adhesion. To overcome these problems, glass fibers for composites are always surface treated with complex mixtures of sizing and coupling agents immediately after spinning. Similarly, asbestos fibers with surface treatments have recently been introduced commercially and surface treatments for graphite are now being recognized as a necessary requirement for broad industrial acceptance.

High efficiency of reinforcement depends on both the inherent fiber properties and the fiber surface treatment. The fiber treatments increase the reinforcement efficiency by two distinct mechanisms, namely:

a. by improving the fiber/matrix adhesion - which is a principal function of the coupling agent, and

b. by protecting the fiber from surface damage and thus assure retention of high fiber tensile strength - which is a principal function of the sizing agent.

These improvements must further be maintained under varying environmental conditions, e.g. at elevated temperature (to assure high heat distortion temperature, i.e., low creep at elevated temperature), in water (to permit exposure to high humidity), etc. Also, depending on the ultimate application

Union Carbide trial exhibit UC-1507: W. A. Fraser, Micromechanical Characterization of Surface Treated Reinforcin... Published by AsbestosClaims.Law
ACL Doc 16612 · Page 6 of 88 asbestosclaims.law/library/16612/6

of the fibers, other properties such as prevention and dissipation of static charge build-up, fiber handling characteristics in filament winding and weaving processes, etc., may be additional requirements.

Optimization of fiber surface treatments is inherently a difficult physical/chemical problem because individual components of practical formulations often perform more than one function and in many instances may interfere with each other. Furthermore, traditional composite evaluation techniques measure only the overall fiber reinforcement efficiency and thus provide little insight into the micromechanics effects of the fiber treatments. Specialized evaluation techniques capable of distinguishing between the basic coupling agent effect (interfacial adhesion) and the basic sizing agent effect (fiber protection) have been too tedious to find general utility for optimization of practical fiber treatments.

In recognition of these problems, it was the aim of this project to develop an improved technique for direct experimental determination of the fundamental micromechanics parameters characterizing both the adhesion promoting capabilities and the fiber protection performance of a given fiber treatment formulation for a given fiber/polymer composite. The method is based on a convenient experimental procedure and is, thus, practical for the routine screening and evaluation of new coupling/sizing agent systems. The procedure provides detailed insight into the micromechanical effects of the various physico-chemical fiber treatments and should facilitate the development of new and improved coupling/sizing systems and processes. Furthermore, by correlating fundamental fiber and interface characteristics with other important composite properties such as fracture toughness, impact strength, fatique and creep resistance, significant contributions may be realized in understanding and eventually in optimizing these properties.

The new single filament test and data analysis procedure developed during this program has been summarized in a recent report [1], issued in the form of a paper submitted to the 1975 SPI Conference on Reinforced Plastics/Composites. The present report covers in detail the evolution of this new technique, the underlying basic concepts, the experimental procedures, including illustrative examples of the application of the technique to specific fiber/polymer systems. Finally, a complete listing of the computer program package is included in an appendix.

A cooperative program has been initiated with the silane coupling agent group at Tarrytown aimed at utilizing this technique for optimizing coupling/sizing agent systems for specific fiberglass/polymer composite systems.

Union Carbide trial exhibit UC-1507: W. A. Fraser, Micromechanical Characterization of Surface Treated Reinforcin... Published by AsbestosClaims.Law
ACL Doc 16612 · Page 7 of 88 asbestosclaims.law/library/16612/7

1. Fiber Reinforcement Theory

The experimental procedure and theoretical analysis scheme to be outlined in this report provide fundamental micromechanics parameters which describe the specific adhesion promoting capabilities and fiber protection performance of a given fiber treatment formulation. To understand the technique and appreciate the utility of the information it provides, one must have some insight into the fundamentals of fiber reinforcement theory. Several aspects of this subject will be discussed in this section.

1.1 Composite Properties: "Thermoelastic" and "Strength"

The following brief review of the micromechanics of uniaxially aligned, fiber reinforced composites will be limited to the analysis of static properties. These properties, using a classification due to McCullough[2], fall into two categories: "thermoelastic" and "strength". Thermoelastic properties, which include tensile modulus, shear modulus, thermal expansion etc., can usually be treated in terms of average properties and average responses of the individual constituents. The simple rule of mixtures has been found, in most cases, to be quite adequate for predicting these composite properties. Longitudinal responses are represented by the parallel reaction of the fiber and resin phase.

$$P_c = \sum_{i=1}^{n} P_i V_i \qquad (1\text{-}1)$$

where

P_c = composite property
P_i = component property
V_i = component volume fraction
n = number of components (two in simple systems)

Transverse responses in the composite consider the series reaction of the fiber and resin phase and are given somewhat less accurately by

$$\frac{1}{P_c} = \sum_{i=1}^{n} V_i / P_i \qquad (1\text{-}2)$$

The rule of mixtures has also been used to describe the strength characteristics of highly idealized composites containing uniform strength, unidirectional, continuous fibers. Implicit in this analysis is the assumption of "unit structural

Union Carbide trial exhibit UC-1507: W. A. Fraser, Micromechanical Characterization of Surface Treated Reinforcin... Published by AsbestosClaims.Law
ACL Doc 16612 · Page 8 of 88 asbestosclaims.law/library/16612/8

behavior" among the constituent elements[3]. This concept implies perfect bonding between matrix and reinforcement, ensuring uniform force transfer between constituents and therefore, their deformation as a single structural unit. For fiber loadings greater than a certain critical value, the composite tensile strength is given by

$$\sigma_c^* = \sigma_f^* V_f + \sigma_m (1-V_f) \qquad (1\text{-}3)$$

where

σ_c^* = composite tensile strength
σ_f^* = breaking stress of fibers
σ_m = stress supported by matrix at breaking strain of fibers
V_f = volume fraction of fibers

With composite strain equal to both the fiber and matrix strain, failure of the fibers results in immediate failure of the composite unless the remaining matrix, $(1-V_f)$, can support the full composite stress, i.e.,

$$\sigma_f^* V_f + \sigma_m (1-V_f) > \sigma_m^* (1-V_f) \qquad (1\text{-}4)$$

where σ_m is the ultimate tensile strength of the matrix. Equation (1-4) defines a minimum fiber volume fraction which must be exceeded for equation (1-3) to be applicable:

$$V_{fmin} = \frac{\sigma_m^* - \sigma_m}{\sigma_f^* + \sigma_m^* - \sigma_m} \qquad (1\text{-}5)$$

At fiber loadings less than V_{fmin}, the fibers undergo multiple fracture, a phenomenon which forms the basis for the fiber treatment evaluation procedure to be described in Section 2. Provided that the yield elongation of the matrix is sufficiently large with respect to the fiber failure strain, the fibers will successively fracture into smaller and smaller fragments depending on the maximum shear stress, τ, which the interface (or matrix) can sustain.

The preceding composite strength model using thermoelastic property analysis procedures, while illustrative, is a vast oversimplification. Strength is a statistical phenomenon, strongly dependent on the nature of local environments and, consequently, cannot be accurately described in terms of average component responses. A prerequisite for the analysis of strength is the identification of the modes of composite failure and the parameters which influence it. Attention must be focused on the

Union Carbide trial exhibit UC-1507: W. A. Fraser, Micromechanical Characterization of Surface Treated Reinforcin... Published by AsbestosClaims.Law
ACL Doc 16612 · Page 9 of 88 asbestosclaims.law/library/16612/9

ways in which "unit structural behavior" breaks down. Coupling and sizing agents have a major influence on the stress limits for this breakdown and on the mechanisms by which it occurs.

1.2 Continuous Fiber Reinforcement: Tensile Failure Modes

In composite systems consisting of strong brittle fibers in ductile and semi-brittle matrices, failure mechanisms can be quite complex with the mode and stress level at failure dependent on matrix, fiber, and interfacial characteristics. A number of failure modes have been observed and distinguished. Consider a composite reinforced with uniaxially aligned continuous filaments and subjected to a tensile load. With semi-brittle resins, fiber breakage can initiate a shear crack which propagates along the fiber/matrix interface separating or decoupling the fiber from the matrix and reducing its effectiveness over a substantial fiber length. Coupling agents, designed for specific fiber/resin systems, are intended to inhibit this type of failure. Another failure possibility is that following a single fiber fracture, a crack propagates through the matrix, parallel to the fibers or perhaps transversely across the composite. These failure modes are influenced, in part, by the toughness of the matrix, i.e., its ability to deform and redistribute shear stresses.

If the preceding failure modes are arrested, increasing the applied tensile load can result in progressive fracture of the fibers accumulating throughout the composite. Parratt[4] and Riley and Reddaway[5] suggested that, in the extreme case, progressive fracture might reduce fiber length to the point that further increases in load cannot be transmitted to the fiber because the maximum interfacial shear strength is exceeded. In essence, what was originally a continuous filament reinforced composite has now been reduced to a system consisting of discontinuous fibers. Composite failure proceeds by shear failure of the matrix and fiber pullout. The concepts of fiber transfer length and critical fiber length are essential to understanding this failure mechanism and will be discussed in more detail in a subsequent section. In proposing this mechanism, the authors also recognized that the statistics of fiber strength must be considered. As the fibers become shorter, breaking at local defects, they become stronger (see Section 4) and can, therefore, sustain a larger load before fracture. Both coupling and sizing agents, affecting the fiber transfer length (fiber/matrix adhesion) and fiber strength (degree of fiber damage) respectively, influence the stress level at which this failure mode occurs.

Union Carbide trial exhibit UC-1507: W. A. Fraser, Micromechanical Characterization of Surface Treated Reinforci... Published by AsbestosClaims.Law
ACL Doc 16612 · Page 10 of 88 asbestosclaims.law/library/16612/10

Hale and Kelly[6] have shown that the preceding failure mode is viable only at low fiber loadings. For higher fiber volume fractions Rosen[7] has hypothesized that composite failure can take place before the conditions for fiber pullout are reached. In this mechanism, composite failure supposedly results from the weakening of a composite cross section by the statistical accumulation of fiber fractures with increasing load. The model considers that in the vicinity of an individual fiber break, a portion of the fiber is ineffective, i.e., it does not support the full composite stress. The composite is modeled as being composed of layers of dimension equal to the ineffective length (fiber transfer length). Any fiber fracturing within this layer is incapable of transmitting a load across the layer, and the applied load at this cross-section is then uniformly distributed among the unbroken fibers that remain. When enough fiber fractures accumulate in any one layer, composite failure results. In developing this composite strength model, Rosen recognized the statistical nature of the phenomenon and tried to describe it quantitatively by incorporating brittle fiber, weakest-link fracture statistics. More will be said about statistical fiber strength models in Section 4 of this report. Sizing agents, which influence fiber strength characteristics (magnitude and variability) clearly affect the ultimate strengths of composites subject to failure via the cumulative weakening mechanism.

Before extending this discussion to include discontinuous fiber reinforced systems, it should be noted that composite properties other than tensile strength show dependencies on fiber coupling and sizing agents. Cooper[8] has shown that both fiber/matrix adhesion and fiber flaw structure strongly influence the energy absorbing processes contributing to the work of composite fracture and hence composite toughness. If fiber surface treatment effects could be accurately characterized, treatment modification might become an important design vehicle for meeting both composite tensile strength and fracture toughness performance requirements.

1.3 Discontinuous Fiber Reinforcement

In a composite reinforced with discontinuous fibers, shear strains in the resin are the origin of the mechanism by which tensile loads on the composite are transferred to the fiber. Consider a fiber of radius r imbedded in a resin matrix which is subjected to a tensile load (Figure 1). Let $\tau(x)$ be the value of the shear stress acting at the fiber matrix interface. A force balance gives

$$\sigma(x)\pi r^2 = 2\pi r \int_0^x \tau(x)\, dx \qquad (1\text{-}6)$$

Union Carbide trial exhibit UC-1507: W. A. Fraser, Micromechanical Characterization of Surface Treated Reinforci... Published by AsbestosClaims.Law
ACL Doc 16612 · Page 11 of 88 asbestosclaims.law/library/16612/11

where:

$\sigma(x)$ = Tensile stress transferred to fiber
$\tau(x)$ = Interfacial shear stress
r = Fiber radius
x = Distance from fiber end

The distribution of tensile stress in the fiber is determined by the distribution of shear stress at the fiber/matrix interface.

A number of models have been proposed for calculating the longitudinal tensile stress distribution in an embedded fiber. The models of Cox[9], Dow[10], and Rosen[7] consider the case of an elastic fiber in an elastic matrix and all assume perfect bonding between matrix and fiber ("unit structural behavior"). This assumption is probably valid at low deformations but at high deformations where interfacial failure may take place the plastic flow model of Kelly and Tyson[11] may be more appropriate.

If we assume that when the interfacial region fails, it does so in shear, by yielding and flowing plastically, $\tau(x)$ in eq. (1-6) can be considered constant. Thus, integration gives

$$\sigma(x) = (2/r)\tau x \qquad (1\text{-}7)$$

This equation, indicating a linear build up of tensile stress from the fiber end, can be used to develop the concept of a critical transfer length. This is the length required to build the stress up to a level to break the fiber and is given by

$$X_c = \sigma_f^* d/4\tau \qquad (1\text{-}8)$$

where:

X_c = critical transfer length
σ_f^* = breaking stress of fiber
d_f = fiber diameter
τ = interfacial shear strength

X_c is observed to decrease as τ increases. Since stress builds up from both ends of a fiber, a critical fiber length, ℓ_c, can be defined as the minimum length of fiber capable of reaching its ultimate strength. From symmetry

$$\ell_c = 2X_c = \sigma_f^* d/2\tau \qquad (1\text{-}9)$$

Union Carbide trial exhibit UC-1507: W. A. Fraser, Micromechanical Characterization of Surface Treated Reinforci... Published by AsbestosClaims.Law
ACL Doc 16612 · Page 12 of 88 asbestosclaims.law/library/16612/12

These ideas are illustrated in Figure 2.

The concept of critical fiber length is essential to understanding the nature of reinforcement in composites containing discontinuous fibers. The rule of mixtures which has been used to describe the strength of ideal, uniaxially aligned, continuous fiber reinforced composites, eq. (1-3), must now include a term which measures the efficiency of reinforcement for short fibers relative to that of continuous fibers. The tensile strength of a uniaxially oriented discontinuous fiber reinforced system is, thus, given by

$$\sigma_c = e_\ell \sigma_f^* V_f + \sigma_m (1-V_f) \qquad (1\text{-}10)$$

Where the meaning of the symbols is as for eq. (1-3). e_ℓ is a fiber length efficiency factor [12] and is given by

$$e_\ell = \ell/2\ell_c \quad \text{for} \quad \ell < \ell c \qquad (1\text{-}11)$$

$$= 1-\ell_c/2\ell \quad \text{for} \quad \ell > \ell c$$

where ℓ is the fiber length

When the composite contains a distribution of fiber lengths, the efficiency factor becomes

$$e_\ell = \sum_{i=o}^{c} (\ell_i/2\ell_c)(V_i/V_f) + \sum_{i=c}^{n} (1-\ell c/2\ell_i)(V_i/V_f) \qquad (1\text{-}12)$$

where

V_i = volume fraction of fibers of length ℓi
V_f^i = total volume fraction of fibers

Eq. (1-11) is shown graphically in Figure 3 (e_ℓ vs. the reduced fiber length, $\ell/\ell c$). When the fiber length equals ℓc, the reinforcing efficiency is observed to be only 50% of that attained in continuous fiber systems. Increasing $\ell/\ell c$ to 5, however, results in a reinforcing efficiency of 90%. The importance of coupling and sizing agents and the necessity for surface treatment optimization in short fiber reinforced composites can be discussed in terms of equations (1-10) and (1-11).

In applications involving the injection molding of short

Published by AsbestosClaims.Law
asbestosclaims.law/library/16612/13

fiber filled plastics, the fibers must be relatively short in order to maintain good flow properties, especially when molding intricate parts. Two factors affecting the reduced fiber length and thus the reinforcing efficiency, eq. (1-11), in such a system are (1) the fiber/matrix adhesion which controls ℓ_c (a function of the coupling agent)and (2) the effectiveness of the fiber treatment in minimizing fiber attrition during molding (one function of the sizing agent). As seen from eq. (1-10), sizing agents can also influence the strength properties of these systems by another mechanism i.e., by preserving the fiber strength, σ_f^*. These effects have recently been studied by Burns et al[13] in chopped fiberglass reinforced nylon 66.[13] This resin is fairly forgiving with respect to fiber/matrix adhesion in that conventional amino-silane treated glass filaments are thought to exhibit interfacial shear strengths approaching the resin shear strength. With adhesion close to optimal, the only mechanisms available for upgrading composite strength depend on sizing agent effectiveness. Relative to systems with fiber lengths tightly distributed about ℓ_c, very significant increases in composite tensile strength can be achieved with only a slight upward shift in average fiber length (see Figure 3). Burns, in fact, reports that substitution of a tough film forming size for the more traditional PVAc coating reduced fiber attrition during molding to the extent that composite strength increased 30%. A portion of this strength increase, as discussed previously, can also be attributed to improved σ_f^* values.

In many resin systems, fiberglass/matrix adhesion can be the strength limiting factor. Coupling agents must be specifically tailored for specific applications. Furthermore, since coupling and sizing agents can interfere with each other,their selection must be carefully coordinated if optimum composite strength is to be realized. Table 1 lists the components of a typical glass treatment formulation. An example of component interference could be the adverse effect of a lubricant on adhesion vs. its effect in minimizing processing induced fiber damage. Another might relate to the protection capabilities of the film former vs. its compatability with the matrix resin. These are just two examples of optimization problems associated with fiber surface treatment formulation.

2. Experimental Method

The experimental method comprises embedding a single continuous filament in a tensile specimen of a particular resin.

Since this is well below the minimum fiber loading for reinforcement, (eq. (1-5)), deformation of the tensile specimen results in the filament fraccuring into small fragments as illustrated in Figure 4. Kelly[14] illustrated this multiple fracture phenomenon in a system consisting of tungsten wires embedded in a copper matrix. After deformation, the copper matrix was dissolved and the wire fragments extracted. On analysis of the fragment length distribution, it was found that its bounds were approximately ℓ_c and $\ell_c/2$. ℓ_c in this case was calculated from eq. (1-9)using the appropriate tungsten wire values for σ_f^* and d and substituting the ultimate shear strength of copper as a value for τ. Recalling the definition of critical fiber length, this result is not unexpected. The longest fibers capable of surviving in this system would have a length just under ℓ_c since longer fibers by definition, must fracture. The shortest fragments would arise with fracture of fibers just longer than ℓ_c, this occurring very near their midpoint.

Analogous experiments were run by Wadsworth and Spilling[15] for carbon fibers embedded in an epoxy resin and by Ongchin, Olender, and Ancker[12] for fiberglass in high density polyethylene. In both these studies it was observed that the range of the fragment length distributions was very much larger than the expected 2:1 predicted from the critical fiber length concept. Both sets of authors recognized that this dispersion in the fragment length distribution is a consequence of the statistical aspects of fiber strength. Glass and carbon fibers are flaw sensitive materials, i.e., when fracture occurs, it is neither preceded nor accompanied by extensive plastic deformation. The appreciable variation in tensile strength characteristic of these materials can be described in terms of statistical strength models, the parameters of which relate to the level of fiber damage (sizing agent effectiveness). Section 4 discusses statistical strength models in more detail and outlines a procedure for determining model parameters from fiber fragmentation data.

2.1 Constituents

The fibers which were investigated included two samples of continuous filament E glass roving prepared for us by Owens Corning Fiberglas in the form of fiber cakes These laboratory spun yarns were treated with two commercially used forming sizes designated OCF 885 and OCF 415. Their properties are listed in Table 2. Also included in the study were samples of PAN based graphite, Thornel 300 (grade WYP 30 1/0)

Union Carbide trial exhibit UC-1507: W. A. Fraser, Micromechanical Characterization of Surface Treated Reinforci... Published by AsbestosClaims.Law
ACL Doc 16612 · Page 15 of 88 asbestosclaims.law/library/16612/15

as well as an experimental sample of Carbon Products new continuous filament pitch based graphite (designated Parma-280-22-9). The Thornel 300 was coated with an epoxy-compatible size whereas the pitch fiber was untreated. The properties of these fibers are listed in Tables 3 and 4. The matrix resins studied were nylon 6 (Plaskon 8201, Allied Chemical), polypropylene (Shell 5524), and polyethylene (DMDJ-7008, Union Carbide). Resin properties are listed in Table 5.

2.2 Procedure

Embedding a single continuous filament in a tensile specimen of a given resin was accomplished using the fiber fork [16] and compression mold shown in Figure 5. Single filaments, carefully teased out of a given yarn, were mounted on the stainless steel fiber fork by epoxying their ends adjacent to positioning notches. The fiber loaded fork was then placed in the mold with each fiber sandwiched between a narrow strip of resin sheeting and a resin plaque overlay. The mold cover plate was carefully positioned on top of the resin plaque and the entire assembly placed in a laboratory scale hydraulic hot press. Molding temperatures were approximately 250°C for nylon 6, 175°C for polypropylene, and 150°C for polyethylene. Molding pressure was of the order of 1000 psi for each resin.

The mold cavity was designed to minimize both longitudinal channel flow, which could cause filament pretensioning or even fiber fracture, and transverse flow, which could result in embedding a curvilinear fiber. The tensile specimen had a cross-section of 0.25 in. x 0.075 in. and an effective gage length of 3.0 in.

The tensile specimens are deformed on an Instron at a jaw speed of 0.02 in./min. to approximately their yield elongation. The specimens are then placed in pyrex glass petri dishes (one specimen per dish) and pyrolyzed on a hot plate at 350°C for six hours. After the resin has been transformed into a carbonized char, the petri dishes are placed in a muffle furnace (1-1-1/2 hrs.) for final ashing. Furnace temperatures are typically 540° C for polyethylene and polypropylene and 600° C for nylon 6. The recovered fiber fragments are then measured using a Nikon comparator projection microscope. The covered petri dishes are placed on the traveling stage of this instrument and fiber length readings are taken directly from the projection screen at 20X magnification using a pair of dial calipers. A fiber diameter measure-

Union Carbide trial exhibit UC-1507: W. A. Fraser, Micromechanical Characterization of Surface Treated Reinforci... Published by AsbestosClaims.Law
ACL Doc 16612 · Page 16 of 88 asbestosclaims.law/library/16612/16

ment was made for a single filament per dish using a conventional optical microscope at 100x magnification. The ashing procedure does not degrade the fiber to the extent of biasing the fragment distribution (even in the case of graphite fibers) since ashing an undeformed tensile bar (thermoplastic matrices) results in the recovery of the unbroken filament.

3. Experimental Data

Fragments normalized by their diameter were ranked according to their size and a fractional cumulative frequency distribution evaluated. These data were then smoothed and differentiated using the moving strip, least squares polynomial method described by Hershey, Zakin and Simha[17] to give an empirical probability curve of fragment aspect ratios. The smoothing and differentiation procedure is outlined in Appendix A and the data reduction and plotting computer programs listed in Appendix E. Figures 6a, b, c show a cumulative distribution curve (raw data), a fragment aspect ratio histogram, and a calculated probability density curve for OCF 885 in polypropylene. This fragment ℓ/d distribution is seen to be quite broad extending well beyond the 2:1 bounds predicted from the simple critical fiber length concept. It should be noted that in order to accumulate a statistically significant number of fiber fragments for analysis, data from six tensile specimens were lumped together in calculating this distribution curve.

3.1 Effect of Total Specimen Strain on ℓ/d Distributions

The data which will be discussed in this and succeeding paragraphs will be presented in the form of smoothed cumulative fragment aspect ratio (ℓ/d) distribution curves. Figure 7 demonstrates that there is little effect of tensile elongation on the cumulative distribution curves of OCF 885 in polypropylene. Fragmentation is essentially complete after a total strain of 0.075 with the measured distribution representing the final curve i.e., the interface has reached its maximum stress limit and appears to be yielding plastically. The slight differences observed in the distribution curves are attributed, at least in part, to the limited amount of data (75-100 fragments) used in characterizing each curve.

3.2 Fiber/Matrix Interactions

Nylon 6: Figure 8 shows the ℓ/d distribution curves for both OCF 885 and OCF 415 in nylon 6 after room temperature

Union Carbide trial exhibit UC-1507: W. A. Fraser, Micromechanical Characterization of Surface Treated Reinforci... Published by AsbestosClaims.Law
ACL Doc 16612 · Page 17 of 88 asbestosclaims.law/library/16612/17

deformation. OCF 885 fractured into much smaller fragments than OCF 415 indicating a considerably higher degree of fiber/matrix interaction. This difference is primarily a reflection of sizing agent/matrix compatibility. The PVAc size of OCF 885 is expected to be considerably more compatible with nylon 6 than the olefinic size of OCF 415. The fact that OCF 415 fractures at all is ascribed to the action of the amine reactive coupling agent present in the treatment formulation.

Polypropylene: As in nylon 6, Figure 9 shows that OCF 885 exhibits a higher degree of fiber/matrix interaction than OCF 415; however, both distributions are shifted, to some extent, on the abscissa to higher ℓ/d values. Interfacial shear strengths for both fibers are somewhat lower in polypropylene than in nylon 6. Both sizing agent/matrix compatibility and coupling agent effectiveness are operating here.

Polyethylene: In HDPE there is a reversal in position of the fragment ℓ/d distribution curves as shown in Figure 10. OCF 415 with its olefinic size exhibits a much higher degree of interaction with polyethylene than the PVAc sized OCF 885. The coupling agents of each treatment formulation probably have little, if any, effect in this resin and thus the observed differences in interfacial shear strength can be interpreted primarily in terms of sizing agent/matrix compatibility.

Summary plots for both glasses in each of the three resins are shown in Figures 11 (OCF 885) and 12 (OCF 415). In resins which show little response to coupling agents, such as HDPE, sizing agent/matrix compatibility becomes a primary factor controlling fiber/matrix interfacial shear strength. In more readily coupled resins such as nylon 6, lack of size/matrix compatibility may be compensated for, somewhat, by including a coupling agent in the treatment formulation. This is clearly demonstrated in Figure 12 where OCF 415 performance in HDPE is observed not to differ markedly from that in nylon 6. The amine reactive coupling agent in the 415 olefinic treatment formulation apparently recoups much of the anticipated loss in interfacial shear strength expected on the basis of size/matrix (olefinic/nylon 6) incompatibility.

3.3 Thermal Stability of Fiber/Matrix Interactions

The thermal stability of specific fiber/matrix interactions can be studied by running the fiber fragmentation test at elevated temperatures. The tensile specimen containing the embedded filament is placed in the environmental test chamber

Union Carbide trial exhibit UC-1507: W. A. Fraser, Micromechanical Characterization of Surface Treated Reinforci... Published by AsbestosClaims.Law
ACL Doc 16612 · Page 18 of 88 asbestosclaims.law/library/16612/18

of a suitably equipped Instron, brought up to temperature and deformed while hot. Figure 13 shows how the fragment ℓ/d distributions for the OCF 885 - nylon 6 system shift to higher ℓ/d values as the temperature is raised from 25°C to 100° C to 150°C. In Figure 14, the OCF 415 - HDPE system is observed to be even more temperature sensitive. Two factors influence these shifts; the temperature dependence of the bulk resin shear strength and the thermal stability of the interfacial interaction. In a given resin, elevated temperature fragmentation data may well be quite useful in distinguishing between fiber treatments that rely merely on treatment/matrix compatibility to promote adhesion and those that provide true chemical coupling.

3.4 Pitch Based Graphite and Thornel 300

Figure 15 shows the fragment ℓ/d distribution curves of untreated, experimental samples of Carbon Products' new continuous filament pitch based graphite fiber in nylon 6 and polypropylene after room temperature deformation. Corresponding Thornel 300 ℓ/d curves for these same two resins are shown in Figure 16. Interfacial shear strength levels for both fibers are observed to be higher in nylon 6 than in polypropylene. This behavior probably reflects the differential in bulk resin shear strength between these matrices in addition to any difference in degree of specific fiber/matrix interaction.

A very preliminary effort was initiated in extending the fiber fragmentation procedure to include thermoset resins. The performance of the pitch based graphite fiber was evaluated in a UCC epoxy matrix (ERLA-4617). Since considerable bulk composite property data existed at Parma on this resin system, it was a natural candidate for study. The ERLA-4617 resin, cured with a near stoichiometric equivalent quantity of methylenediamaline (MDA), was found to have an elongation of 4.5 to 5.0% at a strain rate of 6.7×10^{-3} min^{-1}. Since this elongation was greater than the 1-2% rupture elongation reported for the fiber, utilization of the fiber fragmentation procedure seemed appropriate. Figure 17 shows fragment ℓ/d distribution curves after room temperature and 150°C deformation. As with the thermoplastic resins, the fiber fragments defining these curves were recovered by ashing the matrix resin. On examining this procedure, however, it was found that the distributions may be somewhat biased. With this resin matrix, even undeformed tensile specimens were found to generate a significant number of fragments on ashing. Apparently the thermal expansion coefficient differential existing between fiber and matrix causes thermal stresses in the initial stages

Union Carbide trial exhibit UC-1507: W. A. Fraser, Micromechanical Characterization of Surface Treated Reinforci... Published by AsbestosClaims.Law
ACL Doc 16612 · Page 19 of 88 asbestosclaims.law/library/16612/19

of ashing of sufficient magnitude to fracture the fiber. This was not a problem in thermoplastic matrices where resin yield strength falls off rapidly with increasing temperature. In spite of this undesired spurious fragmentation, the curves of Figure 17 serve to illustrate the sensitivity of the technique for studying fiber/matrix interfacial characteristics in thermoset systems. In future studies involving these resins, alternate fragment recovery procedures will be used. A possible method is acid digestion of the matrix, a technique currently in use at Parma[18] to measure resin content in resin-graphite composite materials.

3.5 Data Interpretation Guidelines

Composite plots of ℓ/d distribution curves for OCF 885, OCF 415, Carbon Products' new pitch based graphite fiber and Thornel 300 in both polypropylene and nylon 6, respectively are shown in Figures 18 and 19. These figures are presented in order to illustrate the potential hazards which exist in making simple interpretations based on raw fiber fragmentation data. Analysis discussed exclusively in terms of relative degrees of fiber/matrix adhesion can be quite misleading. It must be recognized that two factors control the position of the ℓ/d distribution curves: increased interfacial shear strength drives the distributions to lower ℓ/d values as does increased fiber damage (i.e., a weaker fiber will fragment into smaller pieces). The pitch based graphite fiber appears to exhibit excellent interfacial characteristics in both resins. Note, however, that its ℓ/d distribution as measured in polypropylene is quite dispersed, an indication, perhaps, of a highly damaged fiber. This is a reasonable explanation since this fiber has no protective surface coating (sizing agent). This complication in the data interpretation is resolved via the theoretical analysis scheme to be described in the following section.

4. Theoretical Analysis

The sensitivity of the experimental procedure to specific fiber/matrix interactions was demonstrated in Section 3. Furthermore the experimental fragment ℓ/d distribution curves were observed to be quite broad extending well beyond the 2:1 bounds predicted from the simple critical fiber length concept. This dispersion has been attributed to the statistical aspects of brittle fiber strength, a consequence of the distribution of local flaws of varying severity along the length of the fiber. Sizing agents, as discussed previously, are intended to minimize defects and consequently their capabilities

Union Carbide trial exhibit UC-1507: W. A. Fraser, Micromechanical Characterization of Surface Treated Reinforci... Published by AsbestosClaims.Law
ACL Doc 16612 · Page 20 of 88 asbestosclaims.law/library/16612/20

in this respect must be contained in this dispersity of the fragment ℓ/d distribution curves.

4.1 Statistics of Brittle Fracture

Brittle fracture is a much less reproducible phenomenon than fracture preceded by extensive plastic deformation. As Freudenthal[19] so aptly describes,"The process originates in highly localized regions of the material where inherent defects in the microstructure, or defects produced in the course of permanent deformation lead to localized intensities of tensile stresses so high that some of the existing defects are converted into flaws at which the cohesion of the material has actually been destroyed." The strength of a brittle material is a function of its defect structure, and it is this concept that explains the large differences between measured strength values and theoretical values based on calculations of the energy needed to break interatomic bonds.

If it is accepted that fracture at any stress level is dependent on the statistical expectation of encountering a critical or fatal flaw, we see immediately that this probability increases with specimen size. This behavior can be rationalized from purely probabilistic reasoning without making any assumptions concerning the physical nature of material inhomogeneities. A more formal derivation of the functional dependence of fracture probability on specimen size is given in Appendix B.

4.1.1 Weakest Link Strength Models

Assuming flaws to be distributed at random with a certain concentration per unit volume, then the strength of a given specimen is determined by its most severe flaw, i.e., its weakest point. F. T. Pierce[20] in his study of cotton yarns was first to describe this phenomenon mathematically with the introduction of the chain-type weakest link model for fiber strength. This model assumes a fiber to consist of n fiber elements linked together in series. The statistical problem becomes one of relating the distribution of chain strength to the distribution of largest flaws appearing in each of the fiber elements. Pierce recognized the close relation of this model to the generalized asymptotic theory of extreme values developed by Tippet[21], Fisher and Tippet[22], and Frechet[23]. This theory is concerned with finding the distribution of largest (or smallest) values in a sample of size n.

Union Carbide trial exhibit UC-1507: W. A. Fraser, Micromechanical Characterization of Surface Treated Reinforci... Published by AsbestosClaims.Law
ACL Doc 16612 · Page 21 of 88 asbestosclaims.law/library/16612/21

A number of assumptions are required in modeling brittle fiber fracture as a weakest link phenomenon

(1) The total fiber is subdivided into segments of equal length, each containing a number of distributed flaws of varying sizes.

(2) No interaction exists between flaws.

(3) The strength of a fiber element is uniquely determined by the largest flaw present in the element.

(4) The strength of any bulk specimen is uniquely defined by the strength of that segment that contains the most severe flaw. The mathematical formulation of the weakest link model requires the definition of several terms.

σ — A random variable representing strength, either the strength of a fiber element or the strength of an entire fiber.

$f(\sigma)$ — The probability density function (p.d.f) of element strength, i.e. the "underlying" distribution. The fraction of elements having a strength in the interval σ to $\sigma + d\sigma$ is given by $f(\sigma)d\sigma$.

$F(\sigma)$ — The cumulative distribution function (c.d.f.) of element strengths given by $\int_0^\sigma f(\sigma)d\sigma$. The probability of encountering an element of strength $\leq\sigma$.

$g(\sigma)$ — The p.d.f. of fiber (chain) strength. The fraction of fibers having a strength between σ and $\sigma+d\sigma$ is given by $g(\sigma)d\sigma$.

$G(\sigma)$ — The c.d.f. of fiber (chain) strength given by $\int_0^\sigma g(\sigma)d\sigma$. The probability of encountering a fiber of strength $\leq\sigma$

The desired expression is $g(\sigma)$ in terms of $f(\sigma)$, thus the probability that a chain of n links will break at a stress, σ, is simply the probability, $f(\sigma)$, that one link will fail at stress σ, times the probability that the (n-1) links are still surviving, $\left[1-F(\sigma)\right]^{n-1}$, times the number of combinations, n, in which this may occur.

$$g(\sigma) = nf(\sigma)\left[1-F(\sigma)\right]^{n-1} \qquad (4\text{-}1)$$

This is the probability density function of the distribution of smallest values in samples of size n. Integrating equation (4-1) and rearranging yields

Union Carbide trial exhibit UC-1507: W. A. Fraser, Micromechanical Characterization of Surface Treated Reinforci... Published by AsbestosClaims.Law
ACL Doc 16612 · Page 22 of 88 asbestosclaims.law/library/16612/22

$$1-G(\sigma) = \left[1-F(\sigma)\right]^{n} \qquad (4-2)$$

This is the probability that a fiber of n links will survive up to a stress level σ. This equation emphasizes the assumed statistical independence of the elements in that the joint probability of survival equals the product of the individual probabilities of survival for each link.

A number of researchers have described brittle fracture as a weakest link process and have used a variety of distribution functions to characterize f(σ), the underlying fiber element p.d.f. Pierce[20], in his original work on cotton yarns assumed a Gaussian form of f(σ) as did Kontorova and Frenkel[24] in their work on the brittle strength of crystals. Chechulin[25] developed the equations for a gamma distributed elemental strength. The consequence of these different forms of f(σ) is that the moments of g(σ) show different dependencies on n. The true form of f(σ) for a particular fiber could conceivably be determined by the accumulation of statistically significant amounts of tensile strength data at a variety of gage lengths. By examining the variation of the expected value of g(σ) with the fiber length (n), the actual form of f(σ) could be inferred. Generally speaking, however, only a moderate number of test replications is available at any one gage length and consequently discrimination between statistical distribution functions for f(σ) on this basis warrants only a limited degree of confidence.

Experimental research in the field of brittle fracture statistics, as Freudenthal[19] points out, is inherently susceptible to degenerating into indiscriminate data accumulation and curve fitting. A more rational approach is to develop physically relevant probability models which simulate observed phenomenon and can therefore be used for extrapolation of results beyond the range of observation or simply to characterize the brittle fracture characteristics of a given material. It is this latter application which is of concern in this report.

4.1.2 The Weibull Distribution Function

In 1939 Weibull[26], using elementary probability theory, derived an expression for the probability of rupture, S, of an isotropic brittle material of volume, V, subject to any given distribution of stress, σ. This expression is given by

$$S = 1-\exp -\int_{V} n(\sigma)\,dv \qquad (4-3)$$

Union Carbide trial exhibit UC-1507: W. A. Fraser, Micromechanical Characterization of Surface Treated Reinforci... Published by AsbestosClaims.Law
ACL Doc 16612 · Page 23 of 88 asbestosclaims.law/library/16612/23

where

$n(\sigma)$ = a function characteristic of each particular material.

This equation was generalized to model systems in which the material function may not be constant throughout the whole volume of the solid (e.g. materials with distinct surface flaws and interior flaws). In this case the equation becomes

$$s = 1 - \exp\left[-\int_V n_1(\sigma)dv - \int_V n_2(\sigma)dv \right] \qquad (4-4)$$

Based on purely heuristic reasoning, Weibull proposed an expression for $n(\sigma)$ of the form

$$n(\sigma) = \left(\frac{\sigma-\sigma_c}{\sigma_o}\right)^m \qquad (4-5)$$

σ_o, the scale parameter, σ_c, the location parameter and m, the shape parameter are unknowns, characteristic of the particular material. Equation (4-5) was justified purely on the grounds that it was the simplest mathematical expression satisfying the conditions that $n(\sigma)$ be a positive, nondecreasing function vanishing at some stress level, σ_c, which is not necessarily zero. Considering its origins, the distribution function defined by substituting equation (4-5) into (4-3) has been critized as being devoid of any physical meaning. However, as Weibull[27] points out, this same objection could be applied against all other probability functions used to characterize real populations. Furthermore, when applied to statistical strength problems, the parameters of this distribution can, at least, be associated with true material characteristics.

Implicit in Weibull's analysis is the principle that it is the weakest link which determines fracture strength. Thus, if $F(\sigma)$, representing the probability that a unit volume (fiber element) fractures at a stress level σ, is given by

$$F(\sigma) = 1 - \exp-\left(\frac{\sigma-\sigma_c}{\sigma_o}\right)^m \qquad (4-6)$$

then the probability of failure of a chain of n fiber elements is, on substitution of this expression into equation (4-2)

$$G(\sigma) = 1 - \exp-n\left(\frac{\sigma-\sigma_c}{\sigma_o}\right)^m \qquad (4-7)$$

The associated p.d.f. is

$$g(\sigma) = nm\,\sigma_o^{-1}\left(\frac{\sigma-\sigma_c}{\sigma_o}\right)^{m-1} \exp-n\left(\frac{\sigma-\sigma_c}{\sigma_o}\right)^m \qquad (4-8)$$

The mean chain or fiber strength, $\langle\sigma\rangle$, is given by the expected value or first moment of $g(\sigma)$ about the origin.

$$\langle\sigma\rangle = \int_0^\infty \sigma g(\sigma) d\sigma \tag{4-9}$$

Evaluation of this definite integral gives

$$\langle\sigma\rangle = \sigma_c + \sigma_o / n^{1/m} \, \Gamma\left(\frac{m+1}{m}\right) \tag{4-10}$$

Where Γ = the complete gamma function
This equation indicates that average chain strength varies as $n^{-1/m}$
The variance of σ i.e. the square of the standard deviation s is given by

$$s^2 = \sigma_o^2 \; n^{-2/m} \left[\Gamma\left(\frac{m+2}{m}\right) - \Gamma^2\left(\frac{m+1}{m}\right)\right] \tag{4-11}$$

and the coefficient of variation, $cv = s/\bar{\sigma}$, becomes

$$cv = \frac{\left[\Gamma\left(\frac{m+2}{m}\right) - \Gamma^2\left(\frac{m+1}{m}\right)\right]^{1/2}}{\Gamma\left(\frac{m+1}{m}\right)} \tag{4-12}$$

From this expression it is clear that cv is a function only of the Weibull shape parameter, m. In fact Irwin[28] suggested that cv may be closely approximated by

$$cv \simeq 1.2/m \tag{4-13}$$

Thus, in essence, the parameter m is an inverse measure of the coefficient of variation. Using this result we can also gain some insight into the physical significance of the other Weibull parameters, σo and σc. In the limit as m becomes very large ($m \to \infty$) the statistical characterization of strength reduces to the classical theory of fracture, i.e., failure occurs when the material reaches its "fracture strength" a material constant. From equation (4-10) when $m \to \infty$, i.e., $cv \to o$

$$\bar{\sigma} = \sigma_o + \sigma_c \tag{4-14}$$

where σ_c is a lower limiting material strength, possibly zero, and $\sigma_o + \sigma_c$ represents the ultimate strength of the material.

The Weibull distribution function has been applied to a wide variety of problems not directly related to the statistics

Union Carbide trial exhibit UC-1507: W. A. Fraser, Micromechanical Characterization of Surface Treated Reinforci... Published by AsbestosClaims.Law
ACL Doc 16612 · Page 25 of 88 asbestosclaims.law/library/16612/25

of brittle strength, the distribution of particle sizes of fly ash [26], the fatigue of single fibers[29], the abrasion resistance of yarns[9], etc. Its wide applicability is due, in part, to the flexibility of the expression. When m=1, the probability density function becomes the exponential function, with m= 2, the Rayleigh distribution and with m=3.25 most of the Weibull curve is identical with the normal distribution function[31].

Brittle fiber fracture applications of Weibull type statistics have been quite numerous. Wallhaus[32] used it to investigate the effects of time, moisture, static load, and mechanical damage on the strength of single glass filaments. Kies[33] used a modified Weibull distribution in this studies on the strength of glass. Metcalfe and Schmitz[34] investigated the effect of gage length in the tensile testing of E and S glass fibers. Their studies indicated logarithmic strength-length plots were not linear over the entire gage length range investigated (.025-30 cm). For a given fiber, a slope change was observed at some critical gage length. This effect was attributed to the presence of a mixed population of flaws. One type of flaw is severe, has wide spacing and governs failure of long fibers. The other type is less severe, has narrow spacing and determines failure at short gage lengths. Their data suggested that greater fiber damage causes increasing loss of strength at long gage lengths, increasing the slope of the logarithmic strength-length curve in this region, and that it also tends to move the position of the slope change to shorter gage lengths. These trends are illustrated in Figure 20. This bilinear form of the logarithmic strength-length plot indicates that a single exponent Weibull distribution function is inadequate to describe failure processes in fiberglass. The more complex Weibull form of equation (4-4) may therefore be more appropriate.

4.2 The Assumed Fiber Strength Model

Metcalfe and Schmitz[34] demonstrated that a plot of fiber strength vs. fiber length was a very effective means of characterizing flaw structure and assessing the damage level exisiting in fiberglass. This concept forms the basis of our analysis scheme for evaluating the fiber protection capabilities of specific sizing agent systems.

The first step in this procedure is the development of a mathematical model which can simulate the strength-length trends actually observed in the tensile testing of fibers. A simple Weibull distribution function for fiber fracture was found to predict, unsatisfactorily, a linear logarithmic plot

Union Carbide trial exhibit UC-1507: W. A. Fraser, Micromechanical Characterization of Surface Treated Reinforci... Published by AsbestosClaims.Law
ACL Doc 16612 · Page 26 of 88 asbestosclaims.law/library/16612/26

of mean fiber strength vs. fiber length (equation 4-10). The bivariate Weibull distribution function, equation (4-3), proposed for materials with a mixed flaw population has the form

$$G(\sigma) = 1-\exp-n\left[\left(\frac{\sigma-\sigma_{c_1}}{\sigma_{o_1}}\right)^{m_1} + \left(\frac{\sigma-\sigma_{c_2}}{\sigma_{o_2}}\right)^{m_2}\right] \qquad (4\text{-}15)$$

This six parameter probability model should have enough flexibility to accommodate observed bilinear fiber strength-length trends but unfortunately its functional form precludes evaluation of an analytic expression for the expected value (i.e., mean fiber strength). Numerical integration to compute $\langle\sigma\rangle$, while a possibility, was not considered viable because of the excessive expansion in computation time this would necessitate in other aspects of the overall analysis procedure. This limitation of the bivariate Weibull expression rendered it an unacceptable model.

The bilinear logarithmic strength-length behavior observed for fiberglass has been simulated by Rosen[35] in terms of the weakest link model by assuming a double rectangular distribution function for $f(\sigma)$, the underlying fiber element p.d.f. The following analysis is a permutation of Rosen's model.

Using the weakest link, chain type representation of a fiber, the concept of a mixed flaw population can be modeled by assuming that two types of links exist in the fiber chain: virgin or "as spun" links and severely flawed or damaged links. The virgin or "as spun" links, modeling the fiber as it comes out of the spinneret, were assumed to be represented by a simple Weibull expression

$$f(\sigma)_v = (1-P)m/\sigma_o\left(\frac{\sigma-\sigma_c}{\sigma_o}\right)^{m-1} \exp-\left(\frac{\sigma-\sigma_c}{\sigma_o}\right)^{m} \qquad (4\text{-}16)$$

$$F(\sigma)_v = (1-P)\left[1-\exp-\left(\frac{\sigma-\sigma_c}{\sigma_o}\right)^{m}\right] \qquad (4\text{-}17)$$

where

σ_c = a lower limiting virgin link strength not equal to zero.

σ_o = a characteristic link strength related to the flaw free material strength.

Union Carbide trial exhibit UC-1507: W. A. Fraser, Micromechanical Characterization of Surface Treated Reinforci... Published by AsbestosClaims.Law
ACL Doc 16612 · Page 27 of 88 asbestosclaims.law/library/16612/27

m = an inverse measure of the dispersion in link strength .

P = a weighting factor indicating the fraction of the link population with very severe flaws.

The subscripts v on $f(\sigma)$ and $F(\sigma)$ in these equations refer to virgin element expressions. These virgin or "as spun" links were assumed to exhibit some dispersion in strength simply because of the presence of unavoidable, microscopic surface imperfections. A small portion of the links were assumed to contain very severe flaws, a consequence of handling or perhaps environmentally induced damage. These weakened elements were modeled, for simplicity, as possessing a simple rectangular distribution function, $f(\sigma)_f$ isolated at low stress levels (the subscript f refers to flawed elements):

$$f(\sigma)_F = P/(\sigma_b - \sigma_a) \qquad (4\text{-}18)$$

$$F(\sigma)_F = P\left(\frac{\sigma-\sigma_a}{\sigma_b-\sigma_a}\right) \qquad (4\text{-}19)$$

where

σ_a = lower limiting flawed link strength

σ_b = upper bound on flawed link strength

The composite elemental strength p.d.f, i.e., equations (4-16) and (4-18) is plotted in Figure 21 for some assumed model parameter values. In this figure SA=σ_a, SB=σ_b, SC=σ_c SO=σ_o.

Equations (4-16) - (4-19) can now be substituted into the generalized weakest link expressions (equations 4-1 and 4-2) to give the p.d.f. and c.d.f. expressions for a fiber chain of n links. This analysis is detailed in Appendix C as is the calculation of the expected value of $g(\sigma)$ (i.e. the mean fiber strength, $\langle\sigma\rangle$).

The mean strength of a fiber composed of n links drawn from the population characterized by equations (4-16) and (4-18) is given by

$$\langle\sigma\rangle = \sigma_a + (\sigma_b-\sigma_a)\left[1-(1-P)^{n+1}\right]/P(n+1) + (\sigma_c-\sigma_b)\left[1-P\right]^n + \left[1-P\right]^n (\sigma_o/n^{1/m})\,\Gamma\,\frac{m+1}{m} \qquad (4\text{-}20)$$

where

$\sigma_a, \sigma_b, \sigma_c, \sigma_o, m$, and P are defined as before and
Γ = complete gamma function

This expression is plotted in Figure 22 as Ln $\langle\sigma\rangle$ vs. Ln L, where $L=n\ell$ in is the number of fiber elements, and ℓ, the fiber element length is assumed to be .001 in. Several strength-length curves are shown for different values of P, the fraction of the fiber element population containing severe flaws. Arbitrary values were assumed for the other parameters of the fiber element strength distribution function. As the fiber length increases (i.e., n increases) $\langle\sigma\rangle$, the mean fiber or chain strength, falls off rapidly depending on the value of P. For P = .0005 and lengths greater than 0.5 in. fiber strength is essentially controlled by the very few weaker strength elements which are encountered more and more frequently. As P is decreased the strength-length dependence is dimished. The curves of Figure 20 might, thus, be interpreted as characterizing fibers exhibiting varying levels of damage.

The preceding six parameter statistical strength model seems capable of simulating observed mean fiber strength-length behavior while avoiding the complications associated with the bivariate Weibull expression, equation (4-15). The next step requires utilizing experimentally determined fiber fragmentation data to back out values of the parameters associated with this model and thus define characteristic Ln$\langle\sigma\rangle$-Ln L curves for a given fiber systems. These curves will then be used to discriminate between fiber treatments providing various degrees of fiber protection (i.e., sizing agent effectiveness).

4.3 Stochastic Fiber Fragmentation Model

The parameter estimation procedure developed above is based on a coupling of the statistical fiber strength model with a computer simulated stochastic model of the fiber fragmentation process. Discussion of this computer simulation requires an understanding of one additional concept: that of mechanical proof testing.

4.3.1 Proof Testing and Truncated Breaking Strength Distributions

The fracture strength of brittle fibers is characteristically spread over a very wide range. Curve I in Figure 23 might represent a typical cumulative strength distribution curve, $G(\sigma)$. It is bounded on the left by σ_L, the zero probability

Union Carbide trial exhibit UC-1507: W. A. Fraser, Micromechanical Characterization of Surface Treated Reinforci... Published by AsbestosClaims.Law
ACL Doc 16612 · Page 29 of 88 asbestosclaims.law/library/16612/29

strength ($\sim$0) and on the right by σ_u, a value related to the theoretical, flaw free strength of the given material. The expected value or mean strength associated with this initial distribution is $\langle\sigma\rangle_I$. Curve II in Figure 22 is the strength distribution curve obtained after eliminating all specimens of strength less than the proof stress $\sigma_p = \langle\sigma\rangle_I$. Assuming that the surviving elements were all unaffected by the proof test, the truncated cumulative distribution curve, $G_p(\sigma)$ can be related to the original distribution, $G(\sigma)$ by an expression due to Weibull[26].

$$G_p(\sigma) = \frac{G(\sigma) - G(\sigma_p)}{1-G(\sigma_p)} \qquad \sigma \geq \sigma_p$$

$$= 0 \qquad \sigma < \sigma_p \qquad (4\text{-}21)$$

The expected value characterizing this new distribution is $\langle\sigma\rangle_I$. The dispersion of the truncated distribution is observed to be considerably less than the original, in fact, as σ_p increases, approaching, in the limit, the 100% probability stress, σ_u, the surviving elements define a deterministic material, i.e., they all fail at the stress level σ_p. The generalized equations governing proof testing affects in terms of our assumed fiber strength model are outlined in Appendix D.

4.3.2 Computer Simulated Fiber Fragmentation

The following detailed description of the fiber fragmentation model is presented in terms of Figure 24. Consider a single filament of diameter d, 3 inches in length, embedded in some given resin matrix. The mean strength of this fiber, σ_{Fl}* can be computed using the statistical fiber strength model (equation 4-20) for some arbitrary set of model parameter estimates. On tensile deformation of the resin matrix, the model requires that the first fiber break occur at the stress level σ_{Fl}*. Although fiber fragmentation is stochastic in nature there are restrictions on where the break can take place. These arise as a consequence of the mechanism through which stress is transferred from the matrix to the fiber. Recalling the concept of a critical transfer length, i.e., the length required to build the stress up to a level to break the fiber, (equation 1-8), a portion of the fiber end does not realize the stress σ_{Fl}* and consequently the fiber cannot break in these regions. These ineffective regions of the fiber, given by

$$\ell c/2 = \sigma_F^* d/4\tau \qquad (4\text{-}22)$$

depend both on the breaking strength of the fiber and on the

Union Carbide trial exhibit UC-1507: W. A. Fraser, Micromechanical Characterization of Surface Treated Reinforci... Published by AsbestosClaims.Law
ACL Doc 16612 · Page 30 of 88 asbestosclaims.law/library/16612/30

interfacial shear strength, τ, another model parameter. Assuming some reasonable value for τ, the fiber strength, σ_{F1}*, is substituted into equation (4-22) and $\ell c/2$ computed. Excluding these ineffective fiber ends as potential fracture sites, the computer selects a random number which determines the first fiber break location. The resulting two fragments are now stronger than the initial fiber for two reasons: (1) probabilistically they are stronger because of their reduced length and (2) both fragments have essentially been proof tested to the stress level σ_{F1}* (they are at least this strong). A new fragment breaking stress can now be computed which takes into account both strengthening mechanisms. The probabilistic strength increase is based on the length of the longer of the two fragments. The fragment strength equation, as shown in Appendix B, assumes different forms depending on the value of the proof testing stress, σ_{Fi}* and its relation to the fiber model parameters. The general form of this equation is

$$\sigma_{Fi}^* = F(Li, \sigma_{Fi-1}, \sigma_a, \sigma_b, \sigma_c, \sigma_o, m, P) \qquad (4\text{-}23)$$

where

σ_{Fi}* = current fragment breaking stress

Li = length of longest surviving fragment

σ_{Fi-1}* = stress level at which previous break took place (i.e., proof testing stress)

The new fragment breaking stress σ_{F2}* is computed from equation (4-23) and substituted into equation (4-22) (keeping τ constant) to determine a new and somewhat longer critical transfer length. These ineffective, unbreakable regions are subtracted from each fragment end and a new random number is generated. This time, however, the random number is weighted such that the longer fragment is given a higher probability of fracturing but nevertheless a finite probability exists that the smaller fragment breaks. In Figure 24 fragmentation now produces three fibers. The longest is again evaluated and its strength, σ_{F3}*, is determined from equation (4-23) where the proof testing stress is now σ_{F2}*. On calculation of the new (longer) critical transfer length, it is observed (Figure 24) that the middle fragment is now shorter than the current critical fiber length and, therefore, by definition can undergo no further fragmentation. It is essentially decoupled from the system. Stochastic fragmentation continues until, eventually, all fibers are shorter than the current critical fiber length. At this point, fragmentation ceases and the program counts the total number of fiber fragments, assessing whether this constitutes enough for statistical analysis. If not, the process is initiated on a new three inch fiber with the model parameters σ_a, σ_b, σ_c, σ_o, m, P, and τ unchanged. Fragments are accumulated until a theoretical fragment

Union Carbide trial exhibit UC-1507: W. A. Fraser, Micromechanical Characterization of Surface Treated Reinforci... Published by AsbestosClaims.Law
ACL Doc 16612 · Page 31 of 88 asbestosclaims.law/library/16612/31

length or ℓ/d distribution is adequately defined (usually 150 or 200 fragments).

The fundamental characteristics of the theoretical fragmentation model can be demonstrated by several examples. Consider, first, the fragmentation behavior of a flaw free fiber, i.e., one which exhibits a strength independent of length. In terms of our statistical fiber strength model, this implies that σ_a, σ_b, and P = O (i.e., no flawed elements) and as discussed in section 4.1.2, that the Weibull shape parameter, m, is very large. With σ_c = O and m = 100, the fiber breaking strength becomes σ_o (assumed in this case to be 500,000 psi). The slight negative slope of the strength-length curve shown in Figure 25 is a consequence of assuming a finite value for m. These flaw free fiber parameters were substituted into the stochastic fragmentation model to generate theoretical fragment ℓ/d distribution curves at several levels of τ. Figure 26 shows smoothed cumulative ℓ/d curves for interfacial shear strength values of 300, 500, and 700 psi. As the interfacial shear strength is increased, the distribution curves, as expected, shift left to lower aspect ratios. In addition, note that the bounds on these distributions, as predicted from the simple critical fiber length concept, are in a 2:1 ratio. Now consider a flawed fiber exhibiting a mean strength significantly dependent on length and characterized by the model parameters listed in Figure 27. Substituting these values into the stochastic fragmentation model and assuming an interfacial shear strength of 1000 psi resulted in the cumulative fragment length distribution curve of Figure 28a. Smoothing and differentiating, these points numerically gave the associated frequency curve (Figure 28b). Note the considerable dispersion in this distribution, i.e., the bounds are in a 4:1 ratio in contrast to the 2:1 of Figure 26.

Introduction of the concept of a length dependent fiber strength into the stochastic fragmentation model, explains the dispersion observed in measured fragment ℓ/d distribution curves. The next step in the analysis procedure involves the reverse process of using these experimentally determined ℓ/d distribution curves back out values for the interfacial shear strength, τ, and the statistical fiber strength parameters which define a characteristic strength-length function for a given fiber/treatment system. The analysis thus provides, simultaneously, the specific adhesion promoting and fiber protection capabilities (coupling and sizing agent effects) of a particular fiber treatment formulation.

4.4 Parameter Estimation Procedure

The parameter estimation procedure is essentially one of constrained nonlinear optimization. The constraints imposed

Union Carbide trial exhibit UC-1507: W. A. Fraser, Micromechanical Characterization of Surface Treated Reinforci... Published by AsbestosClaims.Law
ACL Doc 16612 · Page 32 of 88 asbestosclaims.law/library/16612/32

on the values of the independent search variables arise from physical considerations of brittle fiber tensile test results and from restrictions implicit in the mathematical formulation of the statistical strength model. The nonlinearity of the problem is obvious.

4.4.1 Objective Function and Search Method

The first step in the estimation process required defining an objective function which measures the goodness of fit between the experimentally determined ℓ/d distribution and that generated theoretically. The function which was devloped operates on the cumulative distribution curves, the smoothed form in the case of the data and the raw curve of the theoretical model. Numerical smoothing of the theoretical points was not done in order to reduce computation time. Each curve was broken into twenty equally spaced cumulative cells and an average fragment ℓ/d value computed for each cell. The objective function was defined as the sum of the squares of the deviations in mean ℓ/d values between correspoinding cells. Cells at the extremes (tails) of the distributions could be excluded, if desired, in cases where the data in these regions was of questionable accuracy.

Function minimization was accomplished using the Nelder-Mead simplex algorithm[36]. As McMaster [37] points out, comparative studies indicate that this direct search method is the most effective algorithm not requiring derivative evaluation for finding the minimum of a function of several variables. Gradient techniques requiring numerical evaluation of derivatives were not used because of the difficulty in obtaining accurate gradient estimates in systems subject to stochastic fluctuation such as this one.

The simplex algorithm, while always convergent to a local optimum if the convergence criterion is strict enough, suffers a serious deficiency (as do other existing algorithms) in that this optimum may or may not be the global optimum. This search code seeks an optimum which, unfortunately, is a strong function of the initial starting point. To obtain a so called, "best" optimum (not necessarily the global optimum) a coarse grid presearch, as recommended by McMaster[37], was incorporated into the algorithm. By using large initial step sizes in defining the simplex of independent variables, one may simulate the preferred but inefficient case of starting a search from many different initial points.

4.4.2 Parameter Constraints

The use of most optimization codes requires that the independent variables be free to move from $-\infty$ to $+\infty$. As stated

Union Carbide trial exhibit UC-1507: W. A. Fraser, Micromechanical Characterization of Surface Treated Reinforci... Published by AsbestosClaims.Law
ACL Doc 16612 · Page 33 of 88 asbestosclaims.law/library/16612/33

previously, however, a number of physical, intuitive, and mathematical constraints on the model parameters distinguish between feasible and non-feasible regions in vector space. These variable restrictions can be expressed as inequality constraints of the form

$$\ell \leq x_i \leq u \tag{4-24}$$

where ℓ = a lower bound on the variable x_i

u = an upper bound on x_i

Constrained search variables can be transformed into unconstrained variables before the search is carried out. A trigonometric transformation originally suggested by Box[38] and found by McMaster[35] to be highly efficient in handling boundary constraints is given by

$$x_i = \ell + (u-\ell) \sin^2 Y_i \tag{4-25}$$

The constrained optimization is performed in the variable Y_i. This transformation is fairly linear near the constraint boundaries and, therefore, eliminates the simplex step size problems characteristic of certain other transformation forms on approaching this region.

The parameters which must be determined include the six variables which define the fiber strength characteristics σ_a, σ_b, σ_c, σ_o, m, and P (sizing agent performance) and the interfacial shear strength τ (coupling agent performance). Since, in essence, it is the quotient of fiber strength and interfacial shear strength which determines the location of experimental σ/d distribution curves, some fundamental information is required if meaningful, unconfounded performance evaluations are to be achieved. This information may be, for example, a knowledge of the mean fiber strength, $\langle\sigma\rangle$, at two different gage lengths as determined experimentally from single filament testing. One of these lengths, L1, is three inches, the length of the initial unfragmented fiber. Substituting the mean strength values and their associated fiber lengths (i.e., number of fiber elements or links) into equation (4-20) defines two equality constraints of the form

$$F_{L1}(\langle\sigma\rangle_1, \sigma_a, \sigma_b, \sigma_c, \sigma_o, m, P) = 0 \tag{4-26}$$

$$F_{L2}(\langle\sigma\rangle_2, \sigma_a, \sigma_b, \sigma_c, \sigma_o, m, P) = 0 \tag{4-27}$$

where $\langle\sigma\rangle_1$ and $\langle\sigma\rangle_2$ are the experimentally determined mean

Union Carbide trial exhibit UC-1507: W. A. Fraser, Micromechanical Characterization of Surface Treated Reinforci... Published by AsbestosClaims.Law
ACL Doc 16612 · Page 34 of 88 asbestosclaims.law/library/16612/34

strength values at gage lengths L1 and L2, respectively. These constraints force the computed fiber strength-length curve to pass through the experimental points and on rearrangement can be used to reduce the number of search variables by two.

In addition to the equality constraints defined by equations (4-26) and (4-27), several inequality constraints also restrict the values available to certain statistical strength parameters. From physical intuition, σ_a, the lower bound on the severely flawed link strength must be some value greater than zero. Fibers of near zero tensile strength will not be realized because of the unconscious proof testing which accompanies sample preparation. These fibers are eliminated simply because they cannot be prepared for testing. This lower stress limit was somewhat arbitrarily assumed to be 10,000 psi which corresponds to a working tensile load of the order of 1 gram for a typical 0.6 mil diameter fiber. This value may be further justified in fiberglass evaluations because it is generally considered to represent the strength of bulk ($\sim$ infinite size) plate glass. From Figure 21 it is observed that the upper bound on σ_a, is σ_b, however, a more critical constraint is $\sigma_a \leq \langle\sigma\rangle_1$. Thus from equation (4-25)

$$\sigma_a = 10^4 + (\langle\sigma\rangle_1 - 10^4) \sin^2 Y_1 \qquad (4\text{-}28)$$

The Weibull distribution shape parameter, m, was constrained between 1.0 and 50.0

$$m = 1.0 + 49.0 \sin^2 Y_2 \qquad (4\text{-}29)$$

The inequality constraint on σ_b is expressed as $\sigma_a \leq \sigma_b \leq \sigma_c$ and the upper bound on σ_c is σ_o, thus

$$\sigma_b = \sigma_a + (\sigma_c - \sigma_a) \sin^2 Y_3 \qquad (4\text{-}30)$$

and

$$\sigma_c = \sigma_b + (\sigma_o - \sigma_b) \sin^2 Y_4 \qquad (4\text{-}31)$$

Equations (4-26) and (4-27) can now be used to solve for P and σ_o, respectively.

$$P = E_{L1}(\langle\sigma\rangle_1, \sigma_a, \sigma_b, \sigma_c, \sigma_o, m) \qquad (4\text{-}32)$$

$$\sigma_o = E_{L2}(\langle\sigma\rangle_2, \sigma_a, \sigma_b, \sigma_c, m, P) \qquad (4\text{-}33)$$

Union Carbide trial exhibit UC-1507: W. A. Fraser, Micromechanical Characterization of Surface Treated Reinforci... Published by AsbestosClaims.Law
ACL Doc 16612 · Page 35 of 88 asbestosclaims.law/library/16612/35

On evaluation of expressions (4-28) and (4-29), equations (4-30) - (4-33) constitute four equations in four unknowns. Since equations (4-32) and (4-33) have nonlinear forms, the set was solved by an iterative process.

The interfacial shear strength, τ, is bounded by zero (no adhesion) and τ_{max}, the shear strength of the polymer itself (optimum adhesion),

$$\tau = \tau_{max} \sin^2 Y_5 \qquad (4\text{-}34)$$

The Nelder-Mead simplex algorithm operates on the unconstrained, five dimensional vector $\underline{y}$. Listings of the everall analysis programs are given in Appendix F.

It is recognized that while the parameter constraints impose severe restrictions on permissible parameter values, the search algorithm is still susceptible to converging to a local optimum. Furthermore, the absolute parameter values which are computed, even if optimal, may not define a unique solution. Experience indicates, however, that the characteristic strength-length curve which they define is unique for a given set of fragment ℓ/d data.

4.5 Data Analysis

Two sets of smoothed cumulative ℓ/d data (OCF 885 in polypropylene and OCF 885 in nylon 6) were processed by the preceding analysis scheme. The fiber strength constraints were determined by tensile testing single filaments of OCF 885 at gage lengths of 1.0 and 3.0 inches. Approximately 100 breaks were made at each gage length with each load value normalized in terms of stress by measuring specific individual filament diameters after rupture. Mean fiber breaking stresses were evaluated and used as the constraints expressed in equations (4-26) and (4-27).

Figure 29 shows the results of an optimization run performed on OCF 885 - polypropylene fragment ℓ/d data. Both the experimental and optimized theoretical, smoothed cumulative ℓ/d distribution curves are plotted. The agreement is observed to be quite good over the major portion of the distribution with the deviation in the lower extremum attributable, in part, to data inaccuracies (i.e., only a few data points characterize this region). The optimized interfacial shear strength, 1200 psi, is about 46% of the von Mises' shear strength value for polyprolylene, 2600 psi (i.e., tensile yield strength/$\sqrt{3}$), thus the general purpose surface treatment of OCF 885 is apparently not optimal for polypropylene. The fiber strength-length curve generated from this optimization is shown in Figure 30. The

crosses represent experimental, mean fiber strength values determined by single filament tensile testing. The computed mean strength-length curve is observed to pass through the constrained points at 1.0 and 3.0 inches and to approximate, reasonably well, the strength-length behavior at other gage lengths.

Figure 31 shows the experimental and optimized theoretical ℓ/d distributions for OCF 885 in nylon 6. 1.0 and 3.0 inch tensile test data was again used as parameter constraints in this optimization. The agreement between the experimental and theoretical curves is, again, quite good over the central portion of the distribution. The optimized interfacial shear strength, 4130 psi, is about 60% of the von Mises' shear strength value for nylon 6, 6800 psi, indicating that the general purpose size of OCF 885 is somewhat better for nylon 6 than for polypropylene. There is, however, still room for improvement. The strength-length curve generated from this analysis and shown in Figure 32 is observed to pass through the 1.0 and 3.0 gage length strength values and to approximate, quite well, the shorter gage length strength-length behavior.

In analyzing OCF 885 fragmentation data in two different resin matrix systems, the stochastic fiber fragmentation model is seen to be quite successful in simulating the experimental data. Furthermore, the back calculated strength-length curve computed for OCF 885 was found to be essentially independent of the resin in which the fiber was embedded. This was a critical test in assessing the validity of the analysis scheme. The dispersity of experimental fragment ℓ/d distribution curves is, thus, truly characteristic of the degree of damage inherent in a given fiber and can, via this analysis procedure, be translated into a more readily interpretable and useful form, i.e., a mean fiber strength-length curve.

5. CONCLUSIONS

- The embedded single filament test is highly sensitive to specific fiber/matrix interactions (coupling agent effect).
- The dispersity of the fiber fragmentation distributions is characteristic of the damage level of the fiber and thereby of the protection afforded by the fiber treatment (sizing agent effect).
- The strength/length dependency of fiberglass, within the range of observed fragment lengths, is accurately described by a mixed element, weakest link fiber strength model.

Union Carbide trial exhibit UC-1507: W. A. Fraser, Micromechanical Characterization of Surface Treated Reinforci... Published by AsbestosClaims.Law
ACL Doc 16612 · Page 37 of 88 asbestosclaims.law/library/16612/37

- A stochastic model of the embedded fiber fracture sequence using the above fiber strength model simulates observed trends in fiber fragment distributions.

- Computer analysis of fiber fragment data in terms of the above models result in reasonable interfacial shear strength values for the individual fiber/polymer systems.

- The computed fiber strength/length relations are in good agreement with independently determined glass fiber strength data. Furthermore, the computed strength/length curve is independent of the matrix resin in which the fiber is embedded.

- The embedded single filament technique and associated analysis is valuable in elucidating the principal coupling the sizing effects of fiber surface treatments. This is of particular value in the optimization of commercial fiber treatment formulations.

ACKNOWLEDGEMENTS

The author wishes to express his appreciation to Mr. John Stenstrom for his efforts in conducting much of the experimental work and to Mr. Gideon Salee of the University of Connecticut for performing the single filament tensile tests. Thanks is also extended to Professor A. T. DiBenedetto (Univ. of Conn.) and Mr. Fred H. Ancker for their assistance and contributions concerning the theoretical aspects of this project.

W. A. Fraser

W. A. Fraser

WAF:PLK

Attachments: References
Tables
Appendices

REFERENCES

1. Fraser, W. A. and Ancker, F. H., "A Computer Modeled Single Filament Technique for Measuring Coupling and Sizing Agent Effects in Fiber Reinforced Composites," Project Report File #4208, November 11, 1974.

2. McCullough, R. L., "Concepts of Fiber Resin Composites," Marcel Dekker, Inc., New York, (1971).

3. Corten, Herbert T., in "Modern Composite Materials," Broutman, Lawrence J. and Krock, Richard H., Editors, Addison-Wesley, Inc., Reading, Massachusetts, (1967).

4. Parratt, N. J., "Defects in Glass Fibers and Their Effect on the Strength of Plastic Mouldings," Rubber and Plastics Age, Vol. 41, p. 263, (1960).

5. Riley, V. R. and Reddaway, J. L., "Tensile Strength and Failure Mechanics of Fiber Composites," J. Mat. Sci., Vol. 3, p.41 (1968).

6. Hale, D. K. and Kelly, A., Strength of Fibrous Composite Materials in Annual Review of Materials Science, Vol. 2, Huggins, R. A., ed., Annual Reviews, Inc., Palo Alto, Calif. (1972).

7. Rosen, B. W., "Tensile Failure of Fibrous Composites," AIAA J., Vol. 2, No. 11, p. 1985-1991, (1964).

8. Cooper, G. A., "The Fracture Toughness of Composites Reinforced with Weakened Fibers," J. Mat. Sci., Vol. 5, p. 645-654, (1970).

9. Cox, H. L., "The Elasticity and Strength of Paper and Other Fibrous Materials," Brit. J. Appl. Phys., Vol. 3, p. 72, (1952).

10. Dow, N. F., "Study of Stresses Near a Discontinuity in a Filament Reinforced Composite Metal," General Electric Report TIS R635D61, AD-414673 (1963).

11. Kelly, A. and Tyson, W. R., "Tensile Properties of Fiber Reinforced Metals: Copper/Tungsten and Copper/Molybdenum," J. Mech. Phys. Solids, Vol. 13, p. 329 (1965).

12. Ongchin, L., Olender, W. K., and Ancker, F. H., "Fiber/Matrix Adhesion and the Fracture Behavior of Glass Reinforced High Density Polyethylene," Proc. 27th Conf. SPI Reinforced Plastics Division, February, 1972, Sect. 11-A.

Union Carbide trial exhibit UC-1507: W. A. Fraser, Micromechanical Characterization of Surface Treated Reinforci... Published by AsbestosClaims.Law
ACL Doc 16612 · Page 39 of 88 asbestosclaims.law/library/16612/39

13. Burns, R., Hankin, A. G., and Johnson, A. E., "Glass Fiber Reinforcement of Polyamide Polymers," Proc. 29th Conf. SPI Reinforced Plastics Division, February, 1974, Sect. 20-A.

14. Kelly, A., "The Strengthening of Metals by Dispersed Particles," Proc. Roy Soc. (London) A282, p. 63-79, (1964).

15. Wadsworth, N. J. and Spilling, I., "Load Transfer From Broken Fibers in Composite Materials," Brit. J. Appl. Phys., (J. Phys. D.) Ser 2, Vol. 1, p. 1049-1058, (1968).

16. Brady, W. C., Tiede, R. L., and Veagie, F. M., "Glass Fiber Manufacturing Process Development," AFML-TR-68-361, Dec., 1968.

17. Hershey, Harry C., Zakin, Jacques L., and Simha, Robert, "Numerical Differentiation of Equally Spaced and Not Equally Spaced Experimental Data," I & EC Fund., Vol. 6, No. 3, p. 413-421, (1967).

18. Parma Standard Test Method - PSM 101, "Gravimetric Determination of Resin Content in Resin-Graphite Composite Materials," Revised 4/26/73.

19. Freudenthal, Alfred M., "Statistical Approach to Brittle Fracture," in Fracture, Vol. II, Ed. H. Liebowitz, New York, Academic Press, (1968).

20. Pierce, F. T., "Tensile Tests for Cotton Yarns Part V: The Weakest Link," J. Text. Inst., Vol. 17, p. 355 (1926).

21. Tippet, L. H. C., "On the Extreme Individuals and the Range of Samples Taken From a Normal Population," Biometrika, Vol. 17, p. 364 (1925).

22. Fisher, R. A. and Tippet, L. H. C., Proc. Cambridge Phil Soc. Vol. 24, p. 180, (1928).

23. Frechet, M., Ann. Soc. Polon. Mat. Cracow, Vol. 6, p. 93, (1927).

24. Kontorova, T. A., "A Statistical Theory of the Brittle Strength of Real Crystals," J. Tech. Phys. (USSR), Vol. 10, p. 886, (1940).

25. Chechulin, B. B., "Statistical Theory of Brittle Strength," Zhm. Tekh. Fiz., Vol. 24, p. 292, (1954).

26. Weibull, W., "A Statistical Theory of the Strength of Materials," Proc. Roy. Swedish Inst. Engr. Res., Ing. Vetenskaps Acad. Handl Vol. 151, (1939).

Union Carbide trial exhibit UC-1507: W. A. Fraser, Micromechanical Characterization of Surface Treated Reinforci... Published by AsbestosClaims.Law
ACL Doc 16612 · Page 40 of 88 asbestosclaims.law/library/16612/40

27. Weibull, W., "A Statistical Distribution Function of Wide Applicability," J. Appl. Mech., Vol. 18, p. 293, (1951).

28. Irwin, G. R., "Relatively Unexplored Aspects of Fracture Mechanics," Univ. of Illinois, TAM Report No. 240, Sect. V., Feb., 1963.

29. Prevorsek, Dusan, Lyons, James, and Whitwell, J.C., "Statistical Treatment of Data and Extreme Value Theory in Relation to Fatigue in Textiles," Text. Res. J., Vol. 33, p. 963-973, (1963).

30. Barella, A., "On Certain Applications of Weibull's Distribution to Fatigue Phenomena in Yarns," Text. Res. J., Vol. 35, p. 1051-3, (1965).

31. Steiger, F. H., "Practical Applications of the Weibull Distribution Function," Chem. Technol. Vol. 1, p. 225-231, (1971).

32. Wallhaus, R. A., "A Statistical Study of the Factors Influencing the Strength of Glass Fibers," TAM Report No. 217, May, 1962, Dept. of Theoretical and Appl. Mech., Univ. of Illinois.

33. Kies, J. A., "The Strength of Glass," NRL Report 5908, Naval Res. Lab., Washington, D. C., April 3, 1958.

34. Metcalfe, A. and Schmitz, G. K., "Effect of Length on the Strength of Glass Fibers," ASTM, Vol. 64, p. 1075-1093, (1964).

35. Rosen, B. W., "Mechanics of Composite Strengthening in Fiber Composite Materials," ASM, Metals Park, Ohio, (1965).

36. Nelder, J. A. and Mead, R., "A Simplex Method for Function Minimization," Computer J., Vol. 7, p. 308, (1965).

37. McMaster, L. P., "Modifications of the Optimization Algorithm and the Integration Procedure for the Mathematical Models of the Styrene Reactors," UCC R&D Report, File No. 2775, March 30, 1971.

38. Box, M. J., "A Comparison of Several Current Optimization Methods and the Use of Transformations in Constrained Problems," Computer J., Vol. 9, p. 67, (1966).

39. Knox, L. J., "Studies of Breaking Stress Distributions of Viscose Filaments," Ph.D. Thesis, Dept. of Chem. Eng. Princeton University, 1970.

40. Abramowitz, M., Stegun, I. A., ed. "Handbook of Mathematical Functions," N.B.S. Applied Mathematics, Series 55, (1964).

Union Carbide trial exhibit UC-1507: W. A. Fraser, Micromechanical Characterization of Surface Treated Reinforci... Published by AsbestosClaims.Law
ACL Doc 16612 · Page 41 of 88 asbestosclaims.law/library/16612/41

TABLE I

COMPONENTS OF A TYPICAL GLASS TREATMENT FORMULATION

Coupling Agent - Promotes fiber/matrix adhesion

Sizing System

Film Former - Usually applied as an aqueous emulsion, protects filaments from damage and gives some integrity to the bundles of individual glass filaments, gives a stable forming package (a fiber cake)

Lubricant - Lubricates filaments while being drawn and aids passage over guide points.

Antistat - Prevents build-up of static charges due to friction in winding

Micellaneous -

TABLE II

FIBERGLASS DESCRIPTIONS

DESIGNATION	OCF 885	OCF 415
Glass Type	E Roving	E Roving
Treatment		
Coupling Agent	UCC A-1100	Amine Reactive
Sizing System	PVA_C + Lubricants	
Treatment Loading	1.6 Wt. %	0.7 Wt. %
Mean Fiber Diameter (50 Filaments)	0.58 mils	0.59 mils
Tensile Modulus	10.5×10^6 psi	10.5×10^6 psi

Union Carbide trial exhibit UC-1507: W. A. Fraser, Micromechanical Characterization of Surface Treated Reinforci...
Published by AsbestosClaims.Law
ACL Doc 16612 · Page 42 of 88
asbestosclaims.law/library/16612/42

TABLE III

PROPERTIES OF THORNEL 300

(Grade WYP 30 1/0)

No. of Filaments	2000
Filament Diameter	0.3 mils
Density	1.70 g/cc
Strand Tensile Strength	325 kpsi
Young's Modulus	34 mpsi

TABLE IV

PROPERTIES OF CARBON PRODUCTS' PITCH BASED, CONTINUOUS FILAMENT GRAPHITE

Experimental Yarn (280-22-9) - untreated.

No. of Filaments	120
Filament Diameter	0.43 mils
Density	2.08 g/cc
Strand Tensile Strength	226 kpsi
Young's Modulus	40 mpsi

Union Carbide trial exhibit UC-1507: W. A. Fraser, Micromechanical Characterization of Surface Treated Reinforci... Published by AsbestosClaims.Law
ACL Doc 16612 · Page 43 of 88 asbestosclaims.law/library/16612/43

TABLE V

MATRIX RESIN PROPERTIES

MATERIAL	NYLON 6 (DRY)	POLYPROPYLENE	HDPE
Density	1.13	0.905	0.962
Tensile Yield Strength	11,800 psi	4,450 psi	4,000 psi
Elongation at Yield	10%	15%	15%
Secant Modulus	380,000 psi	200,000 psi	150,000 psi

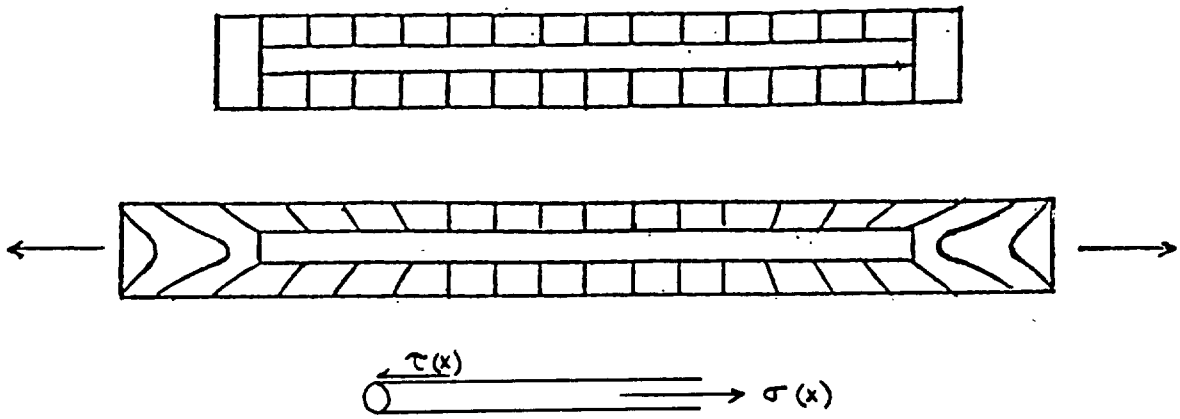


FIGURE 1: Stress Transfer to a Uniaxially Loaded Fiber in a Matrix

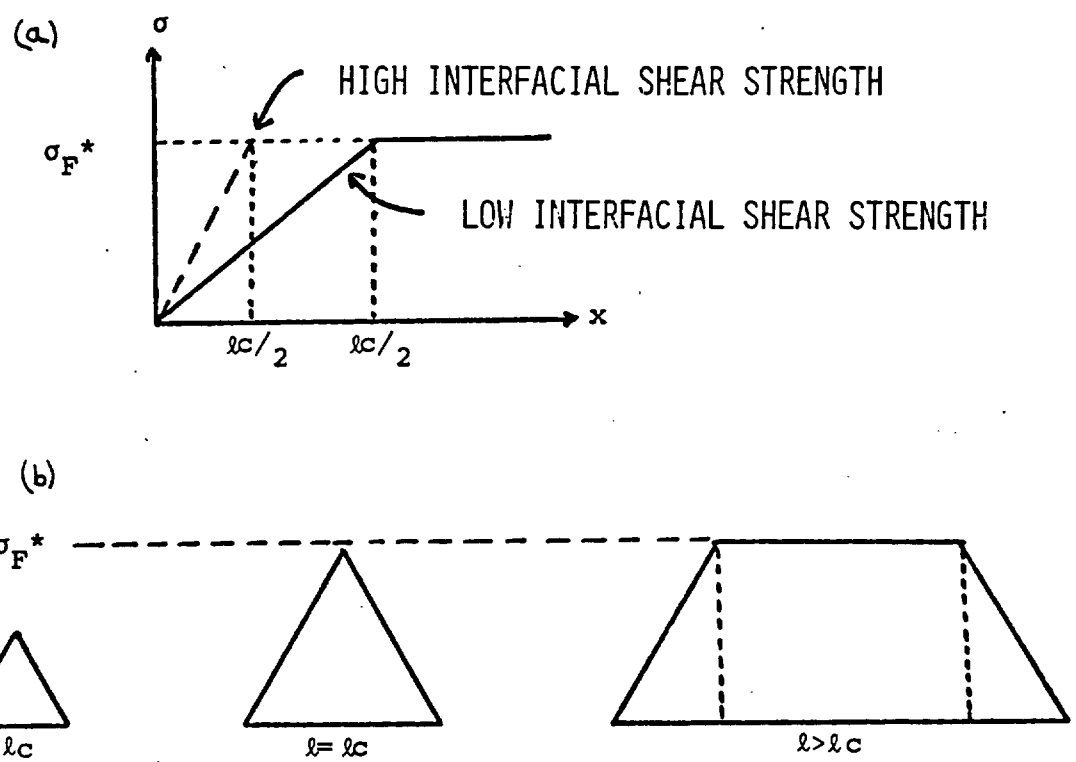


FIGURE 2: (a) Critical Transfer Length-Length Required to Build the Stress up to a Level to Break the Fiber. (b) Critical Fiber Length-Minimum Length of Fiber Capable of Reaching its Breaking Strength

Union Carbide trial exhibit UC-1507: W. A. Fraser, Micromechanical Characterization of Surface Treated Reinforci...
Published by AsbestosClaims.Law
ACL Doc 16612 · Page 45 of 88
asbestosclaims.law/library/16612/45

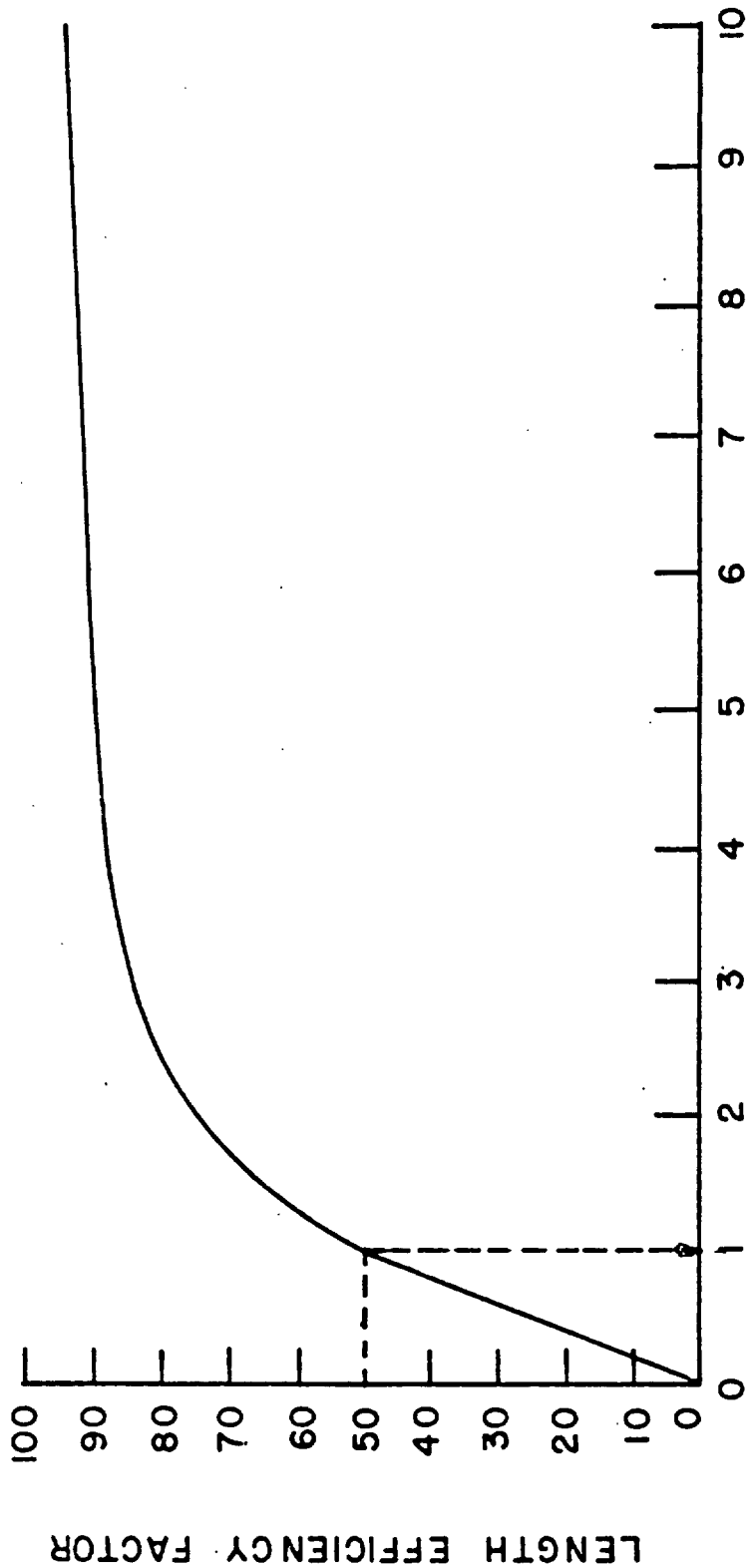


FIGURE 3: Fiber Length Efficiency Factor

FIBER FRAGMENTATION

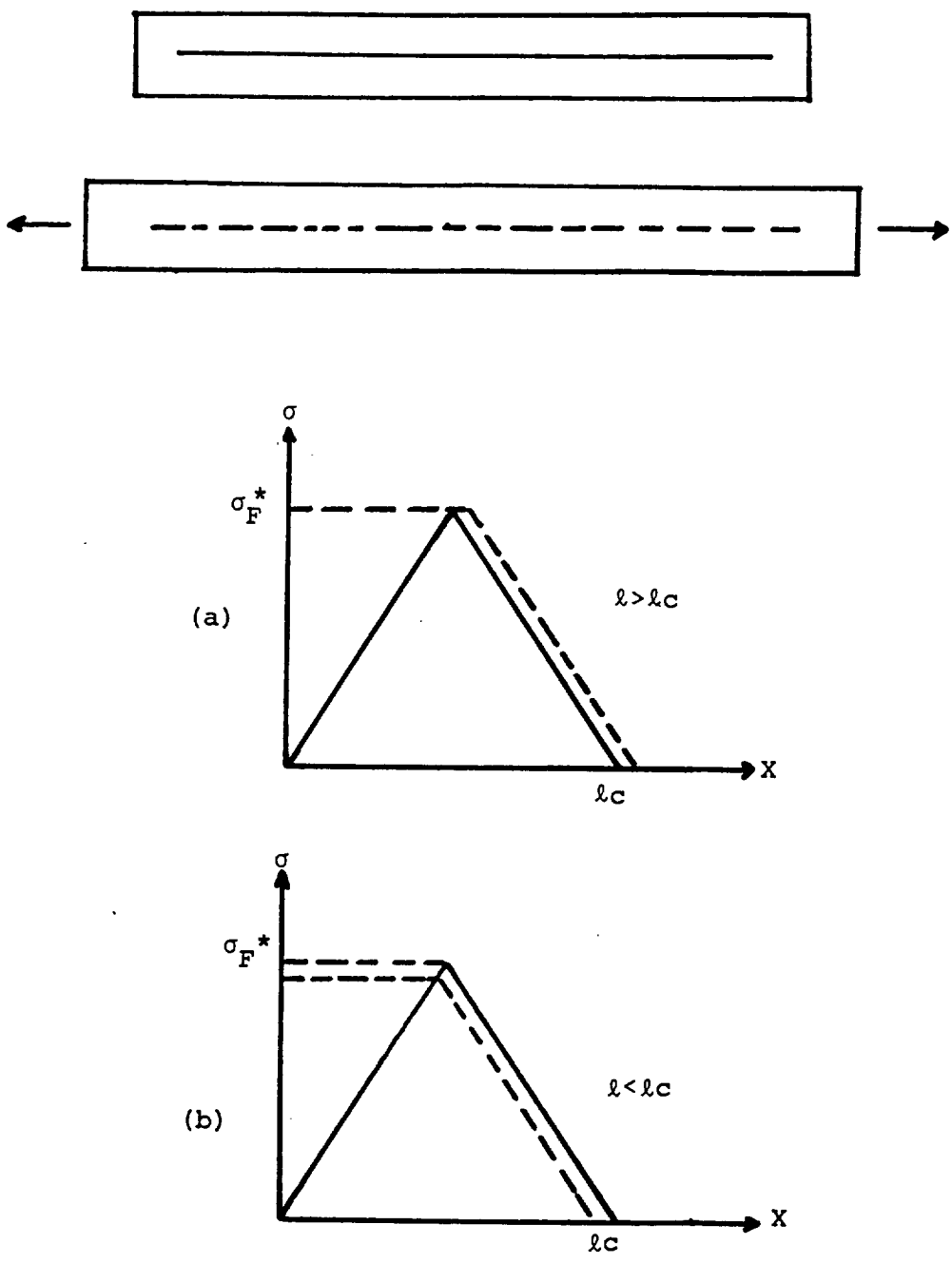


FIGURE 4: Multiple Fiber Fracture (a) Generating Shortest Fragments ∿ℓc/2 (b) Generating Longest Fragments ∿ℓc

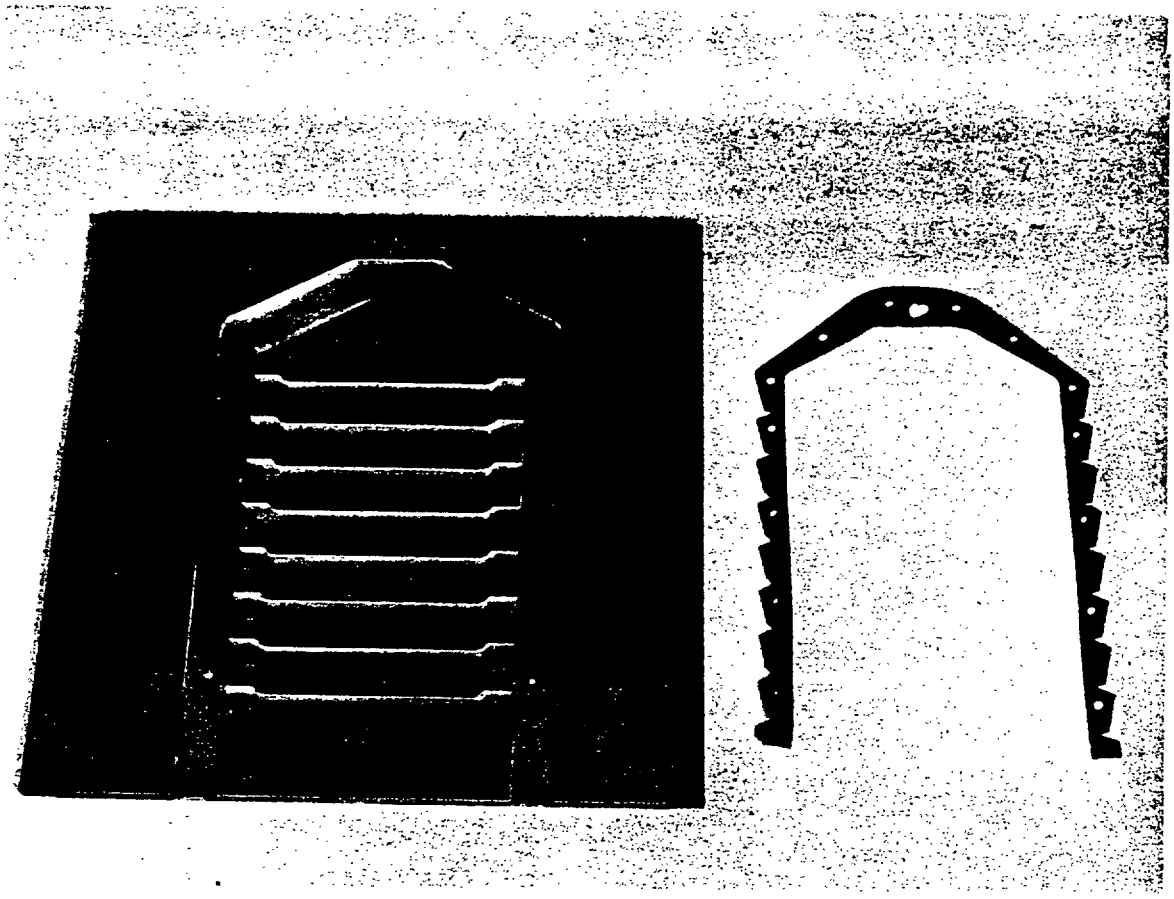


FIGURE 5: Compression Mold and Fiber Fork for Molding Single Filament Embedded Tensile Specimens

Published by AsbestosClaims.Law
asbestosclaims.law/library/16612/48

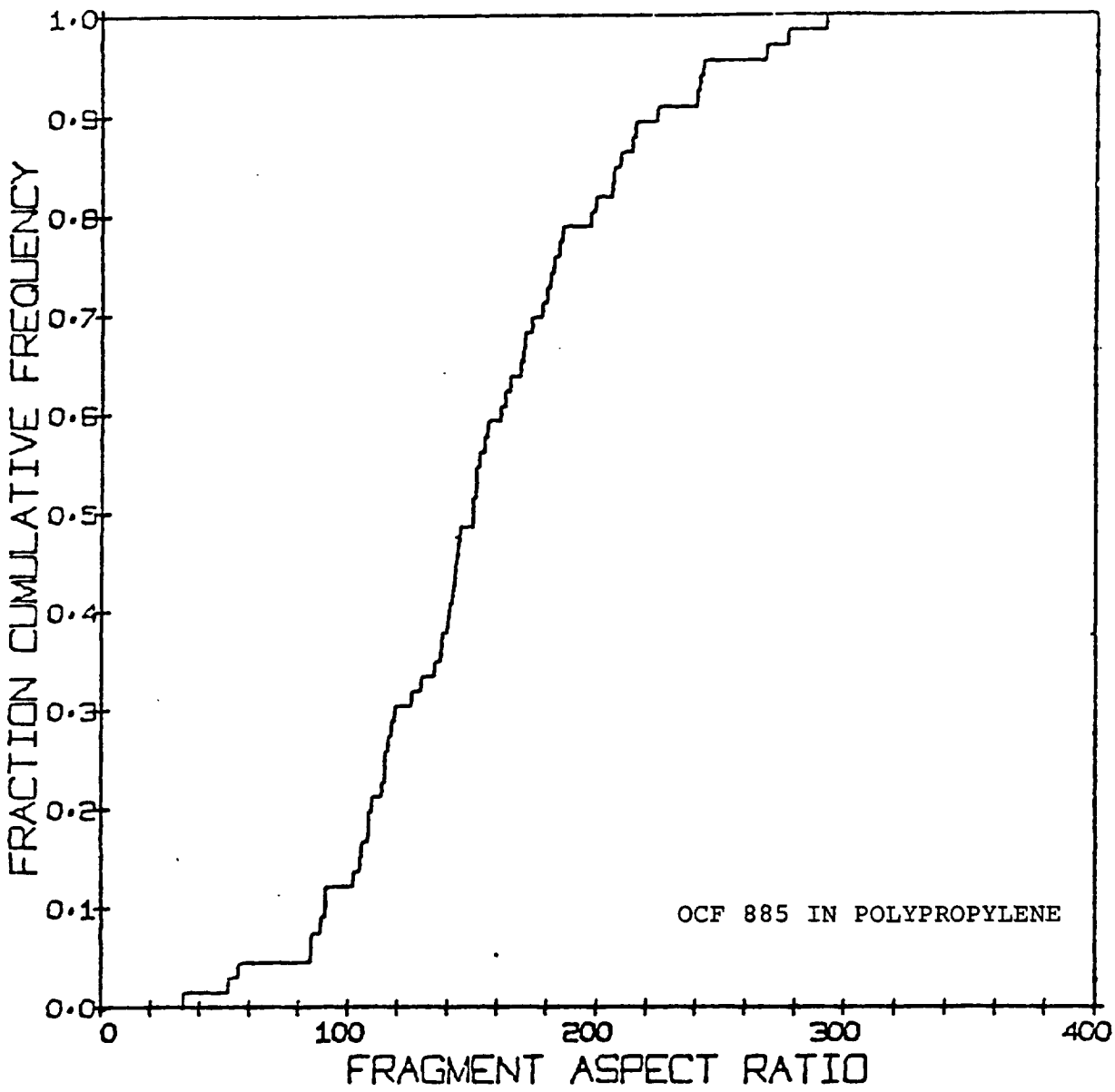


FIGURE 6a: Fragment ℓ/d Cumulative Distribution (OCF 885 in Polypropylene)-Raw Data

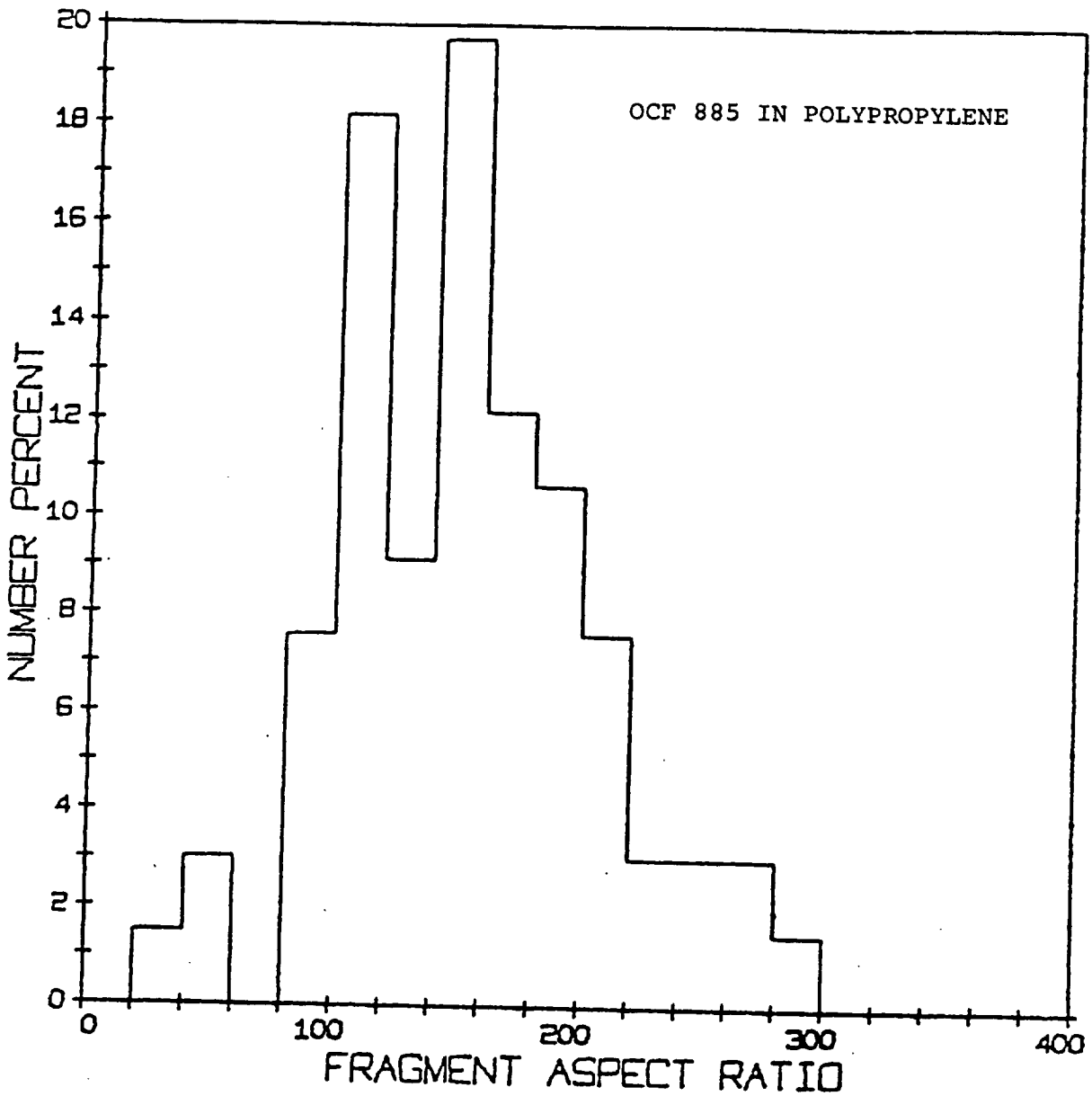


FIGURE 6b: Fragment ℓ/d Histogram (OCF 885 in Polypropylene)

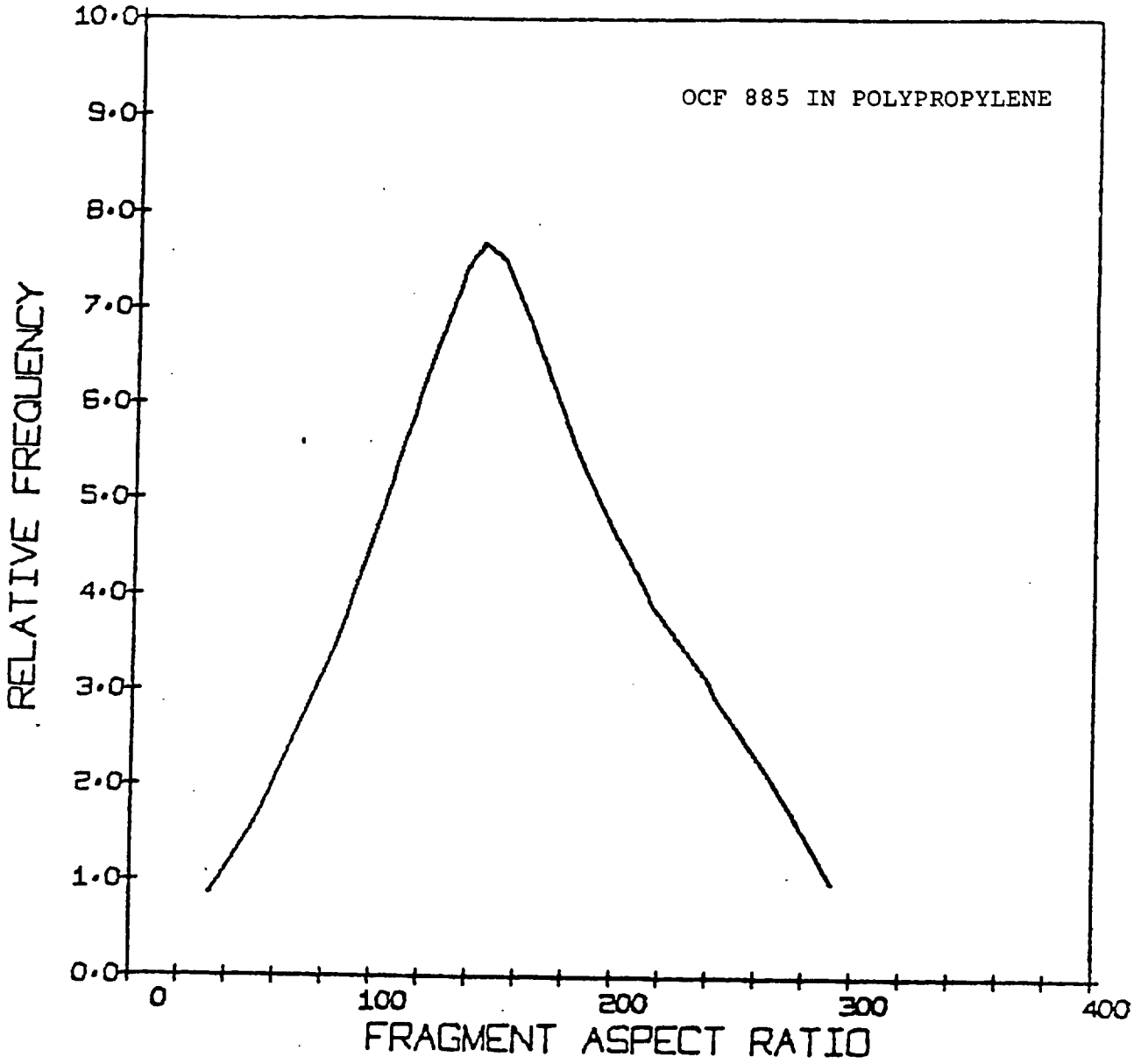


FIGURE 6c: Numerically Smoothed Fragment ℓ/d Frequency Curve (OCF 885 in Polypropylene)

Published by AsbestosClaims.Law
asbestosclaims.law/library/16612/51

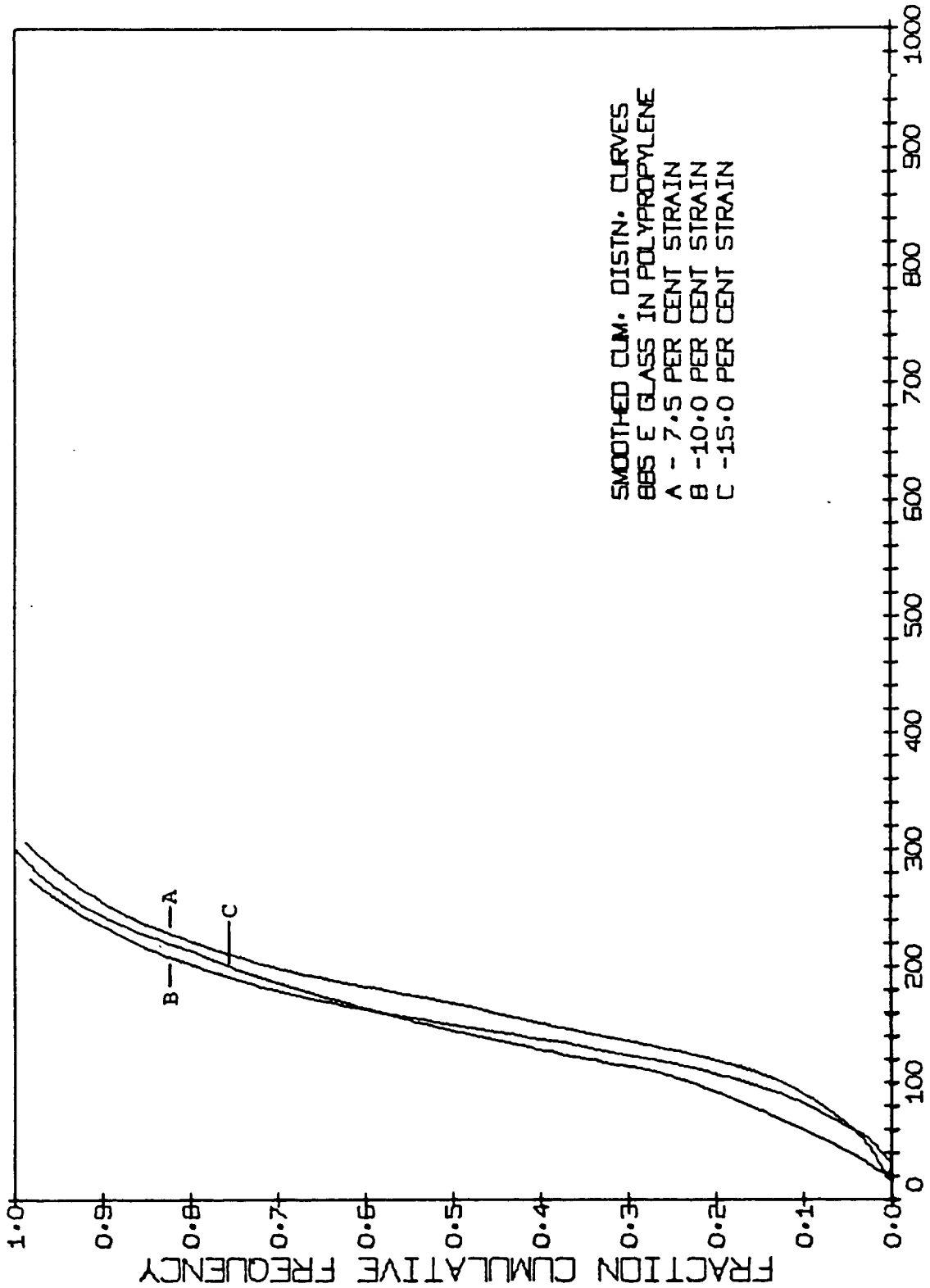


FIGURE 7: Effect of Total Specimen Strain on Experimental ℓ/d Distribution Curves (OCF 885 in Polypropylene)

Published by AsbestosClaims.Law
asbestosclaims.law/library/16612/52

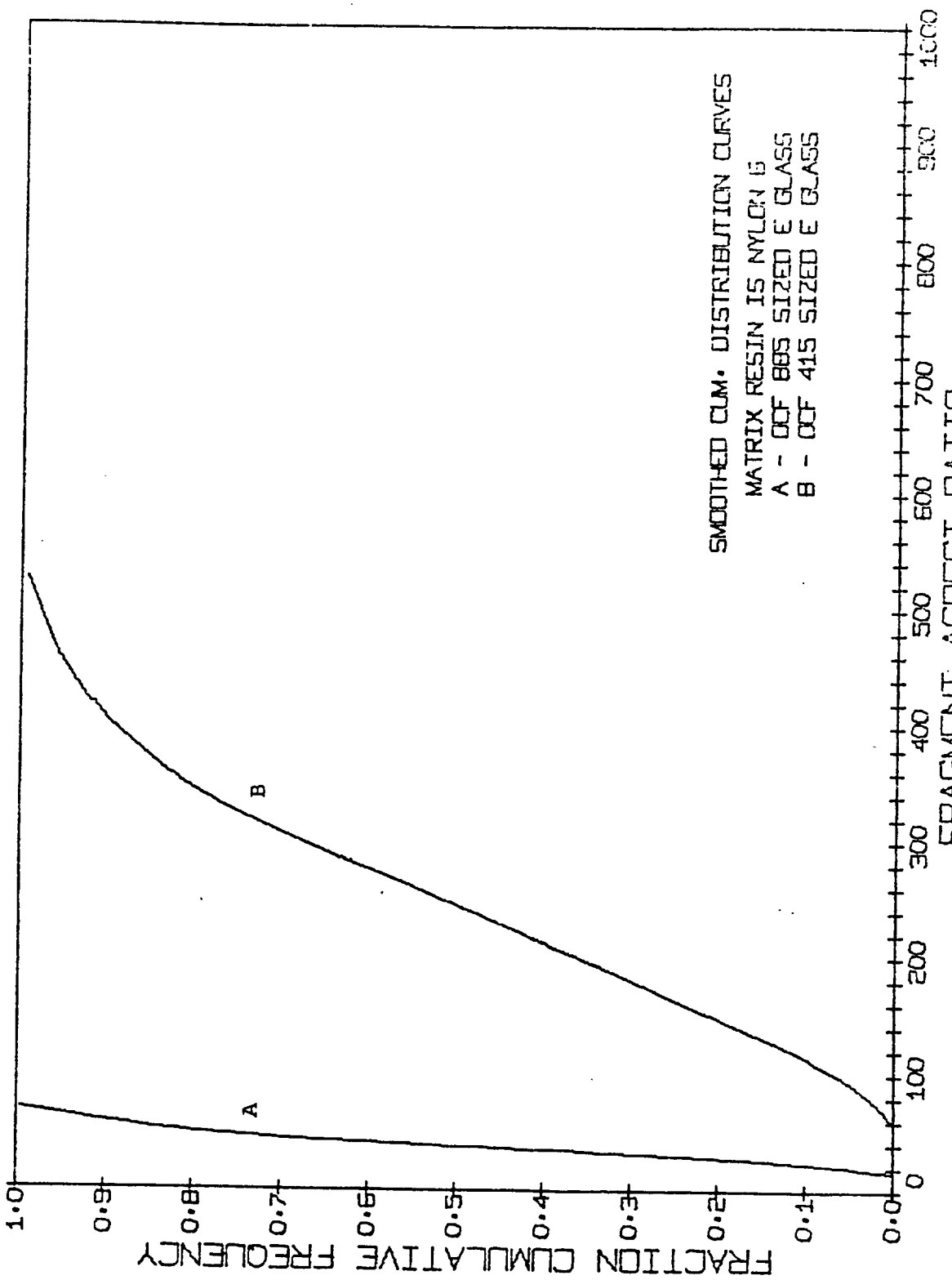


FIGURE 8: Experimental Fragment ℓ/d Distributions of OCF 885 and OCF 415 in Nylon 6

Union Carbide trial exhibit UC-1507: W. A. Fraser, Micromechanical Characterization of Surface Treated Reinforci...
Published by AsbestosClaims.Law
ACL Doc 16612 · Page 53 of 88
asbestosclaims.law/library/16612/53

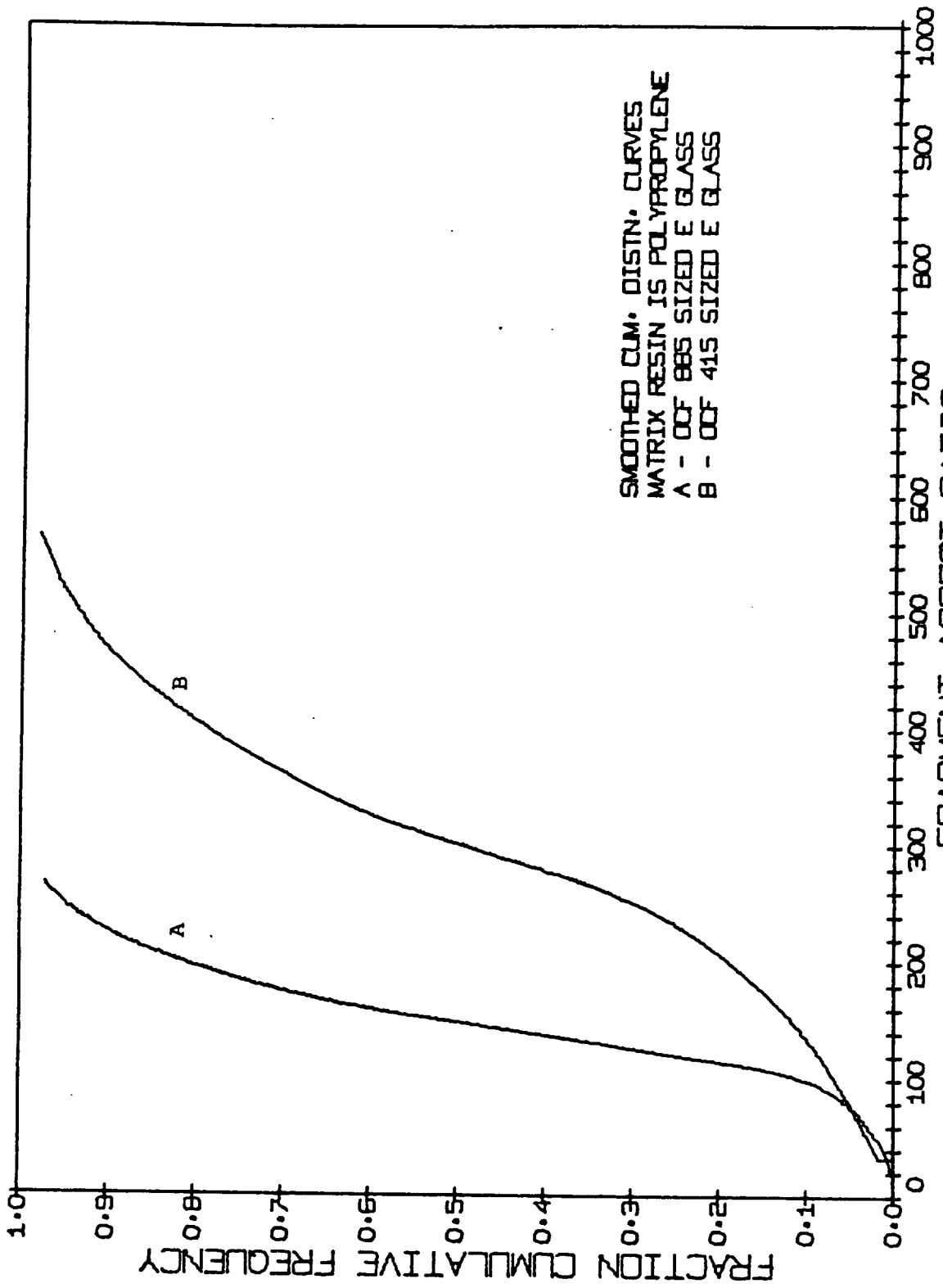


FIGURE 9: Experimental Fragment ℓ/d Distributions of OCF 885 and OCF 415 in Polypropylene

Published by AsbestosClaims.Law
asbestosclaims.law/library/16612/54

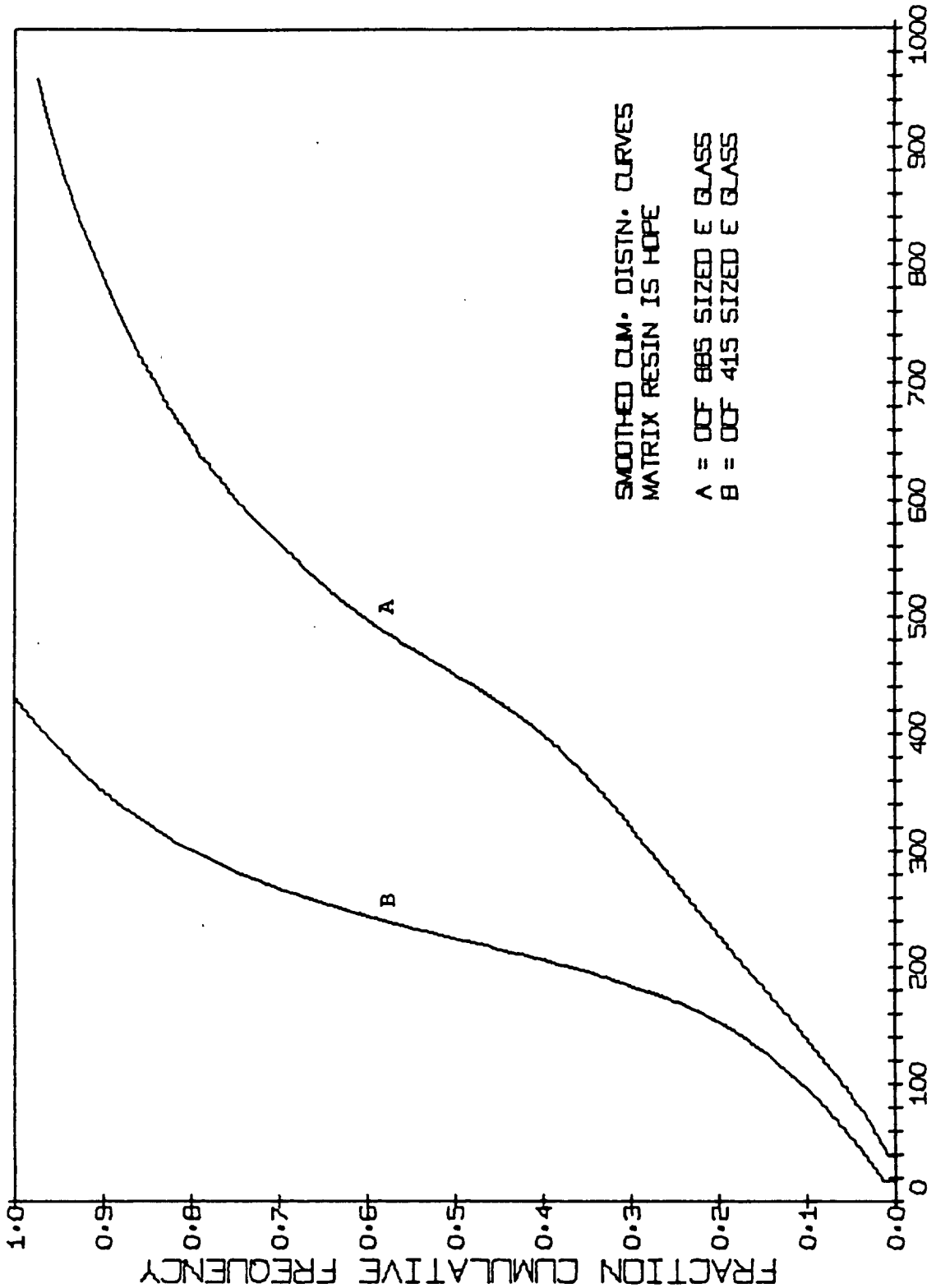


FIGURE 10: Experimental Fragment ℓ/d Distributions of OCF 885 and OCF 415 in High Density Polyethylene

Published by AsbestosClaims.Law
asbestosclaims.law/library/16612/55

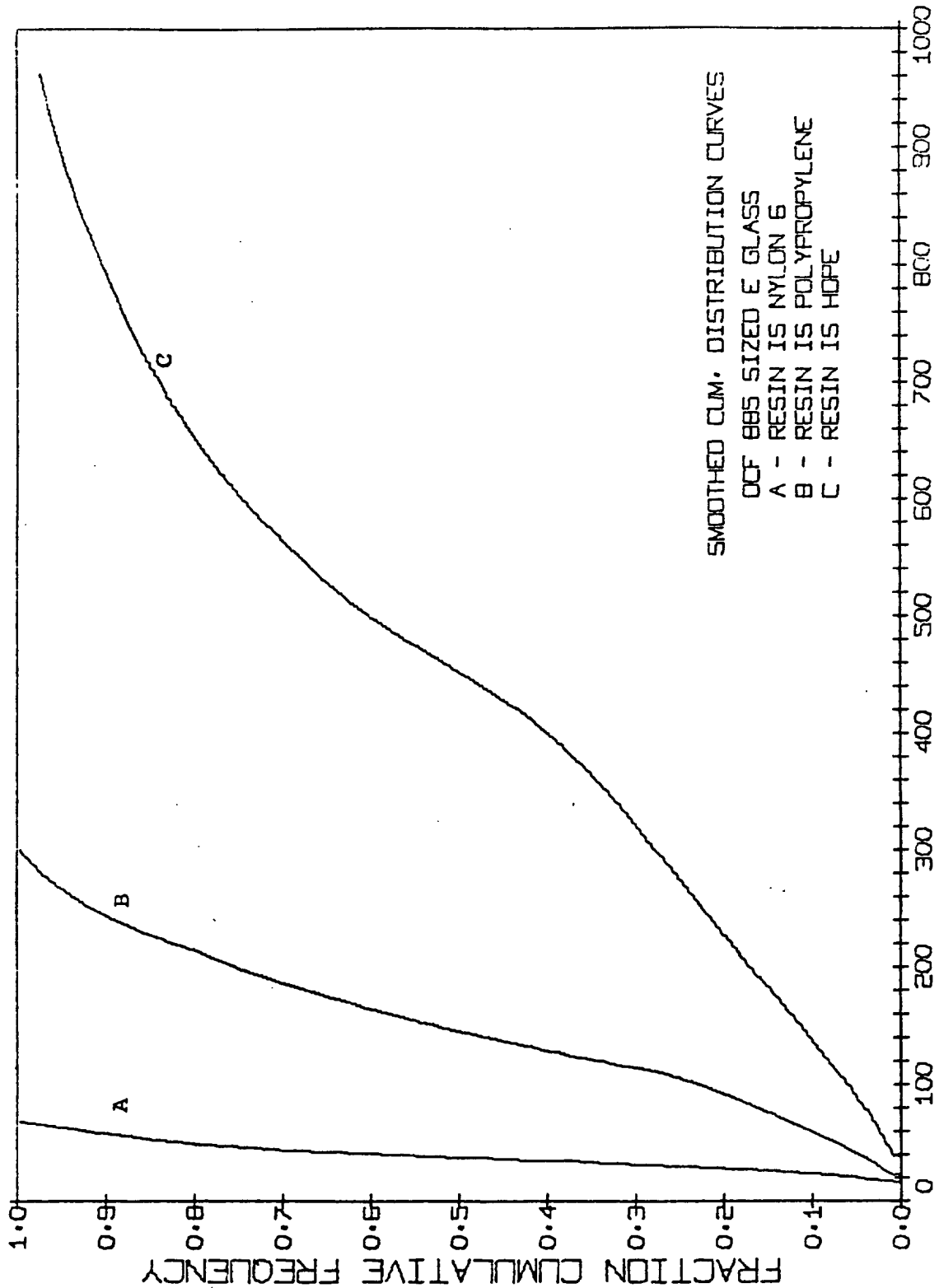


FIGURE 11: Summary Plot, Experimental ℓ/d Distributions of OCF 885 in Nylon 6, Polypropylene and HDPE

Published by AsbestosClaims.Law
asbestosclaims.law/library/16612/56

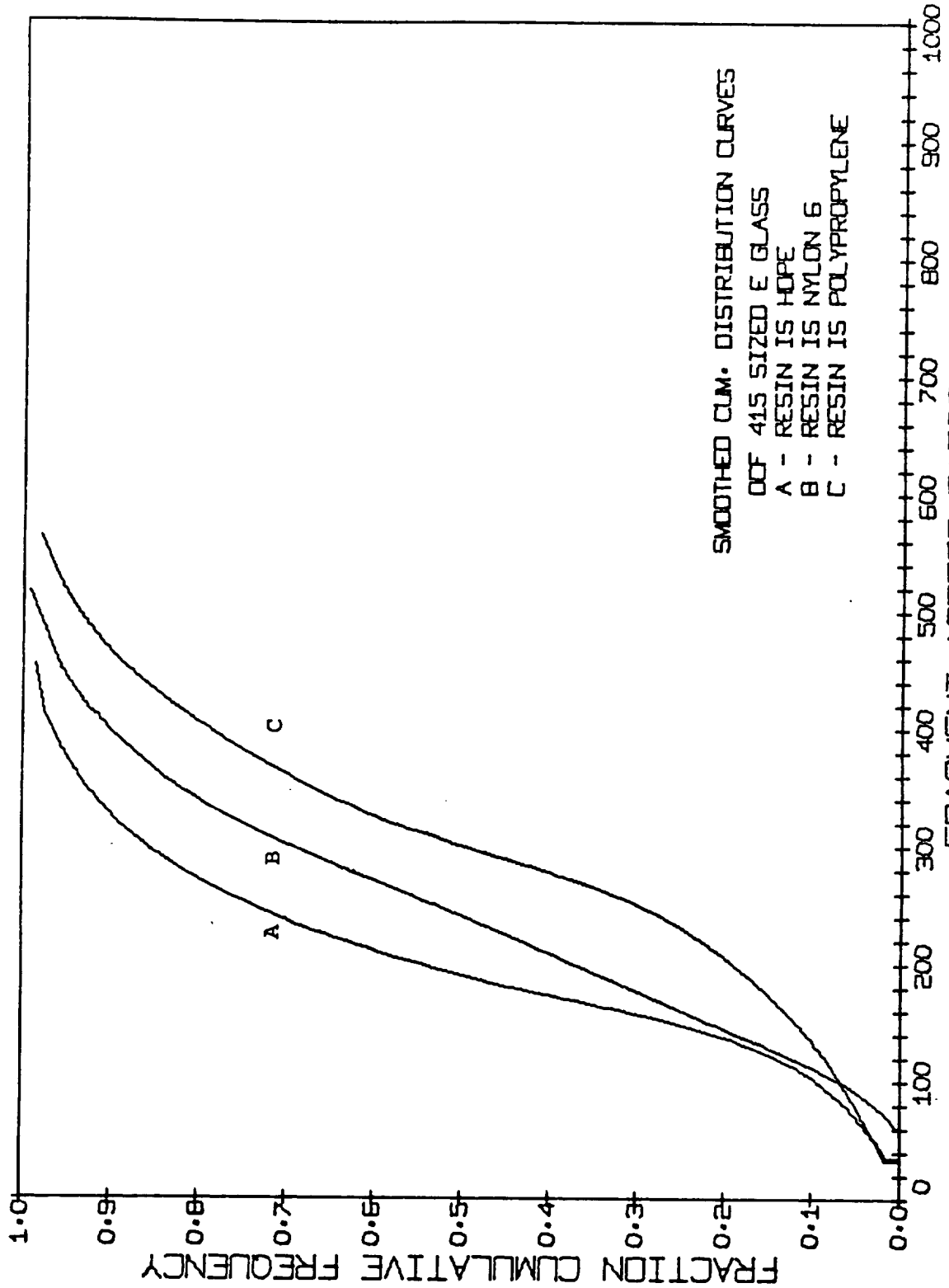


FIGURE 12: Summary Plot, Experimental ℓ/d Distributions of OCF 415 in Nylon 6, Polypropylene and HDPE

Union Carbide trial exhibit UC-1507: W. A. Fraser, Micromechanical Characterization of Surface Treated Reinforci…
Published by AsbestosClaims.Law
ACL Doc 16612 · Page 57 of 88
asbestosclaims.law/library/16612/57

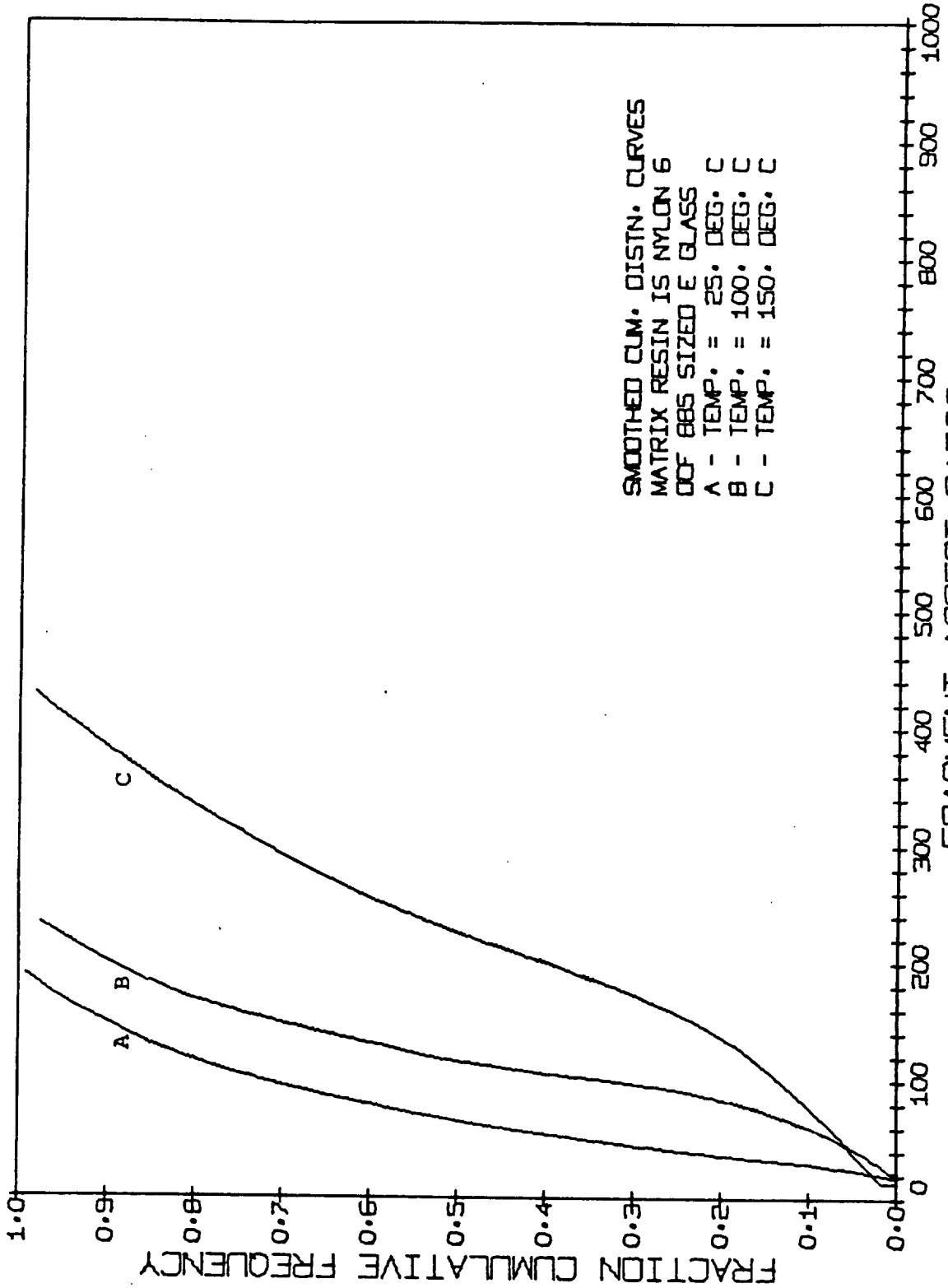


FIGURE 13: Effect of Test Temperature on Fragment ℓ/d Distribution of OCF 885 in Nylon 6

Published by AsbestosClaims.Law
asbestosclaims.law/library/16612/58

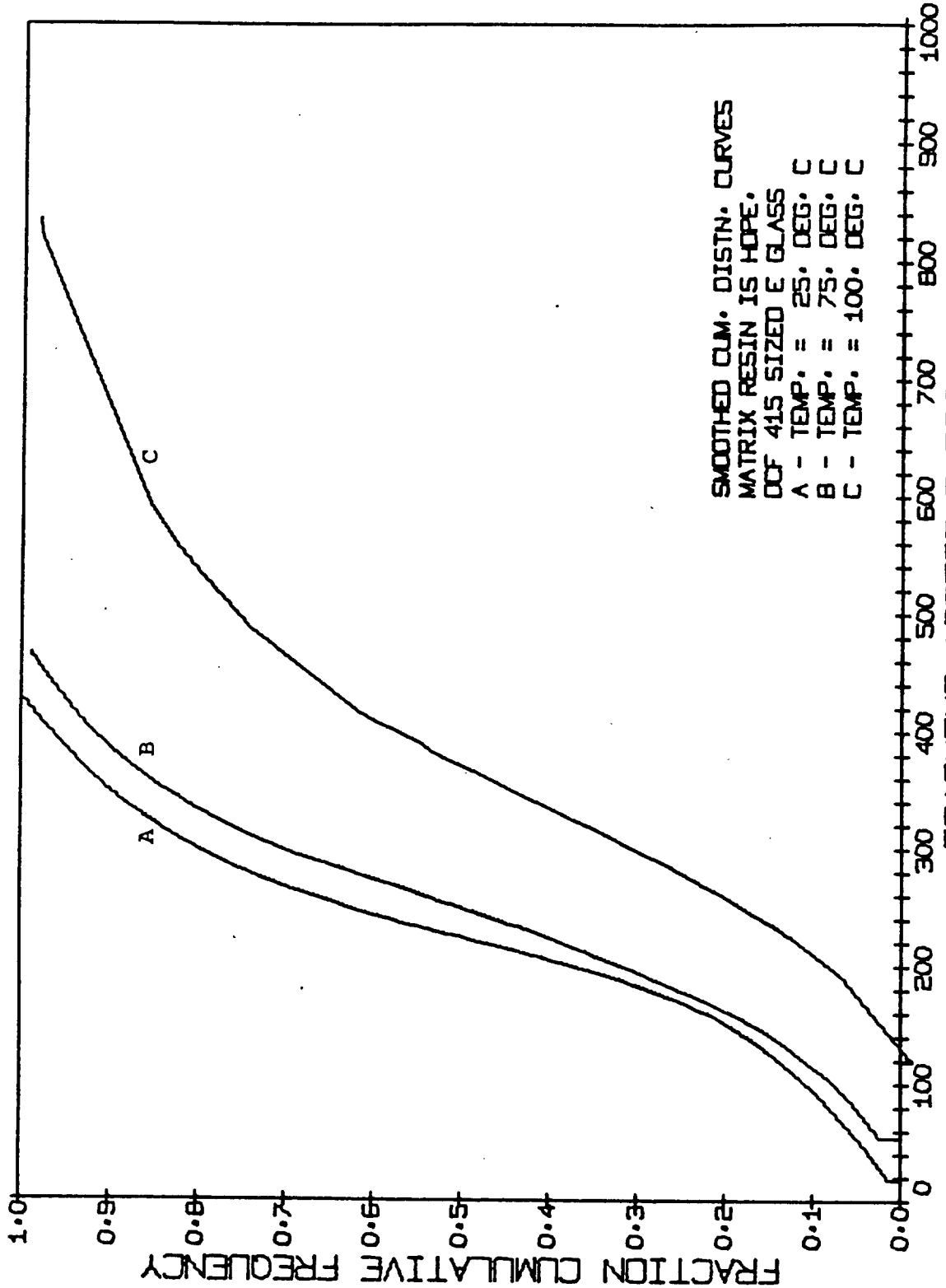


FIGURE 14: Effect of Test Temperature on Fragment ℓ/d Distribution of OCF 415 in HDPE

Union Carbide trial exhibit UC-1507: W. A. Fraser, Micromechanical Characterization of Surface Treated Reinforci...
Published by AsbestosClaims.Law
ACL Doc 16612 · Page 59 of 88
asbestosclaims.law/library/16612/59

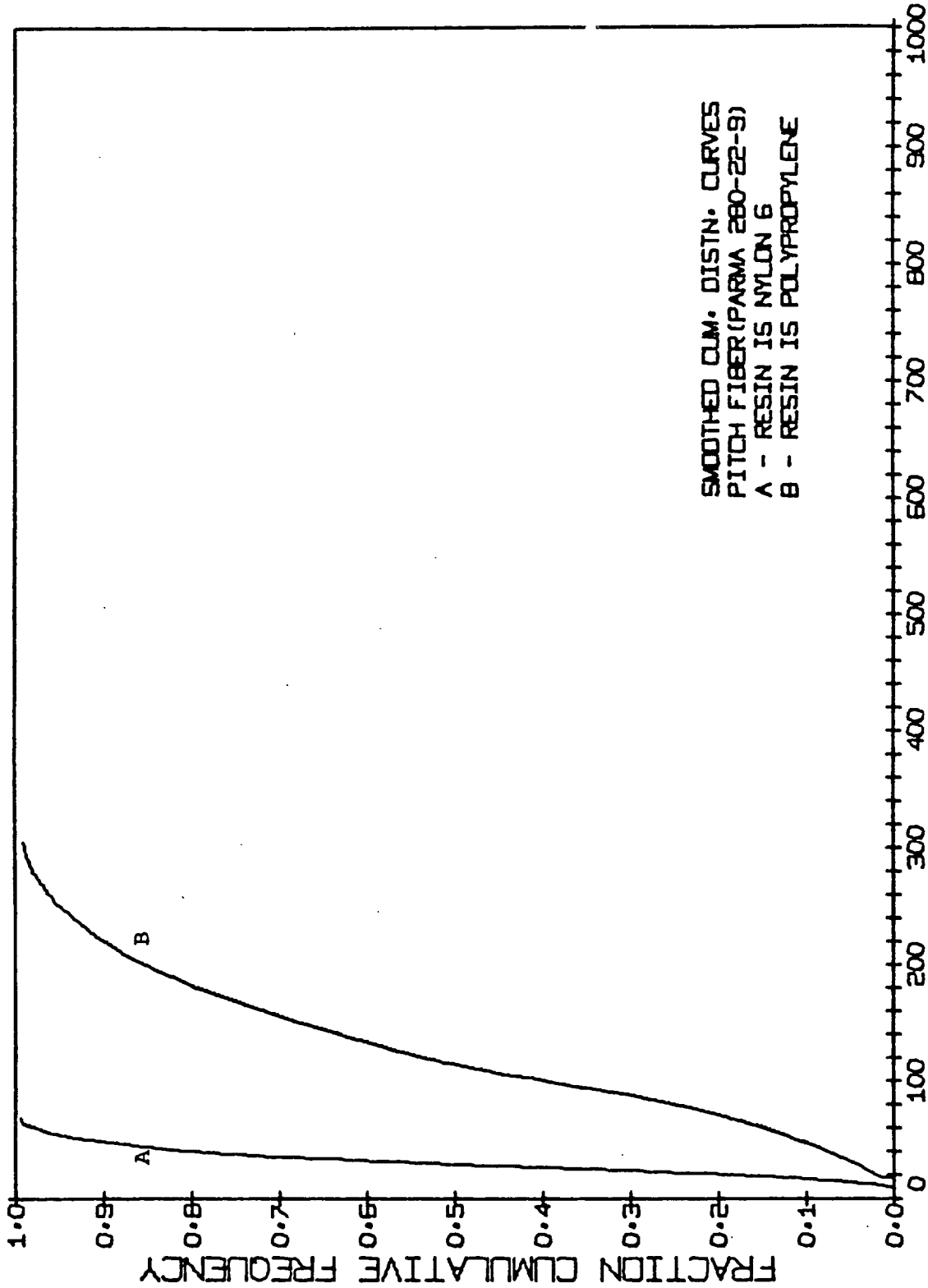


FIGURE 15: Experimental Fragment ℓ/d Distributions of Carbon Products' Untreated, Continuous Filament, Pitch Based Graphite Fiber in Nylon 6 and Polypropylene

Published by AsbestosClaims.Law
asbestosclaims.law/library/16612/60

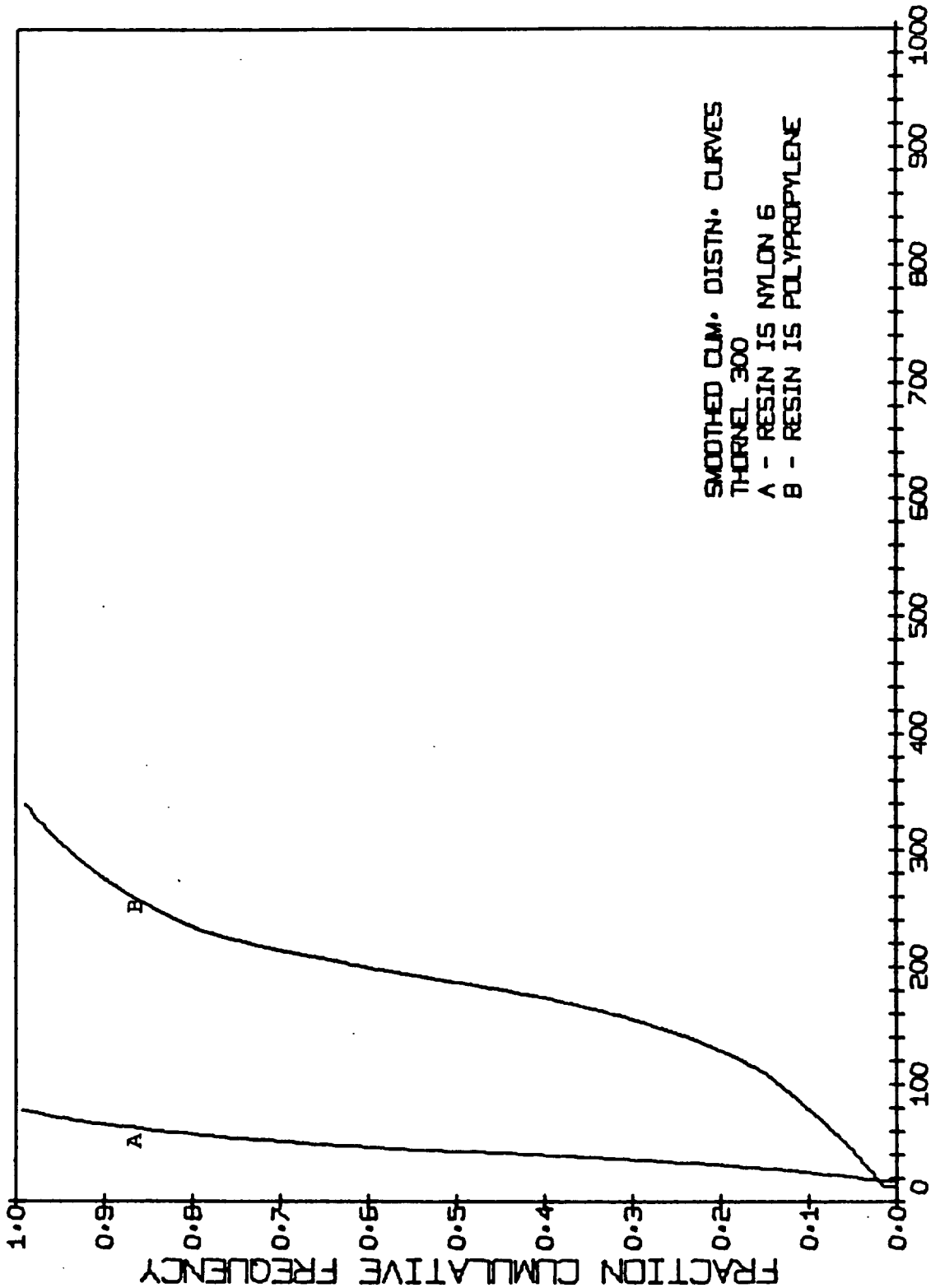


FIGURE 16: Experimental Fragment ℓ/d Distributions Thornel 300 in Nylon 6 and Polypropylene

Published by AsbestosClaims.Law
asbestosclaims.law/library/16612/61

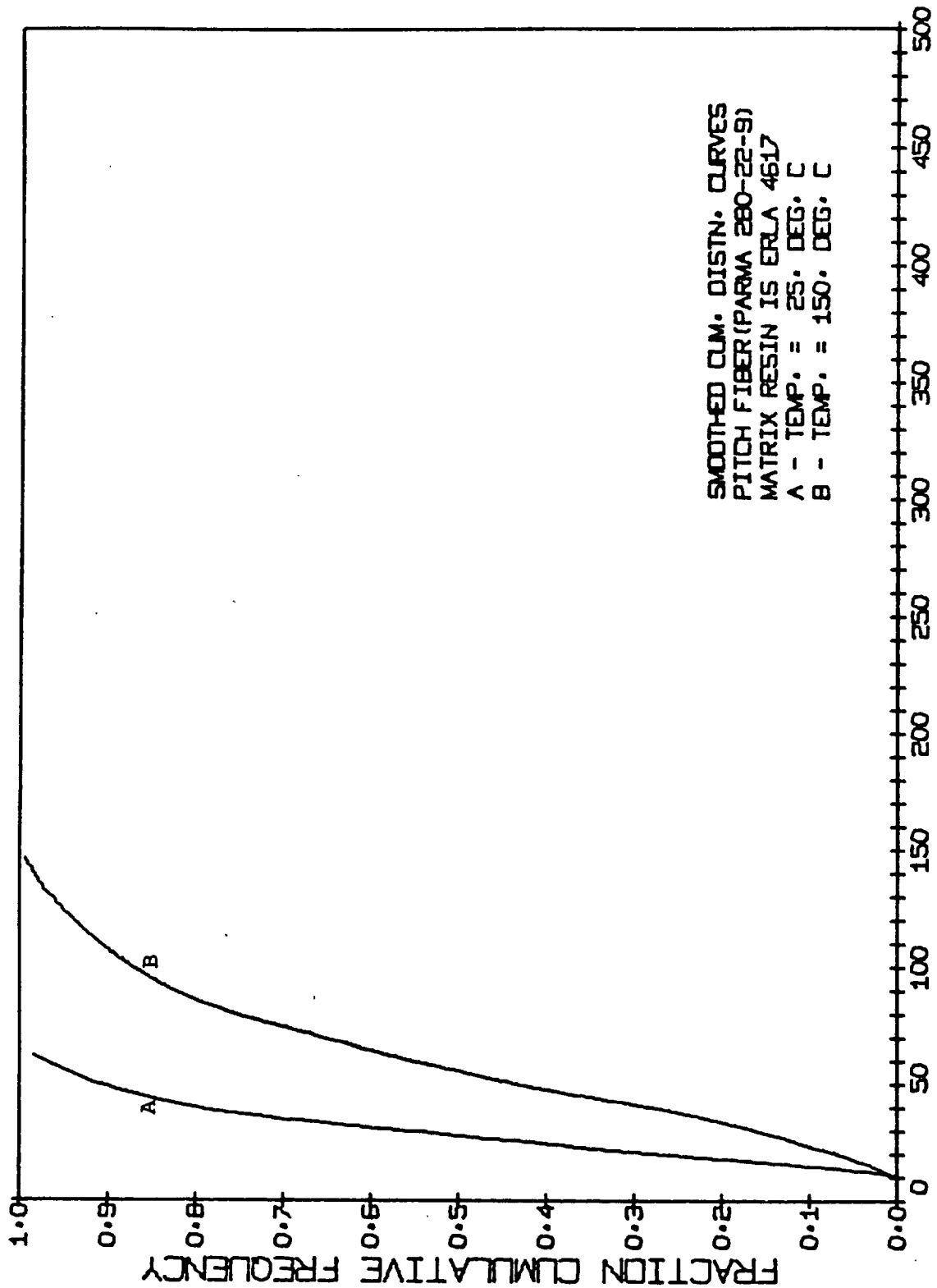


FIGURE 17: Effect of Test Temperature on Fragment ℓ/d Distributions of Carbon Products' Untreated, Continuous Filament, Pitch Based Graphite Fiber in ERLA 4617 (an epoxy matrix)

Published by AsbestosClaims.Law
asbestosclaims.law/library/16612/62

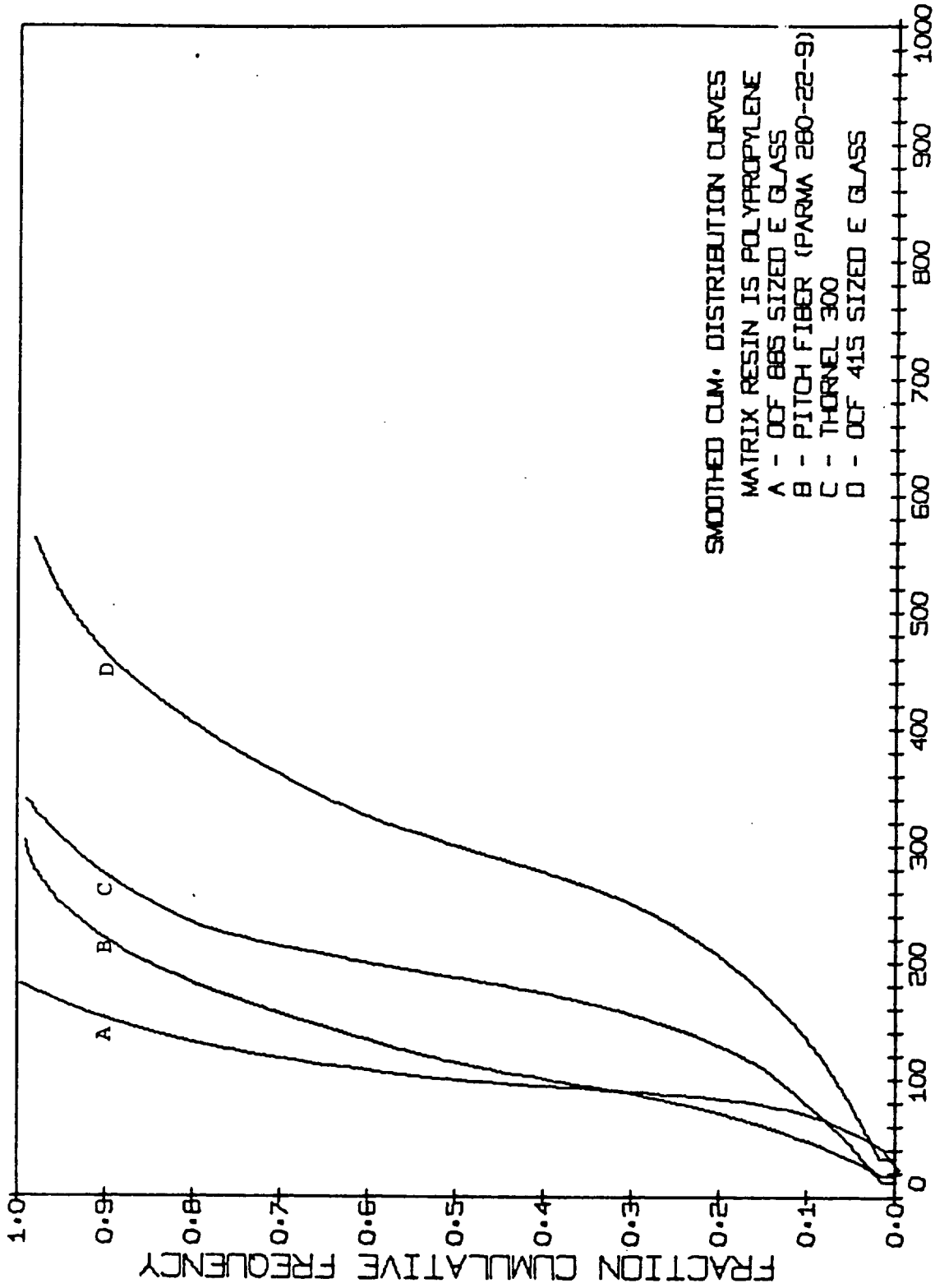


FIGURE 18: Summary Plot, Experimental ℓ/d Distributions of OCF 885, Pitch Based Graphite, Thornel 300, and OCF 415 in Polypropylene

Published by AsbestosClaims.Law
asbestosclaims.law/library/16612/63

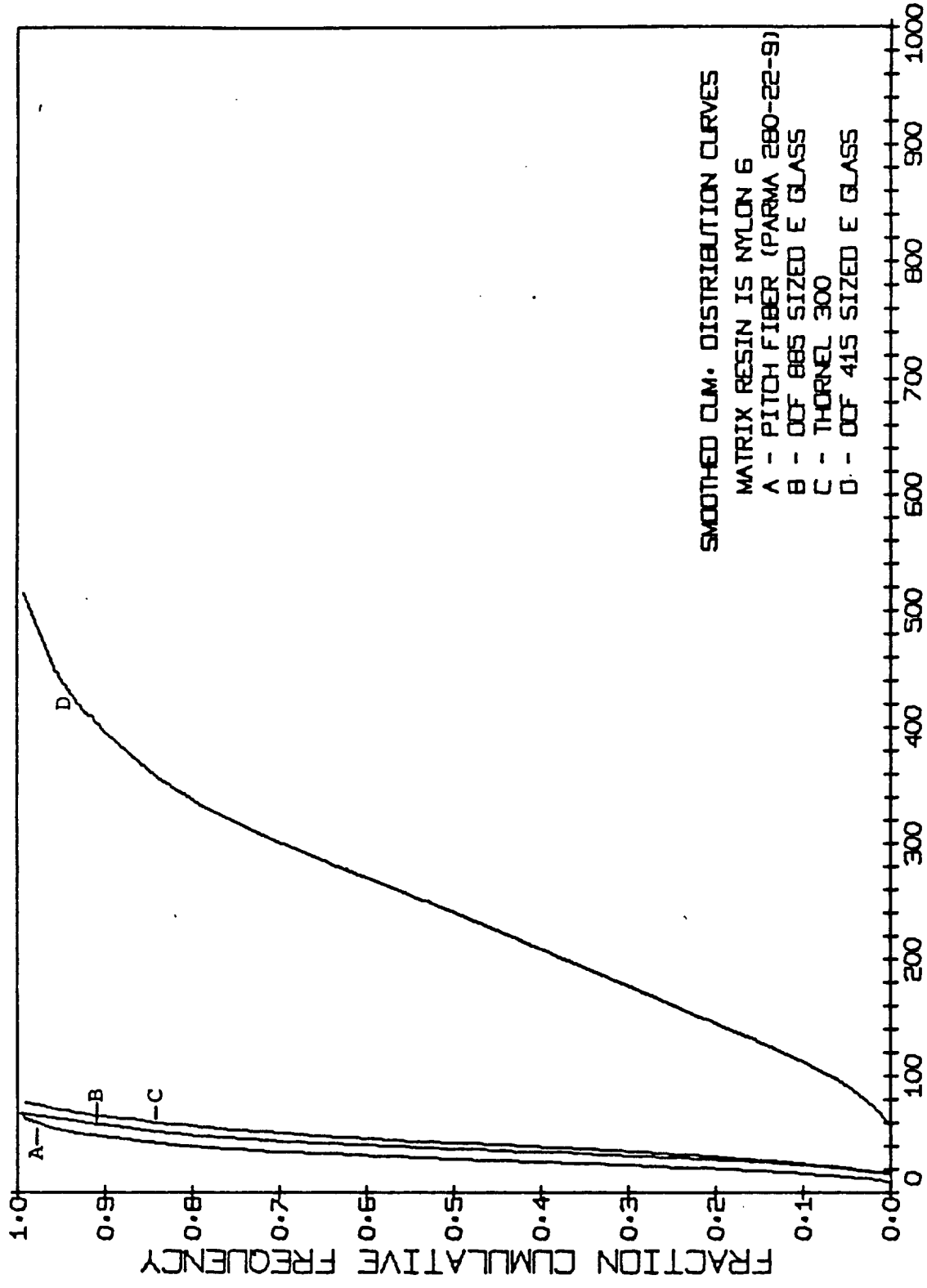


FIGURE 19: Summary Plot, Experimental ℓ/d Distributions of Pitch Based Graphite, OCF 885, Thornel 300, and OCF 415 in Nylon 6

Published by AsbestosClaims.Law
asbestosclaims.law/library/16612/64

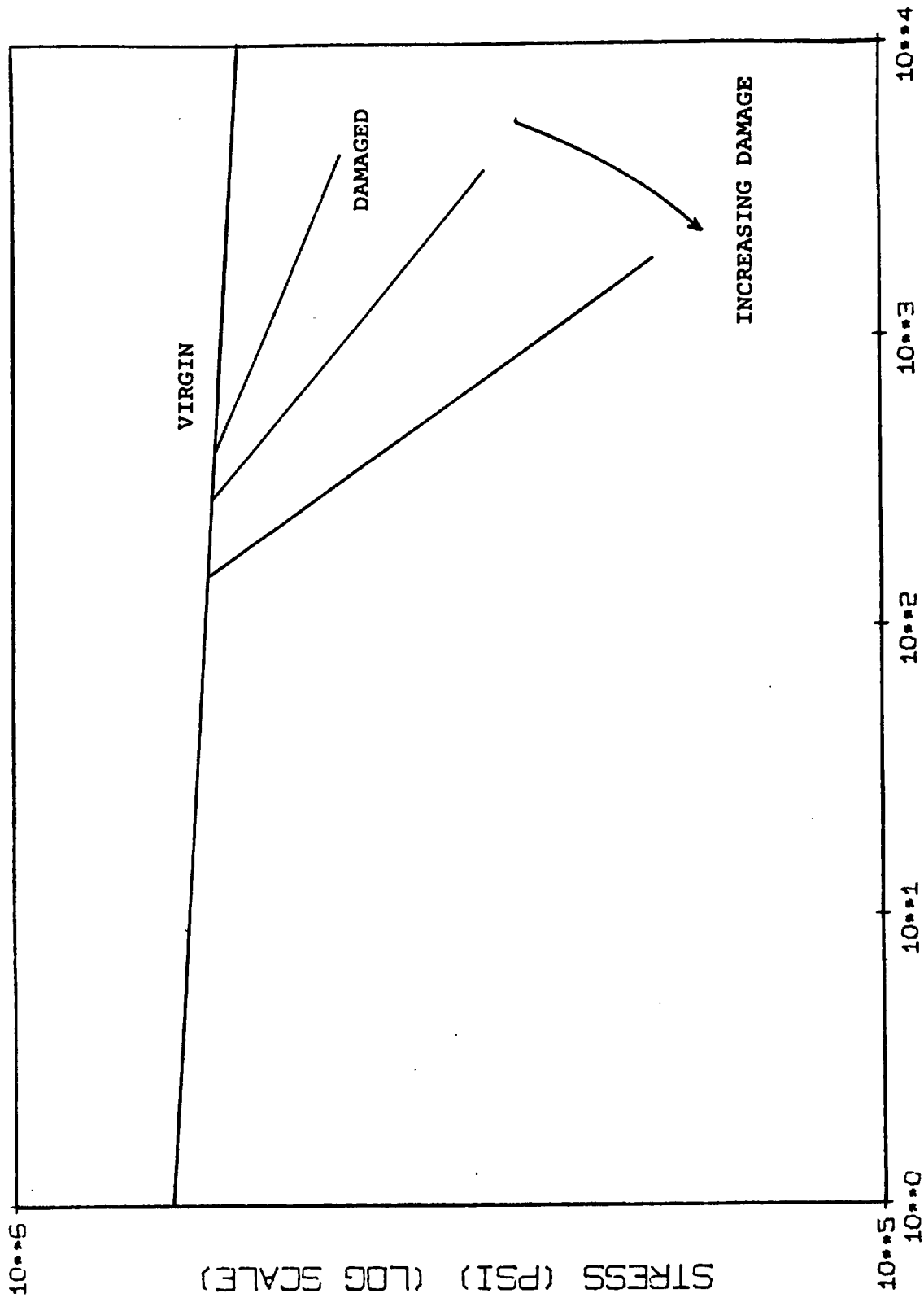


FIGURE 20: General Strength-Length Relationship for Glass Fibers (from Metcalfe and Schmitz[34])

Published by AsbestosClaims.Law
asbestosclaims.law/library/16612/65

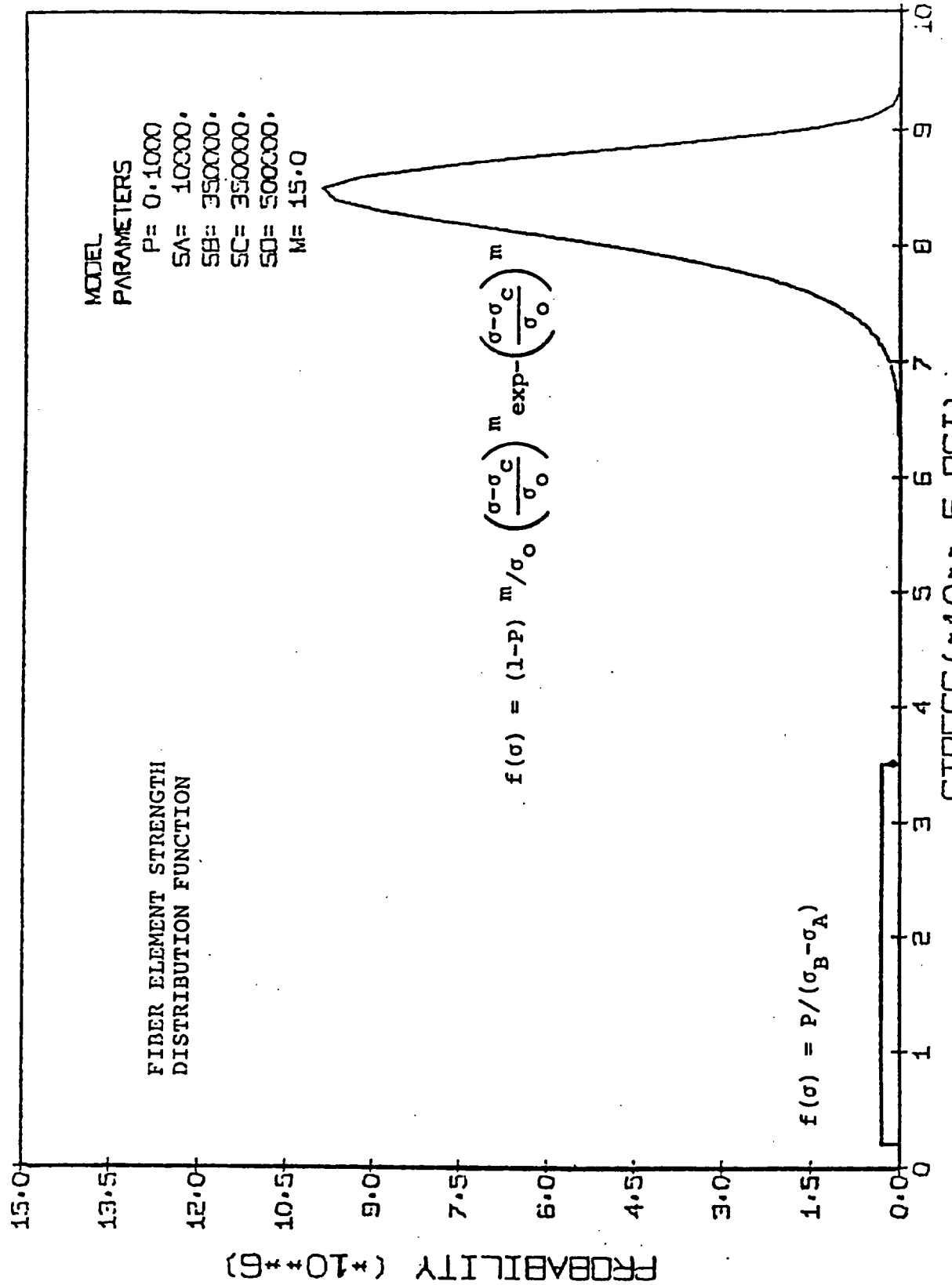


FIGURE 21: Assumed Fiber Element (Link) Strength Distribution Function

Union Carbide trial exhibit UC-1507: W. A. Fraser, Micromechanical Characterization of Surface Treated Reinforci…
ACL Doc 16612 · Page 66 of 88
Published by AsbestosClaims.Law
asbestosclaims.law/library/16612/66

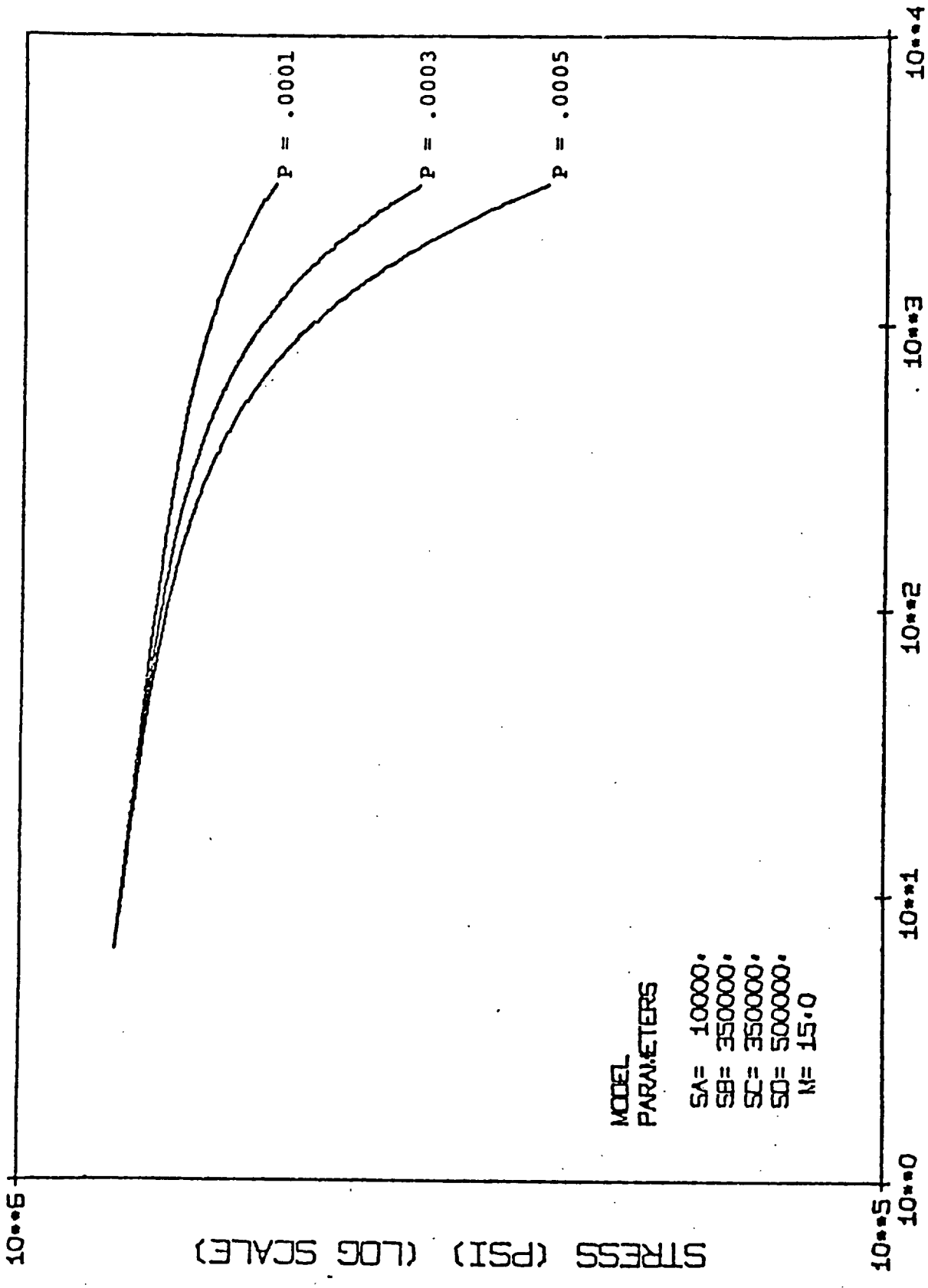


FIGURE 22: Hypothetical Fiber Strength-Length Curves as a Function of P, the Fraction of the Link Population Containing Severe Flaws

Published by AsbestosClaims.Law
asbestosclaims.law/library/16612/67

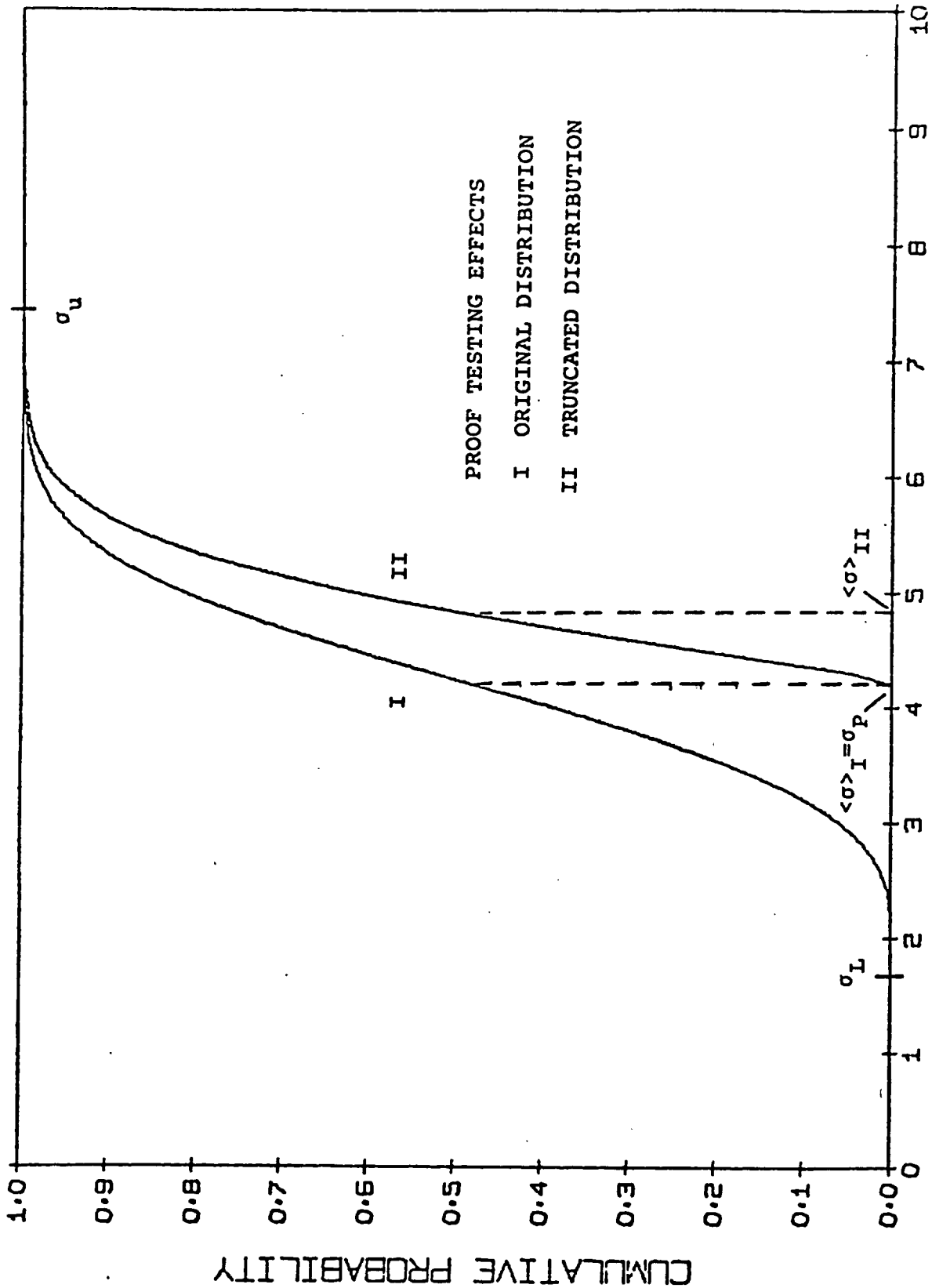


FIGURE 23: The Effect of Proof Testing on the Strength Distribution Function of a Typical Brittle Material

Union Carbide trial exhibit UC-1507: W. A. Fraser, Micromechanical Characterization of Surface Treated Reinforci…
ACL Doc 16612 · Page 68 of 88
Published by AsbestosClaims.Law
asbestosclaims.law/library/16612/68

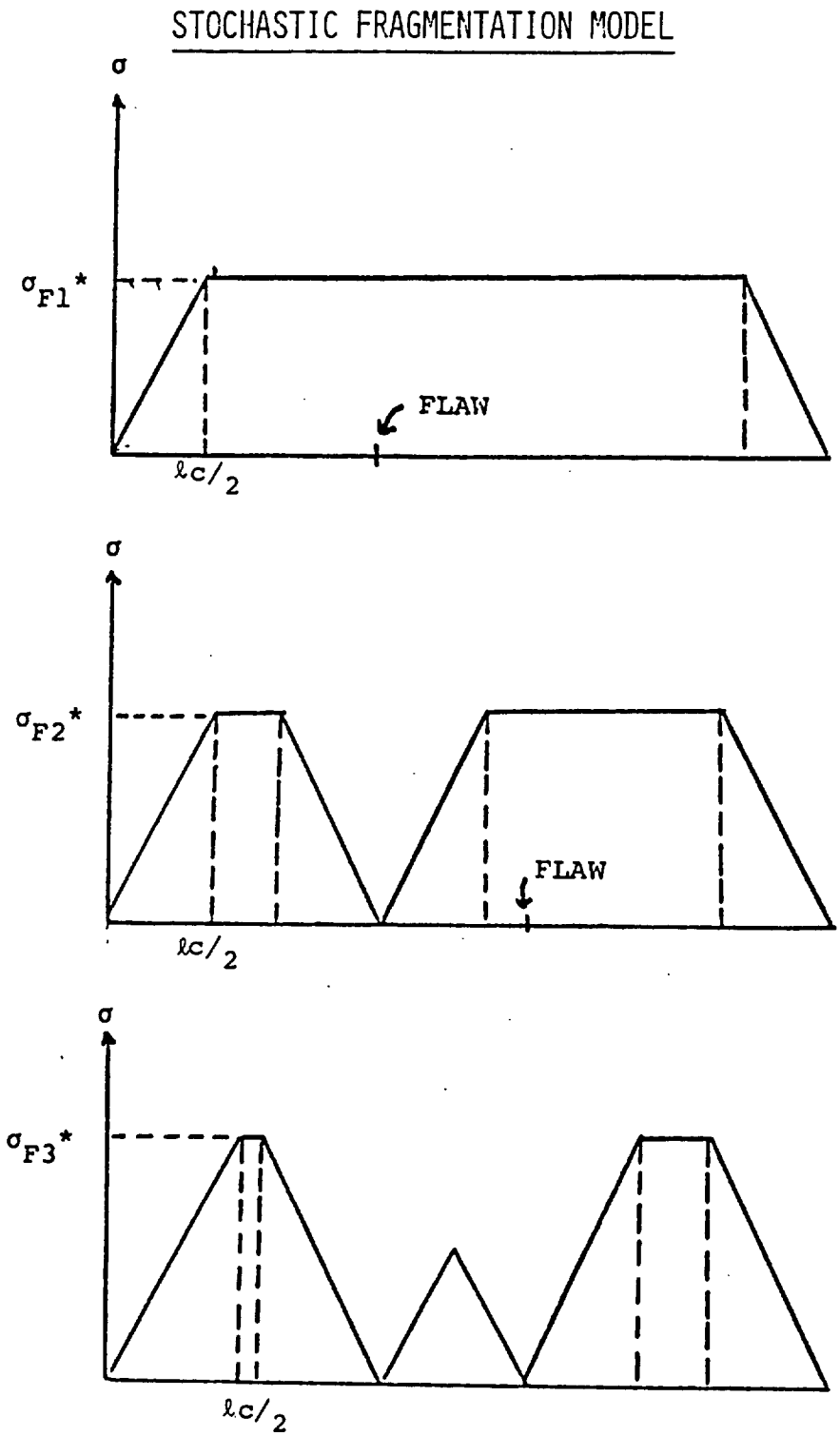


FIGURE 24: The Stochastic Fiber Fragmentation Model Flow Sheet

Published by AsbestosClaims.Law
asbestosclaims.law/library/16612/69

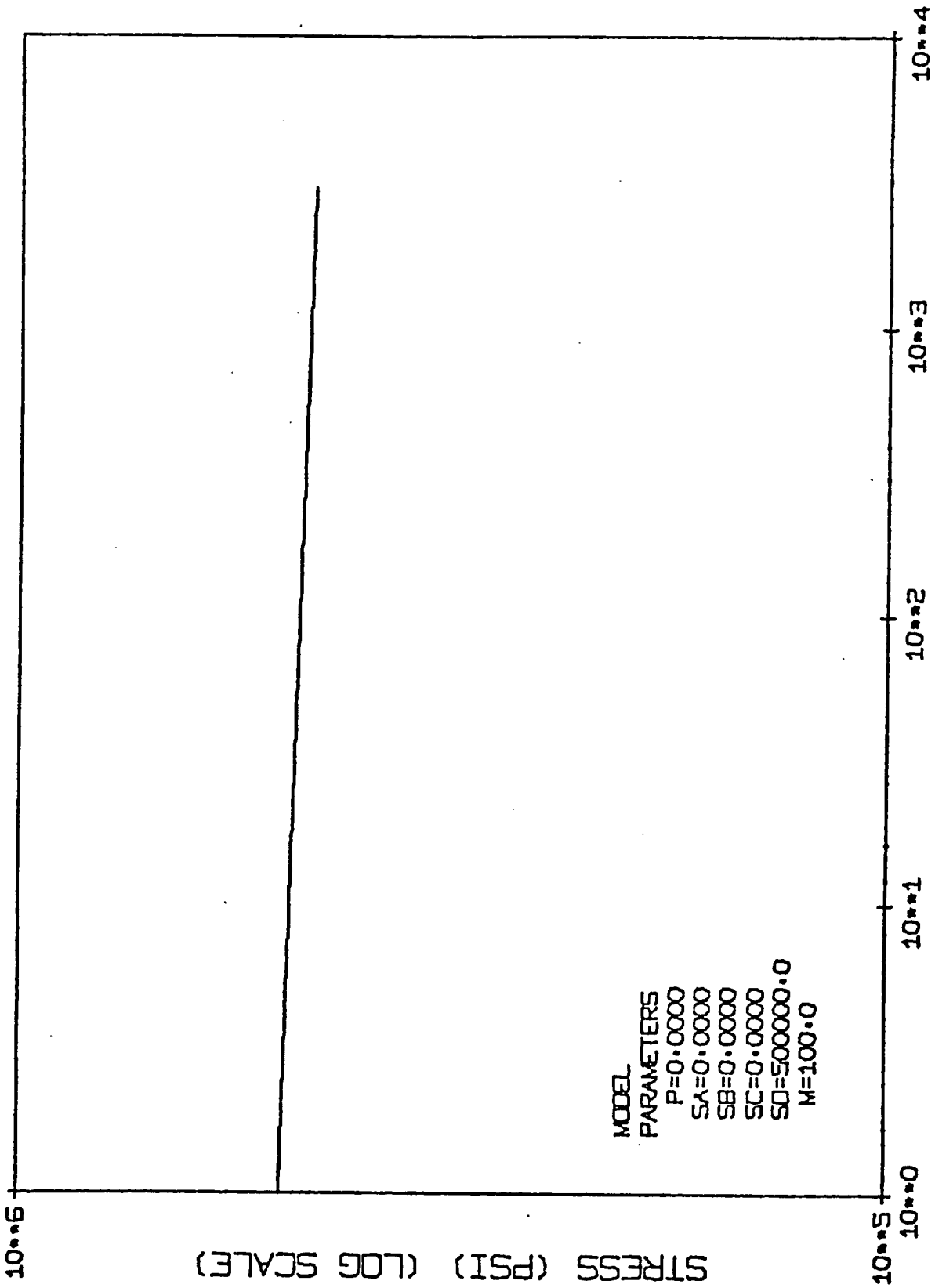


FIGURE 25: Strength-Length Curve for a Theoretical Flaw Free Fiber

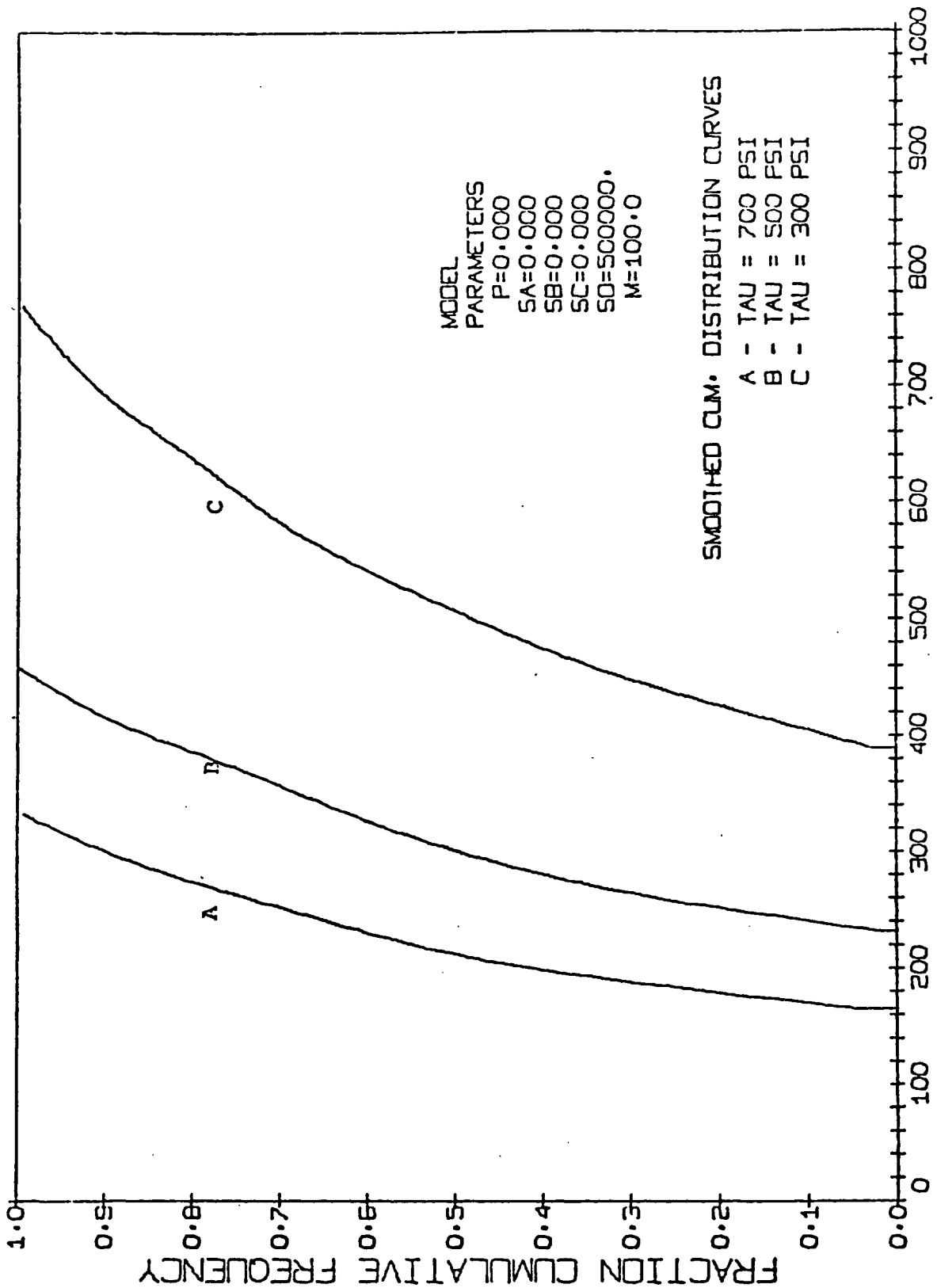


FIGURE 26: Theoretical Fragment ℓ/d Distributions Assuming a Flaw Free Fiber

Published by AsbestosClaims.Law
asbestosclaims.law/library/16612/71

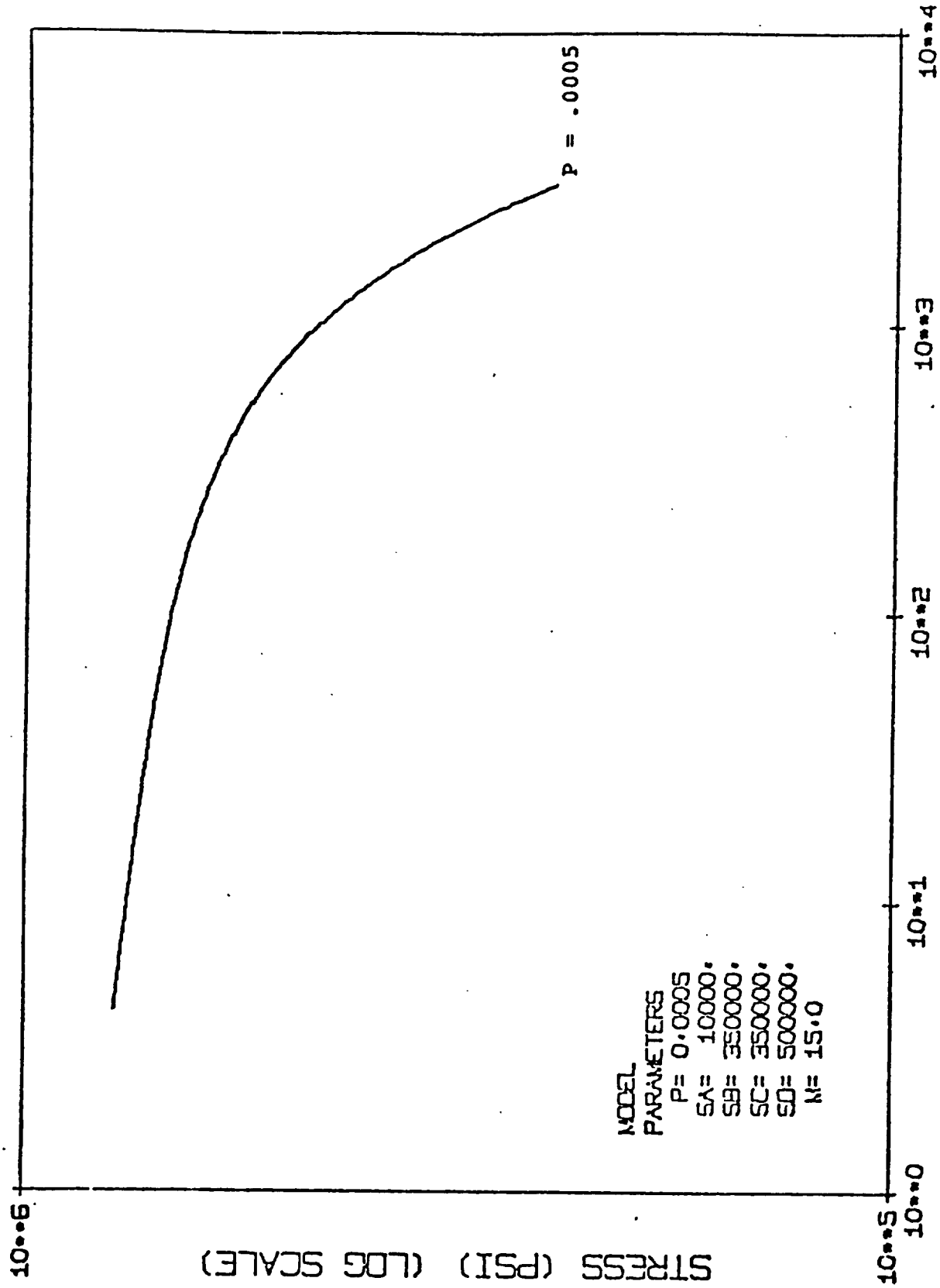


FIGURE 27: Strength-Length Curve for a Theoretical Flawed Fiber

Published by AsbestosClaims.Law
asbestosclaims.law/library/16612/72

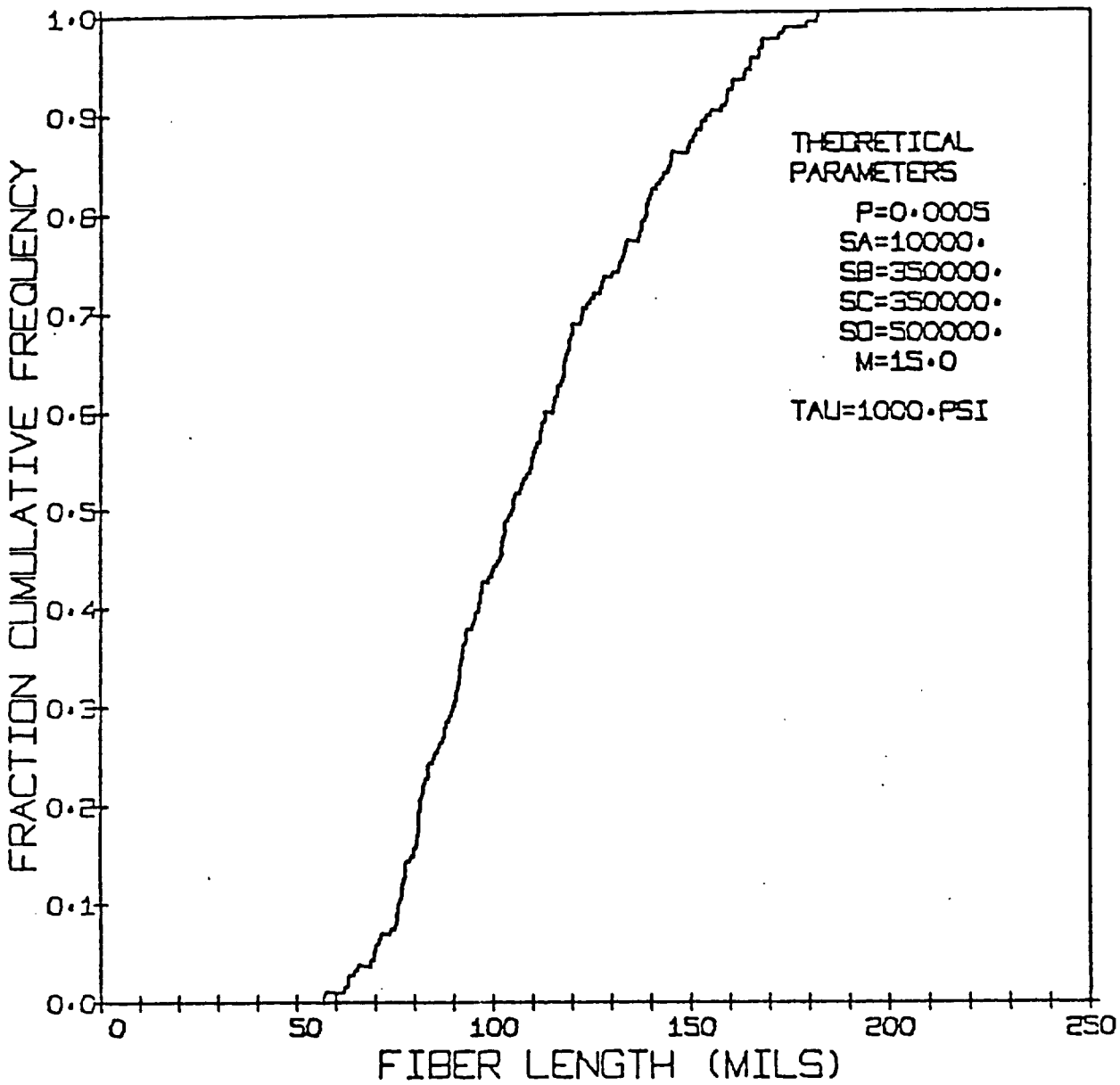


FIGURE 28a: Theoretical Fragment ℓ/d Cumulative Distribution Assuming a Flawed Fiber

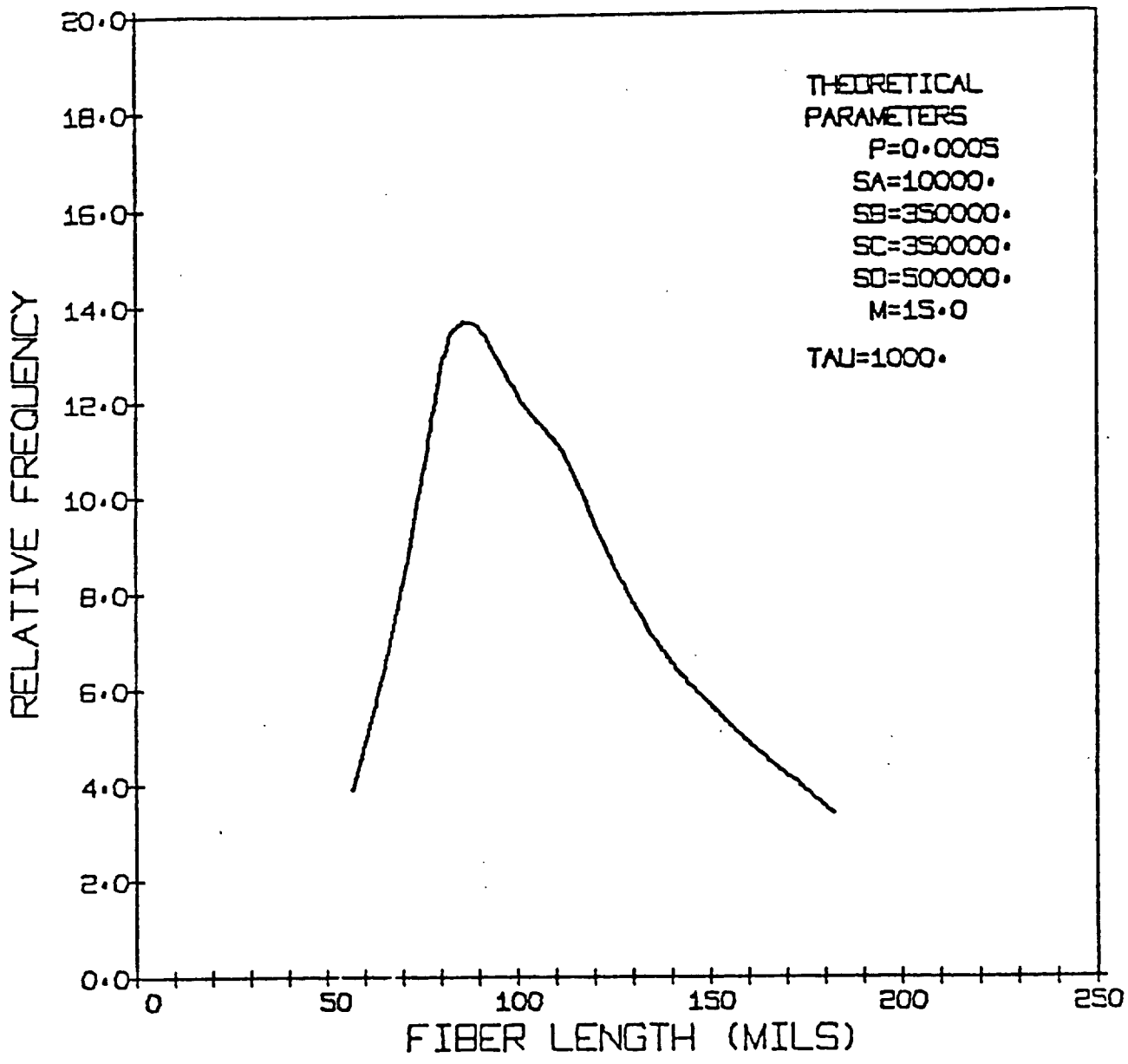


FIGURE 28b: Theoretical Fragment ℓ/d Distribution Assuming a Flawed Fiber (Numerically Smoothed Frequency Curve)

Published by AsbestosClaims.Law
asbestosclaims.law/library/16612/74

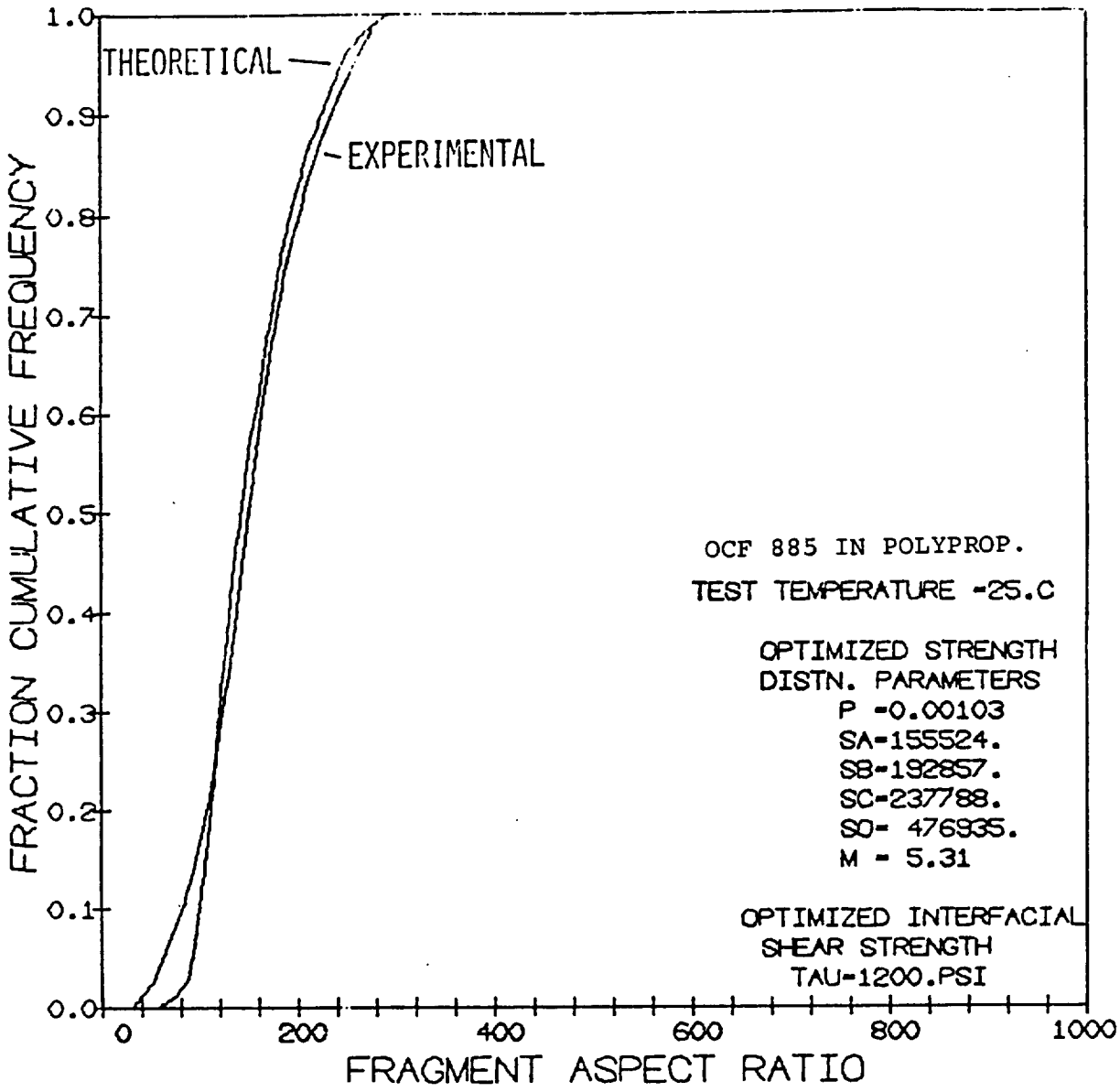


FIGURE 29: Experimental and Optimized Theoretical ℓ/d Distribution Curves for OCF 885 in Polypropylene

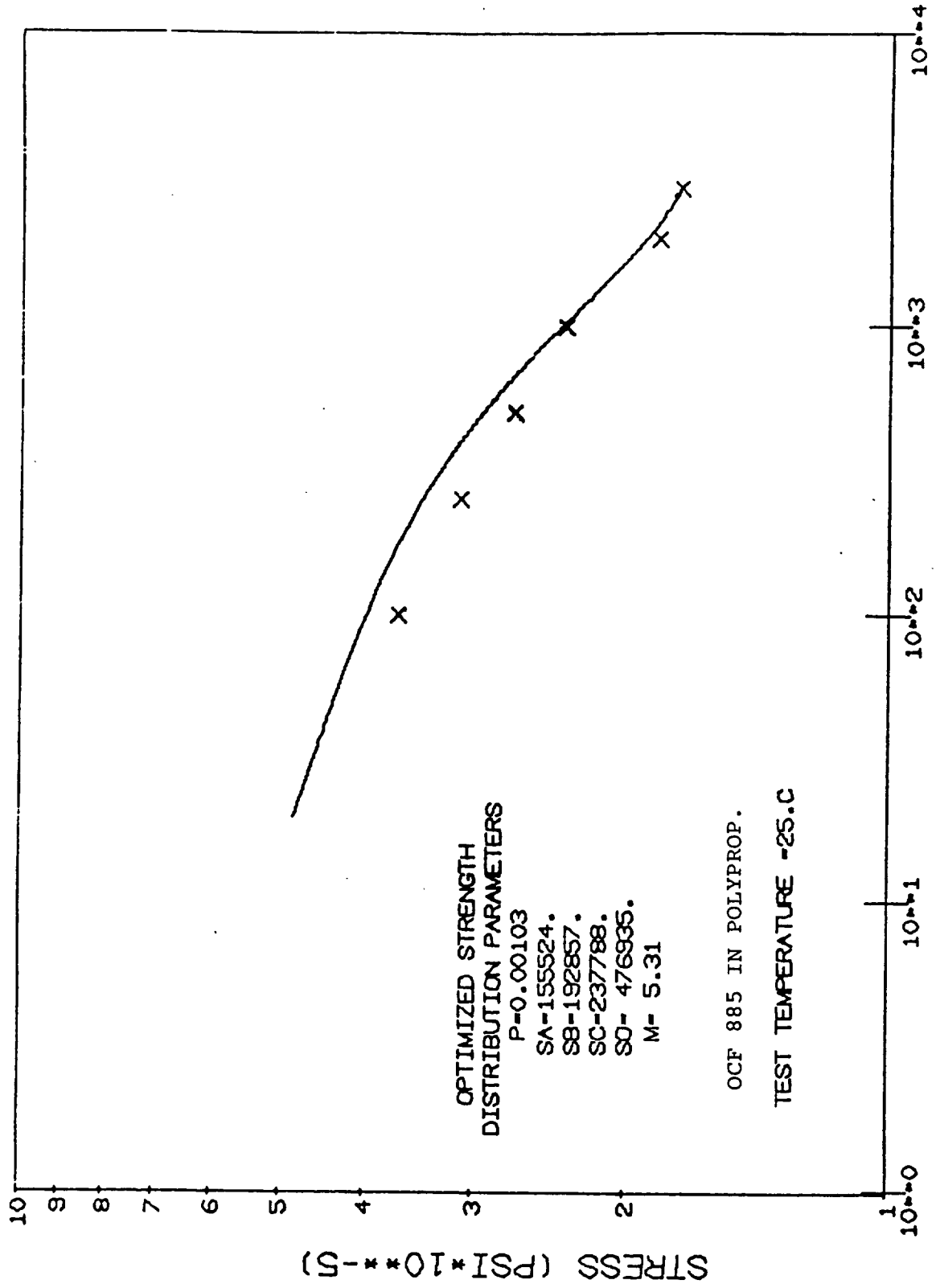


FIGURE 30: Mean Fiber Strength-Length Curve as Computed from OCF 885/Polypropylene Fragmentation Data. x's Represent Single Filament Tensile Test Results

Published by AsbestosClaims.Law
asbestosclaims.law/library/16612/76

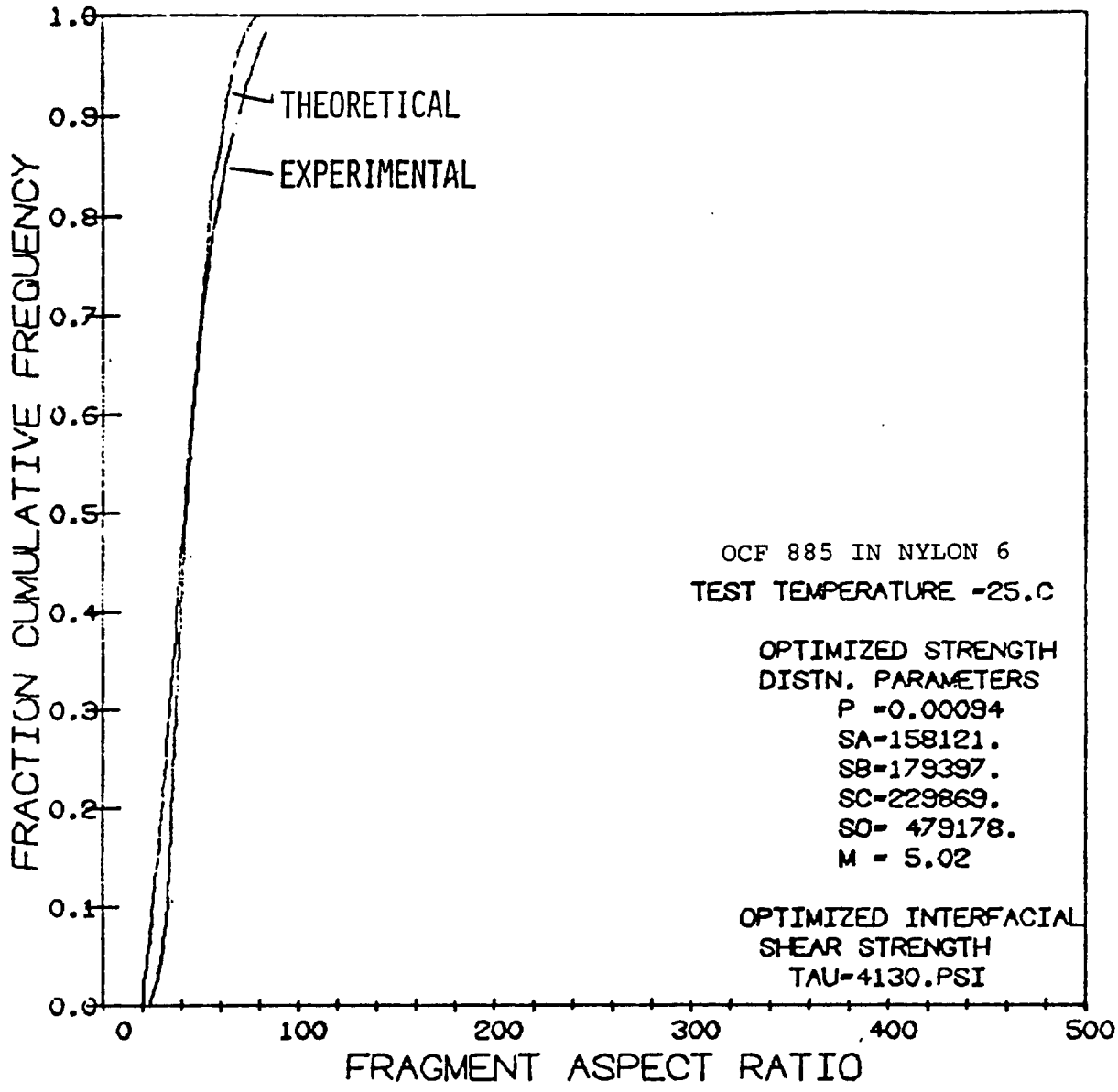


FIGURE 31: Experimental and Optimized Theoretical ℓ/d Distributions for OCF 885 in Nylon 6

Published by AsbestosClaims.Law
asbestosclaims.law/library/16612/77

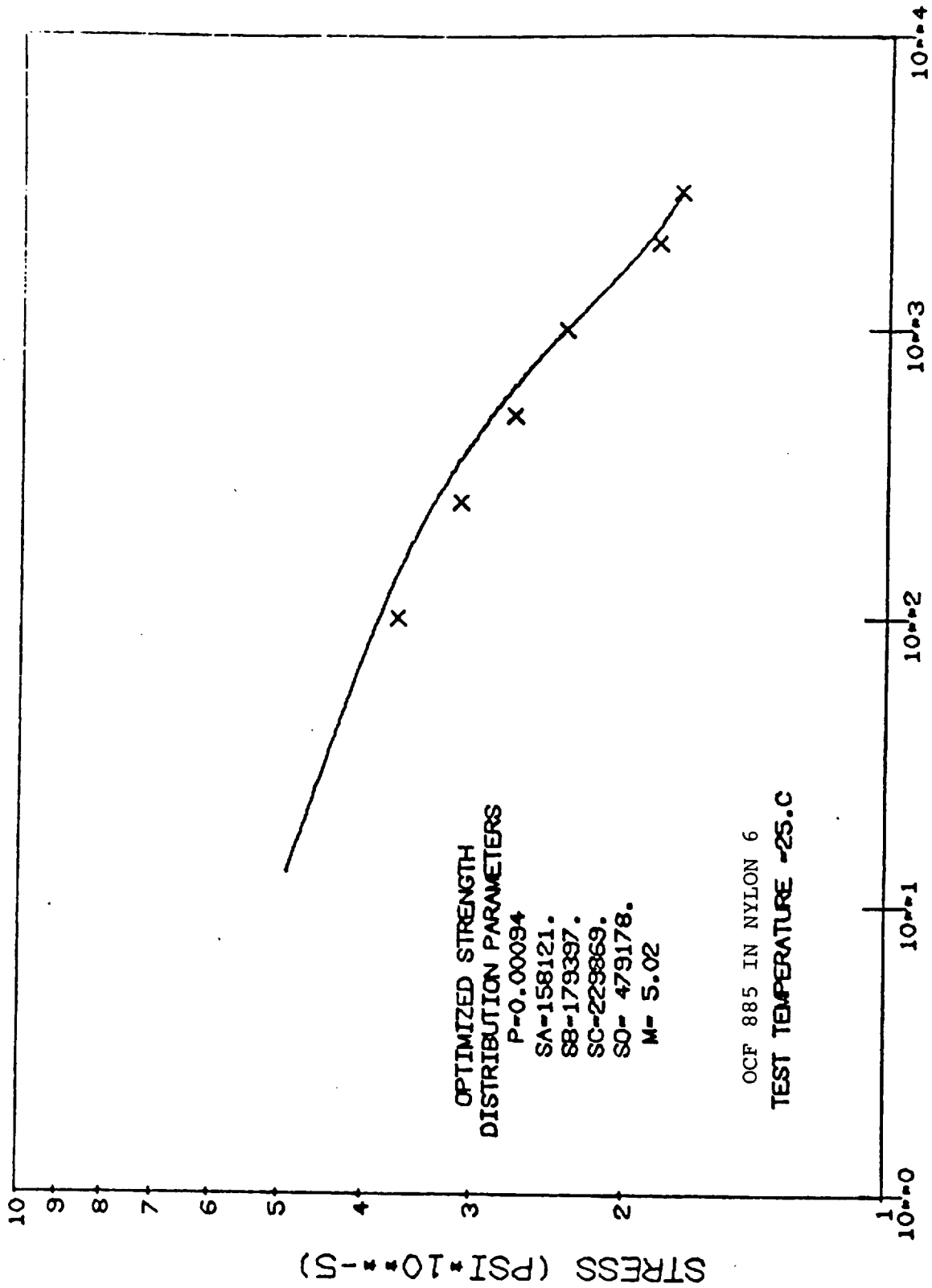


FIGURE 32: Mean Fiber Strength-Length Curve as Computed from OCF 885/Nylon 6 Fragmentation Data. x's Represent Single Filament Tensile Test Results

Published by AsbestosClaims.Law
asbestosclaims.law/library/16612/78

APPENDIX A

Data Smoothing and Differentiation

Fragments, normalized by their diameter, are ranked according to their size and a fractional cumulative frequency distribution is evaluated. These data points are smoothed and differentiated using the moving strip polynomial method of Hershey, Zakin and Sinhma[17] to give an empirical probability density curve of fragment aspect ratios. An odd number of consecutive data points (3, 5, 7, ...) are considered to constitute a strip and a least squares polynomial is fitted to these points. The following model is assumed to represent the data.

$$F(x) = \sum_{j=o}^{m} \beta_j \, x^j + \varepsilon \qquad \text{(A-1)}$$

where

m = degree of the polynomial

β_j = power coefficients

ε = error

The least squares power coefficients, β_j, were solved for by Gauss-Jordan elimination. In data smoothing, $F(x_i)$, the data value at the midpoint of the strip is replaced by its approximation, $Y(x_i)$, as calculated from

$$Y(xi) = \sum_{j=o}^{m} \beta_j \, x_i^j \qquad \text{(A-2)}$$

The strip then advances along the abscissa eliminating the leftmost point and adding a new point to the right-hand side. In the tails of the distribution, points between the strip midpoint and the extremes are approximated by off center formulas. The amount of smoothing increases with the number of points in the moveable strip and decreases with increasing m, the degree of the polynomial. When m=n-1, where n equals the number of points in the strip, the polynomial fits the data exactly (i.e., no smoothing).

To differentiate the data, it is generally smoothed first, then the differential of the least squares polynomial (equation A-2) is evaluated at the strip midpoint.

Union Carbide trial exhibit UC-1507: W. A. Fraser, Micromechanical Characterization of Surface Treated Reinforci... Published by AsbestosClaims.Law
ACL Doc 16612 · Page 79 of 88 asbestosclaims.law/library/16612/79

$$\frac{dY(x_i)}{dx_i} = \sum_{j=1}^{m} j\, \beta_j\, x_i^{j-1} \qquad \text{(A-3)}$$

Ordinarily five or seven point strips are used however, in the central portion of a distribution these points could be nearly coincident and appear to define a steeply inclined line. Derivative evaluation could result in a series of "phantom peaks" appearing in the empirical probability density curve. This effect is particularly troublesome as the total number of data points increases. One approach to eliminating this effect is simply to increase the number of points in the strip. N, thus becomes an empirical variable, the best value is a function of the data being analyzed. Another approach, as suggested by Knox[39], is to define a constant, K. When the ratio of a data point and the current reference point (i.e., last value of x at which Y(x) was evaluated) is less than 1.0 + K, Y(x) is not evaluated at this point. Thus, K is also a variable which must be determined empirically.

The current data analysis program uses a second degree polynomial for both smoothing and differentiation. Multiple smoothing passes (~4) generally precede differentiation and "phantom peaks" are eliminated by the variable strip size technique.

Union Carbide trial exhibit UC-1507: W. A. Fraser, Micromechanical Characterization of Surface Treated Reinforci... Published by AsbestosClaims.Law
ACL Doc 16612 · Page 80 of 88 asbestosclaims.law/library/16612/80

APPENDIX B

Probabilistic Derivation for the Effect of Specimen Size on Strength

The following derivation is due to Freudenthal[19]. Consider that inhomogenerties of critical severity are uniformly distributed over the volume V (or length , or area) of the considered body.

Let

$P^*(V)$ = the probability of nonoccurrence of the critical flaw in volume V.

$P^*(V_1)$ = the probability of nonoccurrence in volume V_1 where V_1 does not include V.

The probability of nonoccurrence in $V + V_1$ is

$$P^*(V + V_1) = P^*(V) \cdot P^*(V_1) \qquad \text{(B-1)}$$

assuming that the probabilities $P^*(V)$ and $P^*(V_1)$ are independent. Differentiating with respect to V gives

$$\frac{d}{dV} P^*(V+V_1) = P^*(V_1) + \frac{d}{dV} P^*(V) \qquad \text{(B-2)}$$

Dividing equation B-2 by B-1 gives

$$\frac{d}{dV} \ln P^*(V+V_1) = \frac{d}{dV} n P^*(V) \qquad \text{(B-3)}$$

This equation equals a constant because it must hold for any arbitrary value of V_1

$$\frac{d}{dV} \ln P^*(V) = C \qquad \text{(B-4)}$$

Integrating with the boundary conditions

$$P^*(O) = 1$$

$$P^*(\infty) = O$$

Union Carbide trial exhibit UC-1507: W. A. Fraser, Micromechanical Characterization of Surface Treated Reinforci... Published by AsbestosClaims.Law
ACL Doc 16612 · Page 81 of 88 asbestosclaims.law/library/16612/81

produces the general expression

$$P^*(V) = e^{-cV} \qquad \text{(B-5)}$$

Where c is related to the flaw concentration (Weibull[26]) and has the units V^{-1}. The probability of fracture, thus becomes

$$P_f(V) = 1 - e^{-cV} \qquad \text{(B-6)}$$

For the same concentration of flaws, the probability of fracture increases rapidly with increasing volume.

Union Carbide trial exhibit UC-1507: W. A. Fraser, Micromechanical Characterization of Surface Treated Reinforci... Published by AsbestosClaims.Law
ACL Doc 16612 · Page 82 of 88 asbestosclaims.law/library/16612/82

APPENDIX C

The Mixed Element, Weakest Link, Fiber Strength Model

$f(\sigma)$, the fiber element probability density function (p.d.f.) is given by

$$
\begin{aligned}
f(\sigma) &= 0 && \text{for } \sigma < \sigma_a \\
f(\sigma) &= P/(\sigma_b-\sigma_a) && \text{for } \sigma_a \leq \sigma \leq \sigma_b \\
f(\sigma) &= 0 && \text{for } \sigma_b < \sigma < \sigma_c \\
f(\sigma) &= (1-P)(m/\sigma_o)\left(\frac{\sigma-\sigma_c}{\sigma_o}\right)^{m-1} \exp-\left(\frac{\sigma-\sigma_c}{\sigma_o}\right)^{m} && \text{for } \sigma \geq \sigma_c
\end{aligned}
\qquad \text{(C-1)}
$$

The fiber element cumulative distribution function (c.d.f.), $F(\sigma) = \int_o^{\sigma} f(\sigma)\, d\sigma$, is given by

$$
\begin{aligned}
F(\sigma) &= 0 && \text{for } \sigma < \sigma_a \\
F(\sigma) &= P(\sigma-\sigma_a)/(\sigma_b-\sigma_a) && \text{for } \sigma_a \leq \sigma \leq \sigma_b \\
F(\sigma) &= P && \text{for } \sigma_b < \sigma < \sigma_c \\
F(\sigma) &= 1-(1-P)\exp-\left(\frac{\sigma-\sigma_c}{\sigma_o}\right)^{m} && \text{for } \sigma \geq \sigma_c
\end{aligned}
\qquad \text{(C-2)}
$$

By employing the weakest link equations, expressions can be derived for the strength distribution functions characterizing a fiber or chain of n fiber elements. The chain p.d.f. is given by

$$g(\sigma) = n\, f(\sigma)\, [1-F(\sigma)]^{n-1} \qquad \text{(C-3)}$$

The chain c.d.f. is given by

$$G(\sigma) = 1 - [1 - F(\sigma)]^{n} \qquad \text{(C-4)}$$

Union Carbide trial exhibit UC-1507: W. A. Fraser, Micromechanical Characterization of Surface Treated Reinforci... Published by AsbestosClaims.Law
ACL Doc 16612 · Page 83 of 88 asbestosclaims.law/library/16612/83

Substituting (C-2) into (C-4) yields

$$G(\sigma) = 0 \qquad \text{for } \sigma < \sigma_a$$

$$G(\sigma) = 1 - \left[1 - P\left(\frac{\sigma-\sigma_a}{\sigma_b-\sigma_a}\right)\right]^n \qquad \text{for } \sigma_a \leq \sigma \leq \sigma_b$$

$$G(\sigma) = 1 - [1 - P]^n \qquad \text{for } \sigma_b < \sigma < \sigma_c \qquad \text{(C-5)}$$

$$G(\sigma) = 1 - \left[(1 - P)\ \exp-\left(\frac{\sigma-\sigma_c}{\sigma_o}\right)^m\right]^n \qquad \text{for } \sigma \geq \sigma_c$$

The average fiber or chain strength can be calculated from

$$\langle\sigma\rangle = \int_o^\infty [1 - G(\sigma)]\, d\sigma \qquad \text{(C-6)}$$

Therefore

$$\langle\sigma\rangle = \int_o^{\sigma_a} d\sigma + \int_{\sigma_a}^{\sigma_b} \left[1 - P\left(\frac{\sigma-\sigma_a}{\sigma_b-\sigma_a}\right)\right]^n d\sigma$$

$$+ \int_{\sigma_b}^{\sigma_c} [1 - P]^n d\sigma + \int_{\sigma_c}^{\infty} \left[(1 - P)\ \exp-\left(\frac{\sigma-\sigma_c}{\sigma_o}\right)^m\right]^n d\sigma \qquad \text{(C-7)}$$

which yields

$$\langle\sigma\rangle = \sigma_a + (\sigma_b-\sigma_a)\left[1 - (1 - P)^{n+1}\right]/P(n+1)$$

$$+ (\sigma_c-\sigma_b)\ [1 - P]^n \qquad \text{(C-8)}$$

$$+ [1 - P]^n \left(\sigma_o/n^{1/m}\right)\ \Gamma\ \frac{m+1}{m}$$

where

Γ = complete gamma function

APPENDIX D

The Sequential Fragment Proof Testing Modifications

The c.d.f. for fibers which have been proof tested to the stress level σ_p can be expressed in terms of the original distribution by the relation

$$G_p(\sigma) = 0 \qquad \text{for } \sigma < \sigma_p$$

$$G_p(\sigma) = \frac{G(\sigma) - G(\sigma_p)}{1 - G(\sigma_p)} \qquad \text{for } \sigma \geq \sigma_p \tag{D-1}$$

$G_p(\sigma)$, in terms of our fiber strength model, thus assumes different forms depending on the value of σ_p and its relation to the model parameters, σ_a, σ_b, and σ_c.

If $\sigma_a \leq \sigma_p \leq \sigma_b$

$$1 - G_p(\sigma) = 1 \qquad \text{for } \sigma < \sigma_p$$

$$= \left[1 - P\left(\frac{\sigma-\sigma_a}{\sigma_b-\sigma_a}\right)\right]^n \Big/ \left[1 - P\left(\frac{\sigma_p-\sigma_a}{\sigma_b-\sigma_a}\right)\right]^n \qquad \text{for } \sigma_p \leq \sigma \leq \sigma_b$$

$$= \left[1 - P\right]^n \Big/ \left[1 - P\left(\frac{\sigma_p-\sigma_a}{\sigma_b-\sigma_a}\right)\right]^n \qquad \text{for } \sigma_b < \sigma < \sigma_c \tag{D-2}$$

$$= \left[1 - P\right]^n \exp n\left(\frac{\sigma-\sigma_c}{\sigma_o}\right)^m \Big/ \left[1 - P\left(\frac{\sigma_p-\sigma_a}{\sigma_b-\sigma_a}\right)\right]^n \qquad \text{for } \sigma \geq \sigma_c$$

If $\sigma_b < \sigma_p < \sigma_c$

$$1 - G_p(\sigma) = 1 \qquad \text{for } \sigma < \sigma_c$$

$$= \exp -n\left(\frac{\sigma-\sigma_c}{\sigma_o}\right)^m \qquad \text{for } \sigma \geq \sigma_c \tag{D-3}$$

If $\sigma_p \geq \sigma_c$

$$1 - G_p(\sigma) = 1 \qquad \text{for } \sigma < \sigma_p$$

$$= \exp -n\left[\left(\frac{\sigma-\sigma_c}{\sigma_o}\right)^m - \left(\frac{\sigma_p-\sigma_c}{\sigma_o}\right)^m\right] \qquad \text{for } \sigma \geq \sigma_p \tag{D-4}$$

Union Carbide trial exhibit UC-1507: W. A. Fraser, Micromechanical Characterization of Surface Treated Reinforci... Published by AsbestosClaims.Law
ACL Doc 16612 · Page 85 of 88 asbestosclaims.law/library/16612/85

The average fiber or chain strength can be evaluated from equation (C-6)

for $\sigma_a \leq \sigma_p \leq \sigma_b$

$$\langle\sigma\rangle = \sigma_p + \frac{(\sigma_b-\sigma_a)}{P(n+1)} \left\{ \left[1 - P\left(\frac{\sigma_p-\sigma_a}{\sigma_b-\sigma_a}\right)\right] - \left[1 - P\left(\frac{\sigma_p-\sigma_a}{\sigma_b-\sigma_a}\right)\right]^{-n} (1-P)^{n+1} \right\}$$

$$+ (\sigma_c-\sigma_b)\ (1-P)^n \left[1 - P\left(\frac{\sigma_p-\sigma_a}{\sigma_b-\sigma_a}\right)\right]^{-n}$$

$$+ (1-P)^n \left[1 - P\left(\frac{\sigma_p-\sigma_b}{\sigma_b-\sigma_a}\right)\right]^{-n} \left(\sigma_o/n^{1/m}\right)\ \Gamma\left(\frac{m+1}{m}\right) \qquad (D-5)$$

Where Γ = complete gamma function

for $\sigma_b < \sigma_p < \sigma_c$

$$\langle\sigma\rangle = \sigma_c + \left(\sigma_o/n^{1/m}\right)\ \Gamma\ \frac{m+1}{m} \qquad (D-6)$$

for $\sigma_p \geq \sigma_c$

$$\langle\sigma\rangle = \sigma_p + \left[\exp\ n\left(\frac{\sigma_p-\sigma_c}{\sigma_o}\right)^m\right] \left(\sigma_o/n^{1/m}\right) \frac{1}{m} \left\{ \Gamma\left(\frac{1}{m}\right) - \gamma\left[\frac{1}{m}, n\left(\frac{\sigma_p-\sigma_c}{\sigma_o}\right)^m\right] \right\}$$

where γ = incomplete gamma function (D-7)

The incomplete gamma function, γ, in equation (D-7) was evaluated using an identity relation with the chi-square probability function. (See Abramowitz[40] pg. 941, eq. 26.4.19).

$$\gamma(a,x) = \Gamma(a)\ \ P(\chi^2/\nu) \qquad (D-8)$$

where $\nu = 2a = 2/m$

$\chi^2 = 2x = 2n\left(\frac{\sigma-\sigma_c}{\sigma_o}\right)^m$

$P(\chi^2/\nu)$ is the probability that the random variable x, distributed according to the chi-square distribution with ν degrees of freedom, is less than or equal to χ^2. It was computed using the IBM SSP subroutine, CDTR.

Union Carbide trial exhibit UC-1507: W. A. Fraser, Micromechanical Characterization of Surface Treated Reinforci... Published by AsbestosClaims.Law
ACL Doc 16612 · Page 86 of 88 asbestosclaims.law/library/16612/86

Since this program is restricted to values of $\nu \geq 0.5$ (i.e., $a \geq 2.5$) the recurrence formula

$$\gamma(a+1,x) = a\gamma(a,x) - x^a e^{-x} \qquad \text{(D-9)}$$

was also used in the calculation (see Abramowitz[40] pg. 262, equation 6.5.22).

DISTRIBUTION

BOUND BROOK

*Ancker, F. H. (6)
Azrak, R. G.
Baker, L. M.
Bertolucci, M. D.
Brown, A.
Carrick, W. L.
Fan, Y. L.
*Fraser, W. A. (8)
Gorham, W. F.
Hale, W. F.
Johnston, N. W.
Leung, M.
*Lynn, J. W.
Marsh, B. D.
McKenna, L. A.
Merriam, C. N.
*Michno, M. J., Jr.
*Nicholas, J. S.
Ongchin, L.
*Pan, F. Y.
*Reinking, N. H.
Sauers, M.
Staub, R. B.
Whelan, J. M.
*White, Dr. C. E.
*Technical Reports Center (10)

NIAGARA FALLS

Byrne, R. E.
Myers, J. L.

NEW YORK

Burnett, L. D.
Ford, C. E.
Forsyth, R. B.
Hiler, D. C.
Hutchinson, K. J.
Jellinek, M. H.
Lutz, A. W.
Shechter, L.
Szabo, T. T.
Thurber, W. C.
Tomfohrde, H. F., III
Townsend, H. N.
Zutty, N. L.

TARRYTOWN

*Marsden, J. G.
Orenski, P.
Ranney, M. W.
Sterman, S.
Tinsley, S. W.
Welch, T. H.
Williams, T. C.

SOUTH CHARLESTON

Atkins, K. E.
Bryant, G. M.
Kayser, R. F.
Koleske, J. V.
Smith, J. J.
Smith, P. L.
Walter, A. T.
Whitehurst, W. E.

PARMA

Bacon, R.
Chambers, W. E.
Chwastiak, S.
Didchenko, R.
Eckstein, B. H.
Kampe, D. J.
Singer, L.
Stroup, R. C.
Volk, H. F.

*Appendicies E and F included.

Published by AsbestosClaims.Law
asbestosclaims.law/library/16612/88